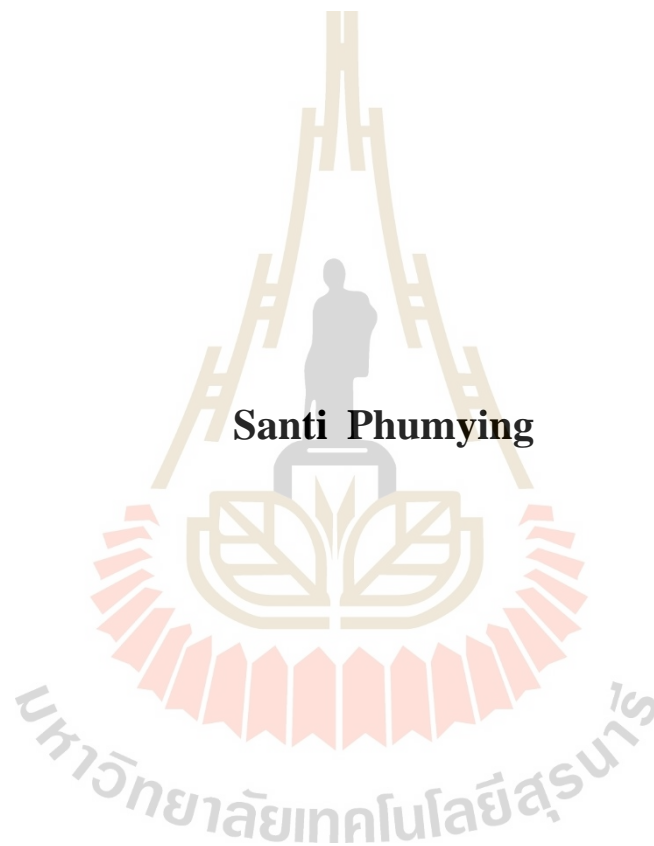


**SYNTHESIS AND STRUCTURAL PROPERTIES OF  
AMMONIUM METAL PHOSPHATE  $\text{NH}_4\text{MPO}_4\cdot\text{H}_2\text{O}$**

**(M = Mg, Co, Fe, Mn, Ni, Zn, Cu)**



**A Thesis Submitted in Fulfillment of the Requirements for the  
Degree of Doctor of Philosophy in Applied Physics**

**Suranaree University of Technology**

**Academic Year 2019**

การสังเคราะห์และสมบัติทางโครงสร้างของแอมโมเนียมเมททอลฟอสเฟต

$\text{NH}_4\text{MPO}_4 \cdot \text{H}_2\text{O}$  (M = Mg, Co, Fe, Mn, Ni, Zn, Cu)



วิทยานิพนธ์นี้สำหรับการศึกษาตามหลักสูตรปริญญาวิทยาศาสตรดุษฎีบัณฑิต

สาขาวิชาฟิสิกส์ประยุกต์

มหาวิทยาลัยเทคโนโลยีสุรนารี

ปีการศึกษา 2562

**SYNTHESIS AND STRUCTURAL PROPERTIES OF  
AMMONIUM METAL PHOSPHATE  $\text{NH}_4\text{MPO}_4\cdot\text{H}_2\text{O}$**

**(M=Mg, Co, Fe, Mn, Ni, Zn, Cu)**

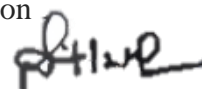
Suranaree University of Technology has approved this thesis submitted in fulfillment of the requirements for the Degree of Doctor of Philosophy.

Thesis Examining Committee



(Assoc. Prof. Dr. Panomsak Meemon)

Chairperson



(Prof. Dr. Santi Maensiri)

Member (Thesis Advisor)



(Assoc. Prof. Dr. Prayoon Songsirithigul)

Member



(Dr. Wiwat Nuansing)

Member



(Dr. Narong Chanlek)

Member



(Assoc. Prof. Dr. Worawat Meevasana)



(Assoc. Prof. Flt. Lt. Dr. Kontorn Chamniprasart)

Vice Rector for Academic Affairs  
and Internationalization

Dean of Institute of Science

สันติ ภูมิขิง : การสังเคราะห์และสมบัติทางโครงสร้างของแอมโมเนียมเมททอลฟอสเฟต  $\text{NH}_4\text{MPO}_4 \cdot \text{H}_2\text{O}$  ( $M = \text{Mg, Co, Fe, Mn, Ni, Zn, Cu}$ ) (SYNTHESIS AND STRUCTURAL PROPERTIES OF AMMONIUM METAL PHOSPHATE  $\text{NH}_4\text{MPO}_4 \cdot \text{H}_2\text{O}$  ( $M = \text{Mg, Co, Fe, Mn, Ni, Zn, Cu}$ )) อาจารย์ที่ปรึกษา : ศาสตราจารย์ ดร.สันติ แม่นศิริ, 147 หน้า.

วิทยานิพนธ์นี้ศึกษาการสังเคราะห์แอมโมเนียมเมททอลฟอสเฟต ( $\text{NH}_4\text{MPO}_4 \cdot \text{H}_2\text{O}$ ,  $M = \text{Mg, Co, Fe, Mn, Ni, Zn, Cu}$ ) ด้วยวิธีการตกตะกอนอย่างง่าย โดยการทดลองแบ่งเป็น 2 ส่วน คือ 1) การสังเคราะห์ผง  $\text{NH}_4\text{MPO}_4 \cdot \text{H}_2\text{O}$  ( $M = \text{Mg, Co, Fe, Mn, Ni, Zn, Cu}$ ) ด้วยวิธีการตกตะกอนอย่างง่ายที่อุณหภูมิห้องในสารละลายน้ำสำหรับทุกเงื่อนไข 2) การสังเคราะห์ผง  $\text{NH}_4\text{MPO}_4 \cdot \text{H}_2\text{O}$  ( $M = \text{Mg, Co, Fe, Mn, Ni, Zn, Cu}$ ) ด้วยวิธีการตกตะกอนอย่างง่ายที่อุณหภูมิห้องในสารลดแรงตึงผิวพอลิเมอร์ที่แตกต่างกัน และได้เสนอกลไกการเกิด  $\text{NH}_4\text{MPO}_4 \cdot \text{H}_2\text{O}$  ( $M = \text{Mg, Co, Fe, Mn, Ni, Zn, Cu}$ ) โดยอาศัยหลักของการการก่อนิวเคลียสผลึก (nucleation) และการเพิ่มขนาดของผลึก (crystal growth)

ในส่วนแรกได้ทำการสังเคราะห์  $\text{NH}_4\text{MPO}_4 \cdot \text{H}_2\text{O}$  ( $M = \text{Mg, Co, Fe, Mn, Ni, Zn, Cu}$ ) ด้วยวิธีการตกตะกอนอย่างง่ายที่อุณหภูมิห้องในสารละลายน้ำสำหรับทุกเงื่อนไข ตัวอย่างที่ได้ถูกตรวจสอบโดยใช้เทคนิคการเลี้ยวเบนรังสีเอกซ์ (XRD) กล้องจุลทรรศน์อิเล็กตรอนแบบส่องกราด ชนิดฟิลด์อิมิสชัน (FESEM) กล้องจุลทรรศน์อิเล็กตรอนแบบส่องผ่าน (TEM) เทคนิคการดูดกลืนรังสีเอกซ์ (XAS) เทคนิคสเปกโทรสโกปีโฟโตอิเล็กตรอนด้วยรังสีเอกซ์ (XPS) ตามลำดับ สมบัติเฉพาะทางแม่เหล็กด้วยเทคนิคแมกนีโตมิเตอร์แบบตัวอย่างสั้น (VSM) และสมบัติการปลดปล่อยไอออนถูกวิเคราะห์ด้วยเทคนิค inductively coupled plasma optical emission spectrometer (ICP-OES) เพื่อศึกษาความเป็นไปได้สำหรับการประยุกต์ด้านปุ๋ย ผลการจำแนกลักษณะพบว่าตัวอย่างที่เตรียมด้วยเงื่อนไขน้ำมีโครงสร้างแบบออร์โธโรมบิก สำหรับตัวอย่าง  $M = \text{Co, Fe, Mn, Ni, Zn, Cu}$  โดยไม่มีโครงสร้างอื่นเจือในขณะที่ยตัวอย่าง  $M = \text{Mg}$  ไม่พบโครงสร้างออร์โธโรมบิกแต่พบโครงสร้างมอนอกlinik และโครงสร้างเฮกซะโกนอล อีกทั้งมีลักษณะสัณฐานวิทยาที่ต่างออกไป เทคนิคการดูดกลืนรังสีเอกซ์ (XAS) และเทคนิคสเปกโทรสโกปีโฟโตอิเล็กตรอนด้วยรังสีเอกซ์ (XPS) ถูกนำมาใช้เพื่อทำนายสถานะเลขออกซิเดชันและโครงสร้างพื้นฐานรอบอะตอมในตัวอย่างที่เตรียมไว้ ผลทดลองแสดงสถานะเลขออกซิเดชันของสารตัวอย่างตรงตามสารมาตรฐานในทุกเงื่อนไข การศึกษาสมบัติทางแม่เหล็กของสารตัวอย่างทุกเงื่อนไขพบว่าที่ทุกเงื่อนไขไม่มีสมบัติทางแม่เหล็กชนิดแอนติเฟอร์โรแมกเนติก (antiferromagnetism) สำหรับตัวอย่าง  $M = \text{Co, Fe, Mn, Ni, Mg}$  และ  $\text{Cu}$  ในขณะที่ตัวอย่าง  $M = \text{Zn}$  แสดงสมบัติทางแม่เหล็กชนิดไดอะแมกเนติก

(diamagnetism) การศึกษาสมบัติการปลดปล่อยไอออนเพื่อศึกษาความเป็นไปได้สำหรับการประยุกต์ด้านปุ๋ยพบว่าสารตัวอย่างทุกเงื่อนไขมีการปลดปล่อยไอออนของโลหะในปริมาณที่น้อย ยกเว้นเงื่อนไขของไอออน Co และ Mn ที่ไม่มีการปลดปล่อยไอออนออกมา แต่มีการปลดปล่อยไอออนของ P ออกมาทุกเงื่อนไข จากผลดังกล่าวพบว่าสารตัวอย่างที่สังเคราะห์ได้เหมาะแก่การนำไปประยุกต์ใช้เป็นปุ๋ยละลายช้าหรือปุ๋ยทางใบ

ในส่วนที่สอง ได้ทำการสังเคราะห์ผง  $\text{NH}_4\text{MPO}_4 \cdot \text{H}_2\text{O}$  ( $M = \text{Mg, Co, Fe, Mn, Ni, Zn, Cu}$ ) ด้วยวิธีการตกตะกอนอย่างง่ายที่อุณหภูมิห้องโดยใช้สารลดแรงตึงผิวพอลิเมอร์ที่แตกต่างกัน ได้แก่ โพลีไวนิลไพโรลิโดน โพลีไวนิลแอลกอฮอล์ ซูโครส และ ซิทิลไตรเมทิลแอมโมเนียมโบรไมด์ ตามลำดับ การเกิดโครงสร้างองค์ประกอบและสัณฐานวิทยาของสารตัวอย่างที่เตรียมได้ได้ทุกเงื่อนไข ถูกวิเคราะห์ด้วยเทคนิคการเลี้ยวเบนด้วยรังสีเอกซ์และกล้องจุลทรรศน์อิเล็กตรอนแบบส่องกราด ชนิดฟิล์มอีมิสชัน ตามลำดับ พบว่าทุกเงื่อนไขมีโครงสร้างแบบออร์โธโรมบิก แต่ไม่พบในตัวอย่าง  $M = \text{Zn}$  ตัวอย่าง  $M = \text{Zn}$  มีโครงสร้างแบบเฮกซะโกนอล จากการทดลองนี้ พบว่าสารละลายที่แตกต่างกันส่งผลต่อโครงสร้างและลักษณะสัณฐานวิทยาของสารตัวอย่าง สถานะเลขออกซิเดชัน จากผลการตรวจสอบธาตุและองค์ประกอบทางเคมีของสารตัวอย่างที่เตรียมได้ถูกตรวจสอบด้วยเทคนิคการดูดกลืนรังสีเอกซ์ และ เทคนิคสเปกโทรสโกปีโฟโตอิเล็กตรอนด้วยรังสีเอกซ์ พบว่าไอออน P มีสถานะเลขออกซิเดชันเป็น  $5+$  และไอออน Mg, Co, Ni, Zn และ Cu มีสถานะเลขออกซิเดชันเป็น  $2+$  ในขณะที่ไอออน Fe และ Mn แสดงสถานะเลขออกซิเดชันเป็น  $2+$  และ  $3+$  ผสมกัน

การศึกษาคูสมบัติการปลดปล่อยไอออนสารตัวอย่างโดยใช้เทคนิค ICP-OES นั้น พบว่า  $\text{NH}_4\text{MPO}_4 \cdot \text{H}_2\text{O}$  ( $M = \text{Mg, Co, Fe, Mn, Ni, Zn, Cu}$ ) แสดงความเป็นปุ๋ยมีการปลดปล่อยไอออนช้า โดยน้อยกว่าร้อยละ 15 ถูกปลดปล่อยออกมาใน 24 ชั่วโมง สำหรับตัวอย่าง  $M = \text{Mg, Fe, Ni, Zn}$  and Cu ยกเว้นเงื่อนไขของ ไอออน Mn และ Co ไม่พบการปลดปล่อยไอออนโลหะ และพบว่ามีการปลดปล่อยไอออนของ P ในทุกเงื่อนไข ผลจากการศึกษานี้แสดงให้เห็นว่าวิธีการตกตะกอนอย่างง่าย โดยใช้ น้ำ โพลีไวนิลไพโรลิโดน โพลีไวนิลแอลกอฮอล์ ซูโครส และซิทิลไตรเมทิลแอมโมเนียมโบรไมด์ เป็นแม่แบบสามารถใช้ในการการสังเคราะห์วัสดุผง  $\text{NH}_4\text{MPO}_4 \cdot \text{H}_2\text{O}$  ( $M = \text{Mg, Co, Fe, Mn, Ni, Zn, Cu}$ ) ได้ นอกจากนี้วิธีการเตรียมอย่างง่ายนี้สามารถนำไปประยุกต์สำหรับเตรียมวัสดุออกไซด์อื่น ๆ ได้

สาขาวิชาฟิสิกส์

ปีการศึกษา 2562

ลายมือชื่อนักศึกษา วิไล นวล  
ลายมือชื่ออาจารย์ที่ปรึกษา ศ.ดร.วิไล

SANTI PHUMYING : SYNTHESIS AND STRUCTURAL PROPERTIES OF  
AMMONIUM METAL PHOSPHATE  $\text{NH}_4\text{MPO}_4\cdot\text{H}_2\text{O}$  (M=Mg, Co, Fe, Mn,  
Ni, Zn, Cu) THESIS ADVISOR : PROF. SANTI MAENSIRI, D.Phil.  
147 PP.

SYNTHESIS AND STRUCTURAL PROPERTIES OF AMMONIUM METAL  
PHOSPHATE  $\text{NH}_4\text{MPO}_4\cdot\text{H}_2\text{O}$  (M=Mg, Co, Fe, Mn, Ni, Zn, Cu)

This dissertation studied the synthesis of  $\text{NH}_4\text{MPO}_4\cdot\text{H}_2\text{O}$  (M = Mg, Co, Fe, Mn, Ni, Zn, Cu) powders prepared by a simple precipitation method. This work consisted of two main parts: 1) the synthesis of  $\text{NH}_4\text{MPO}_4\cdot\text{H}_2\text{O}$  powders by a simple precipitation method at room temperature using water solution, and 2) synthesis of  $\text{NH}_4\text{MPO}_4\cdot\text{H}_2\text{O}$  powders by a simple precipitation route using various polymeric surfactants including water and polymers sources of Polyvinylpyrrolidone (PVP), polyvinyl alcohol (PVA), Sucrose and Hexadecyl trimethylammonium bromide (CTAB). The possible formation of  $\text{NH}_4\text{MPO}_4\cdot\text{H}_2\text{O}$  in different surfactants was proposed based on the two processes of nucleation and crystal growth.

In the first part, the  $\text{NH}_4\text{MPO}_4\cdot\text{H}_2\text{O}$  samples prepared in water solutions were characterized by using X-ray diffraction (XRD), field emission scanning electron microscopy (FESEM), transmission electron microscopy (TEM), X-ray absorption spectroscopy (XAS) and X-Ray Photoemission spectroscopy (XPS), respectively. The magnetic properties were measured by vibrating sample magnetometer (VSM), while the ion release properties were studied by using inductively coupled plasma optical emission spectrometer (ICP-OES). The characterization results showed that all

prepared samples except  $M = \text{Mg}$  had the orthorhombic structure without impurity phase, whereas the sample with  $M = \text{Mg}$  showed monoclinic structure and hexagonal, and this sample also had different morphology from the others. The XAS and XPS results exhibited the oxidation states of metal atoms in the samples with  $M = \text{Mg}$ , Co, Ni, Zn, Cu are  $2+$ , whereas the oxidation states of the samples with  $M = \text{Fe}$ , Mn are mixed with  $2+$  and  $3+$ . All samples exhibited antiferromagnetism except  $M = \text{Zn}$  which is diamagnetism. The results of the ion release properties revealed that all samples released small amounts of P ions which are suitable to be used as slow-release fertilizer or foliar fertilizer application.

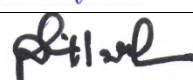
In the second part, the phase formation and morphology of the  $\text{NH}_4\text{MPO}_4 \cdot \text{H}_2\text{O}$  powders prepared with different surfactants were characterized by using XRD and SEM, respectively. It was found that all the prepared samples had orthorhombic structure, except for the sample with  $M = \text{Zn}$  which shows hexagonal structure. This result indicated that the different surfactants affected to the phase formation and morphology of the prepared samples. The XAS and XPS results confirmed that the oxidation states of  $5+$  for P ion and  $2+$  for Mg, Co, Ni, Zn and Cu ions, whereas the mixed oxidation state of  $2+$  and  $3+$  for Fe and Mn ions. The ion release results showed that the prepared  $\text{NH}_4\text{MPO}_4 \cdot \text{H}_2\text{O}$  powders released less than 15% of the ions in 24 h implying that all samples can also be considered as slow-release fertilizer. This study shows that simple precipitation method is a promising technique to synthesize  $\text{NH}_4\text{MPO}_4 \cdot \text{H}_2\text{O}$  powders, which may be extended for other oxide preparation.

School of Physics

Academic Year 2019

Student's Signature

Advisor's Signature

## ACKNOWLEDGMENTS

I would like to express my sincere gratitude to my supervisor, Prof. Dr. Santi Maensiri, School of Physics for his effective scientific supervision, motivation, instructive guidance, generous personal encouragement and support. I benefited from his guidance in every aspect during my PhD study. I wish to thank the Advanced Materials Physics Laboratory (AMP), Center for Scientific and Technological Equipment, Suranaree University of Technology for research facilities supporting. I would like to give special thanks to SUT-PhD scholarship (Grant No.SUT-PhD/05/2556) for my PhD study and financial support for research presentation in both inside and outside the country. I would like to thank NANOTEC-SUT Center of Excellence on Advanced Functional Nanomaterials at the Suranaree University of Technology for the financial support, and the School of Physics, Institute of science, Suranaree University of Technology for having very good laboratory facilities. I specially thank Department of Physics, Faculty of Science, Khon Kaen University for magnetic properties measurement. I would like to thank AMP group members whose direct and indirect support helped and guided me during work and for their friendship.

Finally, I would like to thank my family for their understanding, endless love throughout my life, to bring me up and give me the good life.

Santi Phumying

# CONTENTS

	<b>Page</b>
ABSTRACT IN THAI.....	I
ABSTRACT IN ENGLISH.....	III
ACKNOWLEDGMENTS.....	V
CONTENTS.....	VI
LIST OF TABLES.....	X
LIST OF FIGURES.....	XIII
LIST OF ABBREVIATIONS.....	XX
<b>CHAPTER</b>	
<b>I INTRODUCTION.....</b>	<b>1</b>
1.1 Background and significance of the study.....	1
1.2 Research objectives / Purpose of the study.....	3
1.3 Scope and limitations.....	3
1.4 Location of the research.....	3
1.5 Expected results.....	4
<b>II LITERATURE REVIEWS.....</b>	<b>5</b>
2.1 Fertilizers and importance.....	5
2.2 Controlled release fertilizer.....	7
2.3 Ammonium/transition metal phosphates.....	12
2.4 Preparation of ammonium transition metal phosphates.....	13
<b>III RESEARCH METHODOLOGY.....</b>	<b>20</b>

## CONTENTS (Continued)

	<b>Page</b>
3.1 Materials.....	20
3.2 Instrumentation.....	21
3.3 Synthesis of ammonium metal phosphate $\text{NH}_4\text{MPO}_4\cdot\text{H}_2\text{O}$ (M = Mg, Co, Fe, Mn, Ni, Zn, Cu).....	22
3.4 Morphological characterization of ammonium metal phosphate.....	23
3.5 X-ray diffraction (XRD).....	24
3.6 Fourier transform infrared spectroscopy (FTIR).....	25
3.7 Thermogravimetric analysis.....	25
3.8 X-ray Absorption Spectroscopy (XAS).....	25
3.9 X-ray photoelectron spectroscopy (XPS).....	26
3.10 Magnetic properties measurement.....	27
3.11 Inductively couple plasma optical emission spectrometer (ICP-OES).....	28
3.12 Ion release.....	29
<b>IV RESULTES AND DISCSSION.....</b>	<b>30</b>
4.1 Structural characterization of $\text{NH}_4\text{MPO}_4\cdot\text{H}_2\text{O}$ (M = Mg, Co, Fe, Mn, Ni, Zn, Cu) samples prepared by chemical precipitation method in water solution.....	31
4.1.1 X-ray diffraction (XRD) analysis of $\text{NH}_4\text{MPO}_4\cdot\text{H}_2\text{O}$ (M= Mg, Co, Fe, Mn, Ni, Zn, Cu) samples prepared by chemical precipitation method in water.....	31

## CONTENTS (Continued)

	<b>Page</b>
4.1.2 Thermo gravimetric analysis (TGA) of the $\text{NH}_4\text{MPO}_4\cdot\text{H}_2\text{O}$ (M = Mg, Co, Fe, Mn, Ni, Zn, Cu).....	36
4.1.3 Morphology of $\text{NH}_4\text{MPO}_4\cdot\text{H}_2\text{O}$ powder (M = Mg, Co, Fe, Mn, Ni, Zn, Cu) by SEM.....	39
4.1.4 Morphology of $\text{NH}_4\text{MPO}_4\cdot\text{H}_2\text{O}$ powder (M = Mg, Co, Fe, Mn, Ni, Zn, Cu) by TEM.....	41
4.1.5 X-ray absorption spectroscopy study of the $\text{NH}_4\text{MPO}_4\cdot\text{H}_2\text{O}$ powder (M = Mg, Co, Fe, Mn, Ni, Zn, Cu).....	44
4.1.6 X-Ray Photoelectron spectroscopy study of the $\text{NH}_4\text{MPO}_4\cdot\text{H}_2\text{O}$ powder (M = Mg, Co, Fe, Mn, Ni, Zn, Cu)...	52
4.1.7 The magnetic properties of the $\text{NH}_4\text{MPO}_4\cdot\text{H}_2\text{O}$ (M = Mg, Co, Fe, Mn, Ni, Zn, Cu) samples.....	59
4.2 Effect of solvent on $\text{NH}_4\text{MPO}_4\cdot\text{H}_2\text{O}$ (M= Mg, Co, Fe, Mn, Ni, Zn, Cu) structures.....	61
4.2.1 X-ray diffraction (XRD) analysis of $\text{NH}_4\text{MPO}_4\cdot\text{H}_2\text{O}$ (M= Mg, Co, Fe, Mn, Ni, Zn, Cu) samples within water, PVP, PVA, Sucrose and CTAB solution.....	61
4.2.2 Morphology of $\text{NH}_4\text{MPO}_4\cdot\text{H}_2\text{O}$ powder (M = Mg, Co, Fe, Mn, Ni, Zn, Cu) by SEM.....	82

## CONTENTS (Continued)

	<b>Page</b>
4.2.3 X-ray absorption spectroscopy study of the $\text{NH}_4\text{MPO}_4\cdot\text{H}_2\text{O}$ powders (M = Mg, Co, Fe, Mn, Ni, Zn, Cu) with water, PVP, PVA, Sucrose and CTAB.....	94
4.2.4 X-ray photoelectron spectroscopy study of the $\text{NH}_4\text{MPO}_4\cdot\text{H}_2\text{O}$ powders (M = Mg, Co, Fe, Mn, Ni, Zn, Cu).....	108
<b>V CONCLUSION AND SUGGESTION.....</b>	<b>131</b>
5.1 The structure and morphology characterization.....	131
5.2 The magnetic properties.....	133
5.3 The ion release properties.....	133
5.4 Effect of solvent on $\text{NH}_4\text{MPO}_4\cdot\text{H}_2\text{O}$ (M= Mg, Co, Fe, Mn, Ni, Zn, Cu) structures.....	134
5.5 Suggestion for future work.....	136
REFERENCES.....	138
CURRICULUM VITAE.....	147

## LIST OF TABLES

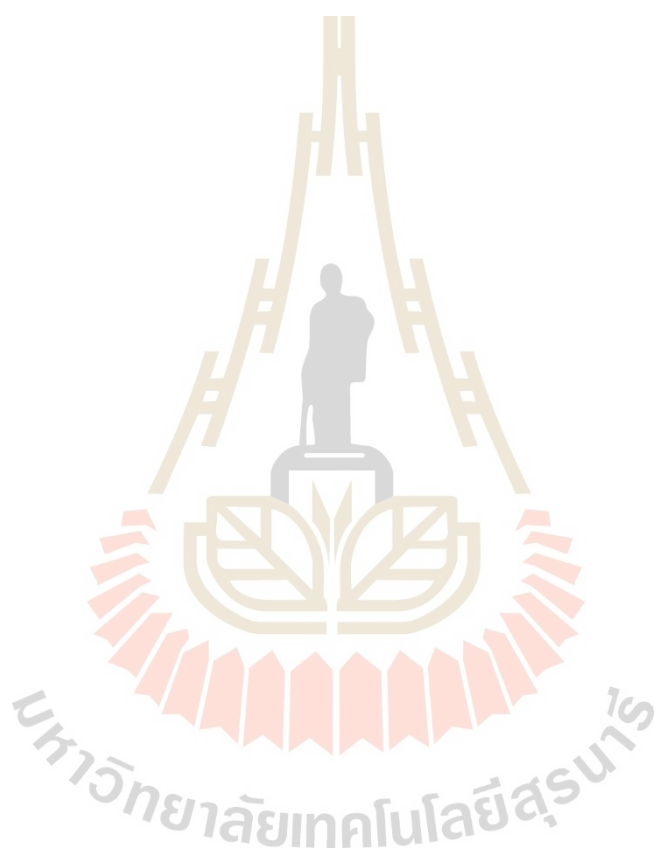
Table	Page
2.1 Summary of ammonium metal phosphate prepared by different synthesis methods.....	16
4.1 Lattice parameter (a, b, and c), $\beta$ angle, cell volume (V), Rietveld refinement parameters ( $R_p$ , $R_{exp}$ , $R_{wp}$ and GOF) and specific magnetization of the $NH_4MPO_4 \cdot H_2O$ (M= Mg, Co, Fe, Mn, Ni, Zn, Cu) powder prepared by chemical precipitation method.....	35
4.2 Lattice parameter (a, b, and c), $\beta$ angle, cell volume (V), Rietveld refinement parameters ( $R_p$ , $R_{exp}$ , $R_{wp}$ and GOF) of the $NH_4CoPO_4 \cdot H_2O$ powders prepared by chemical precipitation method and different medium condition (Water, PVP, PVA, Sucrose and CTAB).....	63
4.3 Lattice parameter (a, b, and c), $\beta$ angle, cell volume (V), Rietveld refinement parameters ( $R_p$ , $R_{exp}$ , $R_{wp}$ and GOF) of the $NH_4CuPO_4 \cdot H_2O$ powder prepared by chemical precipitation method and different medium condition (Water, PVP, PVA, Sucrose and CTAB).....	66
4.4 Lattice parameters (a, b, and c), cell volume (V), Rietveld refinement parameters ( $R_p$ , $R_{exp}$ , $R_{wp}$ and GOF) of the $NH_4MgPO_4 \cdot H_2O$ powder with different medium condition (Water, PVP, PVA, Sucrose and CTAB)...	69

## LIST OF TABLES (Continued)

<b>Table</b>	<b>Page</b>
4.5	Lattice parameters (a, b, and c), cell volume (V), Rietveld refinement parameters ( $R_p$ , $R_{exp}$ , $R_{wp}$ and GOF) of the $NH_4MnPO_4 \cdot H_2O$ powder prepared by chemical precipitation method and different medium condition (Water, PVP, PVA, Sucrose and CTAB).....72
4.6	Lattice parameters (a, b, and c), $\beta$ angle, cell volume (V), Rietveld refinement parameters ( $R_p$ , $R_{exp}$ , $R_{wp}$ and GOF) of the $NH_4FePO_4 \cdot H_2O$ powder prepared by chemical precipitation method and different medium condition (Water, PVP, PVA, Sucrose and CTAB).....75
4.7	Lattice parameters (a, b, and c), cell volume (V), Rietveld refinement parameters ( $R_p$ , $R_{exp}$ , $R_{wp}$ and GOF) of the $NH_4NiPO_4 \cdot 6H_2O$ powders prepared by chemical precipitation method with water, PVP, PVA, Sucrose and CTAB).....78
4.8	Lattice parameters (a, b, and c), $\beta$ angle, cell volume (V), Rietveld refinement parameters ( $R_p$ , $R_{exp}$ , $R_{wp}$ and GOF) of the $NH_4ZnPO_4$ powders prepared by chemical precipitation method and different medium condition (Water, PVP, PVA, Sucrose and CTAB).....81
4.9	Ion release from $NH_4MPO_4 \cdot H_2O$ (M= Mg, Co, Cu) samples by Inductively Coupled Plasma Optical Emission Spectrometry (ICP-OES) method.....128
4.10	Ion release from $NH_4MPO_4 \cdot H_2O$ (M= Fe, Mn) samples by Inductively Coupled Plasma Optical Emission Spectrometry (ICP-OES) method.....129

**LIST OF TABLES (Continued)**

<b>Table</b>	<b>Page</b>
4.11 Ion release from $\text{NH}_4\text{MPO}_4\cdot\text{H}_2\text{O}$ (M= Ni, Zn) samples by Inductively Coupled Plasma Optical Emission Spectrometry (ICP-OES) method.....	130



## LIST OF FIGURES

Figures	Page
2.1 Schematic for classification of controlled release fertilizers. (Adapted from Azeem et al., 2014).....	8
2.2 The structure of $\text{NH}_4\text{CoPO}_4 \cdot \text{H}_2\text{O}$ (Adapted from ICSD 28-0044).....	13
3.1 Diagram represents the principles of XRD.....	24
4.1 XRD patterns of the prepared $\text{NH}_4\text{MPO}_4 \cdot \text{H}_2\text{O}$ (M = Co, Cu, Fe, Mn) powder.....	33
4.2 XRD patterns of the prepared $\text{NH}_4\text{MPO}_4 \cdot \text{H}_2\text{O}$ (M = Zn, Ni, Mg) powder.....	34
4.3 TG-DTG curves of the $\text{NH}_4\text{MPO}_4 \cdot \text{H}_2\text{O}$ (M = Co, Cu, Mg, Mn, Fe, Ni and Zn) powder performed at a heating rate of $5^\circ\text{C min}^{-1}$ in $\text{N}_2$ atmosphere.....	37
4.4 shows the DSC curves of the prepared samples, when heated at a rate of $5^\circ\text{C/min}$ from ambient temperature to $700^\circ\text{C}$ .....	38
4.5 SEM image of $\text{NH}_4\text{MPO}_4 \cdot \text{H}_2\text{O}$ powder with M = (a) Co (b) Cu (c) Mg (d) Mn (e) Fe (f) Ni and (g) Zn.....	40
4.6 TEM images with corresponding selected-area electron diffraction (SAED) patterns of the $\text{NH}_4\text{MPO}_4 \cdot \text{H}_2\text{O}$ powder with M = (a) Co (b) Cu (c) Mg (d) Mn .....	42
4.7 TEM images with corresponding selected-area electron diffraction (SAED) patterns of the $\text{NH}_4\text{MPO}_4 \cdot \text{H}_2\text{O}$ powder with M = Fe (e) Ni (f) and Zn (g).....	43

## LIST OF FIGURES (Continued)

Figures	Page
4.8	XANES spectra at the Co K absorption edge for Co foil, CoO and Co <sub>2</sub> O <sub>3</sub> standard and XANES spectra of the NH <sub>4</sub> CoPO <sub>4</sub> ·H <sub>2</sub> O.....45
4.9	XANES spectra at the Cu K absorption edge for Cu foil and CuCl <sub>2</sub> standard and XANES spectra of the NH <sub>4</sub> CuPO <sub>4</sub> ·H <sub>2</sub> O.....46
4.10	XANES spectra at the Fe K absorption edge for Fe foil, FeO and Fe <sub>2</sub> O <sub>3</sub> standard and XANES spectra of the NH <sub>4</sub> FePO <sub>4</sub> ·H <sub>2</sub> O.....47
4.11	XANES spectra at the Mn K absorption edge for Mn foil, MnO, Fe <sub>2</sub> O <sub>3</sub> and MnO standard and XANES spectra of the NH <sub>4</sub> MnPO <sub>4</sub> ·H <sub>2</sub> O.....48
4.12	XANES spectra at the Ni K absorption edge for Ni foil and NiO standard and XANES spectra of the NH <sub>4</sub> NiPO <sub>4</sub> ·6H <sub>2</sub> O.....49
4.13	XANES spectra at the Zn K absorption edge for Zn foil and ZnO standard and XANES spectra of the NH <sub>4</sub> ZnPO <sub>4</sub> .....50
4.14	XANES spectra at the P K absorption edge for P powder and KH <sub>2</sub> PO <sub>4</sub> standard XANES spectra of NH <sub>4</sub> MPO <sub>4</sub> ·H <sub>2</sub> O (M = Mg, Co, Fe, Mn, Ni, Zn, Cu).....51
4.15	XPS spectra of NH <sub>4</sub> MPO <sub>4</sub> ·H <sub>2</sub> O (M = Mg, Co, Fe, Mn, Ni, Zn, Cu) samples with the survey scan mode.....54
4.16	Curve-fitting for N1s and XPS spectra of NH <sub>4</sub> MPO <sub>4</sub> ·H <sub>2</sub> O (M = Mg, Co, Fe, Mn, Ni, Zn, Cu) samples.....55
4.17	Curve-fitting for Co2p, Cu2p, Fe2p, Mg2s, Mn2p, Ni2p, Zn2p and XPS spectra of NH <sub>4</sub> MPO <sub>4</sub> ·H <sub>2</sub> O (M = Mg, Co, Fe, Mn, Ni, Zn, Cu) samples.....56

## LIST OF FIGURES (Continued)

Figures	Page
4.18	Curve-fitting for O1s and XPS spectra of $\text{NH}_4\text{MPO}_4\cdot\text{H}_2\text{O}$ (M = Mg, Co, Fe, Mn, Ni, Zn, Cu) samples.....57
4.19	Curve-fitting for P2p and XPS spectra of $\text{NH}_4\text{MPO}_4\cdot\text{H}_2\text{O}$ (M = Mg, Co, Fe, Mn, Ni, Zn, Cu) samples.....58
4.20	The specific magnetization as a function of field, measured at 20 °C of the $\text{NH}_4\text{MPO}_4\cdot\text{H}_2\text{O}$ (M= Mg, Co, Fe, Mn, Ni, Zn, Cu) powder.....60
4.21	XRD pattern of $\text{NH}_4\text{CoPO}_4\cdot\text{H}_2\text{O}$ powder prepared by chemical precipitation method with (a) water (b) PVP (c) PVA (d) Sucrose and (e) CTAB.....62
4.22	XRD pattern of $\text{NH}_4\text{CuPO}_4\cdot\text{H}_2\text{O}$ powder prepared by chemical precipitation method with (a) water (b) PVP (c) PVA (d) Sucrose and (e) CTAB.....65
4.23	XRD pattern of $\text{NH}_4\text{MgPO}_4\cdot\text{H}_2\text{O}$ powder prepared by chemical precipitation method with (a) water (b) PVP (c) PVA (d) Sucrose and (e) CTAB.....68
4.24	XRD pattern of $\text{NH}_4\text{MnPO}_4\cdot\text{H}_2\text{O}$ powders prepared by chemical precipitation method with (a) water (b) PVP (c) PVA (d) Sucrose and (e) CTAB.....71
4.25	XRD pattern of $\text{NH}_4\text{FePO}_4\cdot\text{H}_2\text{O}$ powders prepared by chemical precipitation method with (a) water (b) PVP (c) PVA (d) Sucrose and (e) CTAB.....74

## LIST OF FIGURES (Continued)

Figures	Page
4.26 XRD pattern of $\text{NH}_4\text{NiPO}_4 \cdot 6\text{H}_2\text{O}$ powders prepared by chemical precipitation method with (a) water (b) PVP (c) PVA (d) Sucrose and (e) CTAB.....	77
4.27 XRD pattern of $\text{NH}_4\text{ZnPO}_4$ powders prepared by chemical precipitation method with (a) water (b) PVP (c) PVA (d) Sucrose and (e) CTAB.....	80
4.28 The possible formation mechanism of $\text{NH}_4\text{ZnPO}_4$ microstructures prepared by using water and polymer sources of PVP, PVA, sucrose and CTAB.....	86
4.29 SEM image of $\text{NH}_4\text{CoPO}_4 \cdot \text{H}_2\text{O}$ powders prepared by chemical precipitation method with (a) water (b) PVP (c) PVA (d) Sucrose and (e) CTAB.....	87
4.30 SEM image of $\text{NH}_4\text{CuPO}_4 \cdot \text{H}_2\text{O}$ powders prepared by chemical precipitation method with (a) water (b) PVP (c) PVA (d) Sucrose and (e) CTAB.....	88
4.31 SEM image of $\text{NH}_4\text{MgPO}_4 \cdot \text{H}_2\text{O}$ powders prepared by chemical precipitation method with (a) water (b) PVP (c) PVA and (d) CTAB.....	89
4.32 SEM image of $\text{NH}_4\text{MnPO}_4 \cdot \text{H}_2\text{O}$ powders prepared by chemical precipitation method with (a) water (b) PVP (c) PVA (d) Sucrose and (e) CTAB.....	90

## LIST OF FIGURES (Continued)

<b>Figures</b>	<b>Page</b>
4.33 SEM image of $\text{NH}_4\text{FePO}_4 \cdot \text{H}_2\text{O}$ powders prepared by chemical precipitation method with (a) water (b) PVP (c) PVA (d) Sucrose and (e) CTAB.....	91
4.34 SEM image of $\text{NH}_4\text{NiPO}_4 \cdot \text{H}_2\text{O}$ powders prepared by chemical precipitation method with (a) water (b) PVP (c) PVA and (d) CTAB.....	92
4.35 SEM image of $\text{NH}_4\text{ZnPO}_4$ powders prepared by chemical precipitation method with (a) water (b) PVP (c) PVA (d) Sucrose and (e) CTAB.....	93
4.36 Co K-edge XANES spectra of $\text{NH}_4\text{CoPO}_4 \cdot \text{H}_2\text{O}$ powder prepared by chemical precipitation method.....	95
4.37 P K-edge XANES spectra of $\text{NH}_4\text{CoPO}_4 \cdot \text{H}_2\text{O}$ powders prepared by chemical precipitation method.....	96
4.38 Cu K-edge XANES spectra of $\text{NH}_4\text{CuPO}_4 \cdot \text{H}_2\text{O}$ powder prepared by chemical precipitation method.....	97
4.39 P K-edge XANES spectra of $\text{NH}_4\text{CuPO}_4 \cdot \text{H}_2\text{O}$ powder prepared by chemical precipitation method.....	98
4.40 Mn K-edge XANES spectra of $\text{NH}_4\text{MnPO}_4 \cdot \text{H}_2\text{O}$ powders prepared by chemical precipitation method.....	99
4.41 P K-edge XANES spectra of $\text{NH}_4\text{MnPO}_4 \cdot \text{H}_2\text{O}$ powders prepared by chemical precipitation method.....	100

## LIST OF FIGURES (Continued)

<b>Figures</b>	<b>Page</b>
4.42 Fe K-edge XANES spectra of $\text{NH}_4\text{FePO}_4\cdot\text{H}_2\text{O}$ powders prepared by chemical precipitation method.....	102
4.43 P K-edge XANES spectra of $\text{NH}_4\text{FePO}_4\cdot\text{H}_2\text{O}$ powders prepared by chemical precipitation method.....	103
4.44 Ni K-edge XANES spectra of $\text{NH}_4\text{NiPO}_4\cdot\text{H}_2\text{O}$ powders prepared by chemical precipitation method.....	104
4.45 P K-edge XANES spectra of $\text{NH}_4\text{NiPO}_4\cdot\text{H}_2\text{O}$ powder prepared by chemical precipitation method.....	105
4.46 Zn K-edge XANES spectra of $\text{NH}_4\text{ZnPO}_4$ powders prepared by chemical precipitation method.....	106
4.47 P K-edge XANES spectra of $\text{NH}_4\text{ZnPO}_4$ powders prepared by chemical precipitation method.....	107
4.48 Curve-fitting for Co2p and XPS spectra of $\text{NH}_4\text{CoPO}_4\cdot\text{H}_2\text{O}$ samples with water, PVP, PVA Sucrose and CTAB.....	109
4.49 Curve-fitting for Cu2p and XPS spectra of $\text{NH}_4\text{CuPO}_4\cdot\text{H}_2\text{O}$ samples with water, PVP, PVA and Sucrose.....	110
4.50 Curve-fitting for Fe2p and XPS spectra of $\text{NH}_4\text{FePO}_4\cdot\text{H}_2\text{O}$ samples with water, PVP, PVA Sucrose and CTAB.....	111
4.51 Curve-fitting for Mg3s and XPS spectra of $\text{NH}_4\text{MgPO}_4\cdot\text{H}_2\text{O}$ samples with water, PVP, PVA Sucrose and CTAB.....	112

## LIST OF FIGURES (Continued)

Figures	Page
4.52 Curve-fitting for Mn2p and XPS spectra of $\text{NH}_4\text{MnPO}_4 \cdot \text{H}_2\text{O}$ samples with water, PVP, PVA Sucrose and CTAB.....	113
4.53 Curve-fitting for Ni2p and XPS spectra of $\text{NH}_4\text{NiPO}_4 \cdot \text{H}_2\text{O}$ samples with water, PVP, PVA Sucrose and CTAB.....	114
4.54 Curve-fitting for Zn2p and XPS spectra of $\text{NH}_4\text{ZnPO}_4$ samples with water, PVP, PVA Sucrose and CTAB.....	115
4.55 Curve-fitting for P2p and XPS spectra of $\text{NH}_4\text{CoPO}_4 \cdot \text{H}_2\text{O}$ samples with water, PVP, PVA Sucrose and CTAB.....	116
4.56 Curve-fitting for P2p and XPS spectra of $\text{NH}_4\text{CuPO}_4 \cdot \text{H}_2\text{O}$ samples with water, PVP, PVA and Sucrose.....	117
4.57 Curve-fitting for P2p and XPS spectra of $\text{NH}_4\text{FePO}_4 \cdot \text{H}_2\text{O}$ samples with water, PVP, PVA Sucrose and CTAB.....	118
4.58 Curve-fitting for P2p and XPS spectra of $\text{NH}_4\text{MgPO}_4 \cdot \text{H}_2\text{O}$ samples with water, PVP, PVA Sucrose and CTAB.....	119
4.59 Curve-fitting for P2p and XPS spectra of $\text{NH}_4\text{MnPO}_4 \cdot \text{H}_2\text{O}$ samples with water, PVP, PVA Sucrose and CTAB.....	120
4.60 Curve-fitting for P2p and XPS spectra of $\text{NH}_4\text{NiPO}_4 \cdot \text{H}_2\text{O}$ samples with water, PVP, PVA Sucrose and CTAB.....	121
4.61 Curve-fitting for P2p and XPS spectra of $\text{NH}_4\text{ZnPO}_4$ samples with water, PVP, PVA Sucrose and CTAB.....	122

## LIST OF ABBREVIATIONS

SEM = Scanning electron microscopy

SAED = Selected area electron diffraction

TEM = Transmission electron microscopy

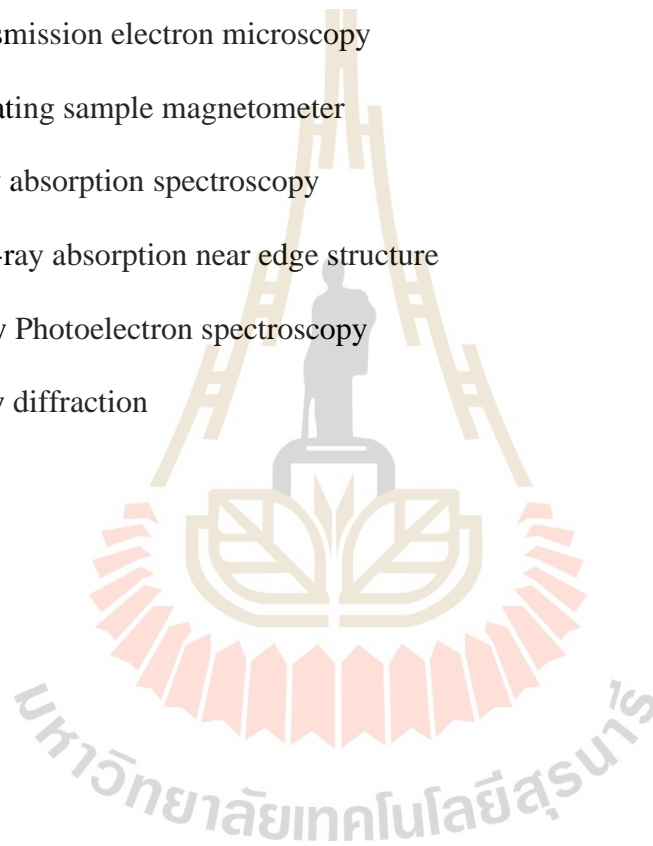
VSM = Vibrating sample magnetometer

XAS = X-ray absorption spectroscopy

XANES = X-ray absorption near edge structure

XPS = X-Ray Photoelectron spectroscopy

XRD = X-ray diffraction



# CHAPTER I

## INTRODUCTION

### 1.1 Background and significance of the study

Agriculture is the backbone of the economic system of most countries supporting the main livelihood of about 75% of the rural population of the developing countries (Mishra, Mishra, Dikshit and Pandey, 2014), which is expected to feed the steadily increasing world population of 9.1 billion by 2050 (FAO, 2012). There is a significantly increasing of the demand for food and residence. While, arable lands diminish due to industrialization, urbanization, desertification and land degradation from human activity (Jie, Jing-zhang, Man-zhi and Zi-tong, 2002). Thus, the decreased agricultural land requires the nutrient load per unit area is steadily increasing. Therefore, this implies that food production will have to be much more intensive and efficient than ever before. Intensive high-yield agriculture is dependent on fertilizer additions, which is intimidating factors threaten global food security and demand modifications to improve agricultural systems. To meet the increasing food demands, the agricultural sector is bound to employ enormous quantities of fertilizers that have thus far demonstrated undesirable environmental impacts. Hence, it is of paramount importance to develop systems that boost production and alleviate environmental problems. Controlled release fertilizers and slow release fertilizers may be one solution, which are believed to enhance crop yield while reducing the environmental pollution of the hazardous emissions such as  $\text{NH}_3$ ,  $\text{N}_2\text{O}$  etc. from current fertilizer applications (Azeem, KuShaari, Man, Basit and Thanh, 2014).

Fertilizers can be defined as organic or inorganic materials, which are applied to the soil and it is provided as essential nutrients for growing plants by absorption through the plant roots. They are used to supplement the natural soil nutrients, to compensate for nutrients lost by the harvesting of crops, leaching or gaseous exchange, and to maintain or improve the fertility of the soil (Park, 2001). The main fertilizer products include Nitrogen, Phosphate and Potash. The ion transition metals such as copper (Cu), iron (Fe), manganese (Mn) and zinc (Zn) are micronutrient, which is involved in all metabolic and cellular functions (Hänsch and Mendel, 2009). The metal ammonium phosphate is controlled release fertilizers because it has low solubility compounds (Azeem et al., 2014). The metal ions are well micronutrient in the plants but they are required in much smaller amounts than those of the primary nutrients such as nitrogen, phosphorus, sulfur, and potassium (Hänsch and Mendel, 2009). However, the metal ions are easily oxidized in the ambient environment. Recently, the metal ammonium phosphates can be released a metal ion by dissolving in the phosphate buffer saline system and this system can prevent oxidation of metal ion (Li et al., 2014). Thus, this system can apply as a long-term foliar fertilizer.

In this work, we focus on the synthesis of ammonium metal phosphate  $\text{NH}_4\text{MPO}_4 \cdot \text{H}_2\text{O}$  ( $M = \text{Mg, Co, Fe, Mn, Ni, Zn, and Cu}$ ) by a using precipitation technique in order to study the structure to potentially apply for the controlled release fertilizers. In this research, the synthesis, structural and ions release properties of the ammonium metal phosphate are investigated by various techniques including thermogravimetric analysis (TGA), differential scanning calorimetric method (DSC), scanning electron microscopy (SEM), transmission electron microscopy (TEM), X-ray diffraction (XRD), fourier transform infrared spectroscopy (FTIR), X-ray

photoelectron spectroscopy (XPS) and X-ray absorption spectroscopy (XAS). The effects of metal in the structure on the ions release properties of the ammonium metal phosphates are investigated and discussed.

## **1.2 Research objectives / Purpose of the study**

1.2.1 To synthesize ammonium metal phosphate  $\text{NH}_4\text{MPO}_4\cdot\text{H}_2\text{O}$  ( $\text{M} = \text{Mg}, \text{Co}, \text{Fe}, \text{Mn}, \text{Ni}, \text{Zn}, \text{Cu}$ ) by precipitation technique.

1.2.2 To study the effect of polymer and surfactant on the structure and morphology of ammonium metal phosphate.

1.2.3 To characterize the synthesized ammonium metal phosphate by thermogravimetric analysis (TGA), differential scanning calorimetric method (DSC), scanning electron microscopy (SEM), transmission electron microscopy (TEM), X-ray diffraction (XRD), ultraviolet-visible spectroscopy (UV-VIS), X-ray absorption spectroscopy (XAS), ion release measurement and X-ray photoelectron spectroscopy (XPS).

## **1.3 Scope and limitations**

1.3.1 This study focuses on the synthesis of the ammonium metal phosphate  $\text{NH}_4\text{MPO}_4\cdot\text{H}_2\text{O}$  ( $\text{M} = \text{Mg}, \text{Co}, \text{Fe}, \text{Mn}, \text{Ni}, \text{Zn}, \text{Cu}$ ) by precipitation route.

1.3.2 The morphology, the microstructure, and the ions release performance of the metal ammonium phosphates are investigated.

## **1.4 Location of the research**

Advanced Materials Physics Laboratory (AMP), School of Physics, Institute of Science, Suranaree University of Technology, Nakhon Ratchasima, Thailand

## 1.5 Expected results

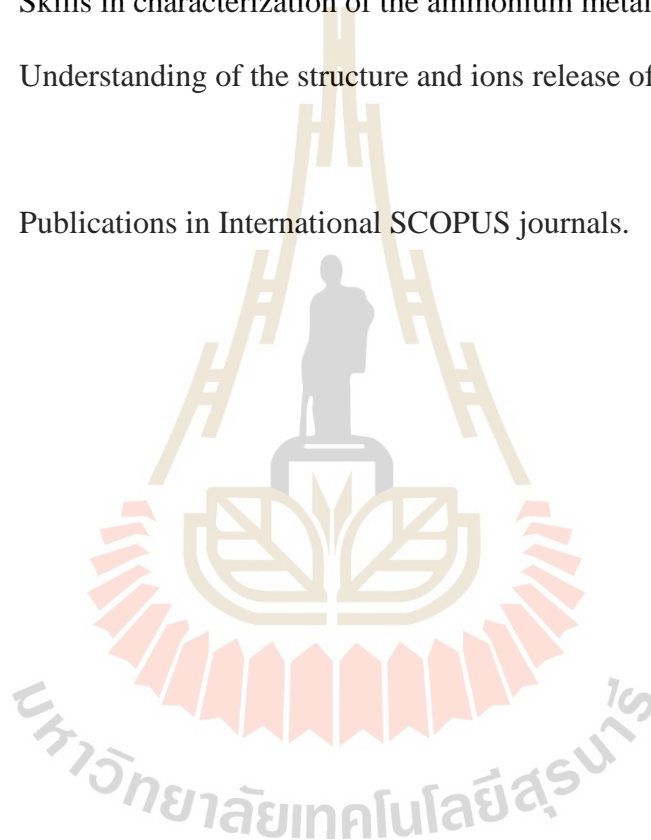
1.5.1 Understanding of the effects of ammonium metal phosphate on the ions release properties of the fabricated ammonium metal phosphate.

1.5.2 Achievable and skills in fabrication of ammonium metal phosphate  $\text{NH}_4\text{MPO}_4 \cdot \text{H}_2\text{O}$  ( $M = \text{Mg}, \text{Co}, \text{Fe}, \text{Mn}, \text{Ni}, \text{Zn}, \text{Cu}$ ).

1.5.3 Skills in characterization of the ammonium metal phosphate.

1.5.4 Understanding of the structure and ions release of the ammonium metal phosphate.

1.5.5 Publications in International SCOPUS journals.



## **CHAPTER II**

### **LITERATURE REVIEW**

The chapter II reviews the literature on the structure, preparation, and potential applications of ammonium metal phosphate materials.

#### **2.1 Fertilizers and importance**

In modern agricultural systems or in developing countries with rapidly growing populations, fertilizers are essential for maintaining or improving agricultural output. The Food and Agriculture Organization (FAO) through its worldwide fertilizer program has shown the enormous contribution that fertilizer can make to increasing food output although the response varies from site to site. For each kg of nutrient is applied in approximately 10 kg of grain are produced. The importance of fertilizers in world food production was given more recently in detailed estimates of the nitrogen cycle and nitrogen flows. Moreover, it is expected that roughly 40% of the world's dietary protein in the mid-1990s was derived from synthetic ammonia and fertilizers (Park, 2001). Although modern fertilizers are products of the chemical industry but most fertilizers such as ammonium sulphate, urea, ammonium nitrate, single or triple superphosphate and potash are all relatively simple inorganic chemicals, which occur naturally in the environment. Single superphosphate is a simple product made from ground phosphate rock which has been digested with sulphuric acid, which widely

used in the chemical industry but it also occurs in nature, in the atmosphere as a result of burning fossil fuels and also in areas subject to volcanic activity.

Fertilizer nutrients are usually defined as primary, secondary and micro-nutrients. The primary nutrients are required by plants in relatively large quantities, are nitrogen (N), phosphorus (P) and potassium (K). Secondary nutrients are calcium, magnesium, sodium and sulphur. There are numerous micro-nutrients but the main ones are iron, zinc, copper, manganese, boron and molybdenum. It is important to note that a deficiency of any nutrient will lead to the poor yield. So that the distinction between primary, secondary and micro- only refers to the amounts taken up by the crop, which does not in any way mean that some are less important than others and can be ignored. They are all important and each needs to be balanced one against the other.

Normally, there are two types of fertilizer: natural fertilizer and chemical fertilizer. The term 'natural' fertilizer usually refers to products such as farmyard manure (FYM) and other organic materials such as farm slurry, chicken manure, green manures, blood and bone meal and compost. Plants absorb nutrients in a simple inorganic form, which are indifferent as to whether they originate from an organic or inorganic fertilizer. However, there are some significant differences between the two types and some of the key features of natural fertilizers are that:

- They are bulky and difficult to handle. FYM and slurry have a high-water content and low nutrient content.
- They provide organic matter which aids soil structure.
- They are slow-release fertilizers and contain micro-nutrients.
- They are usually the expensive per unit of plant food if delivered off-farm.

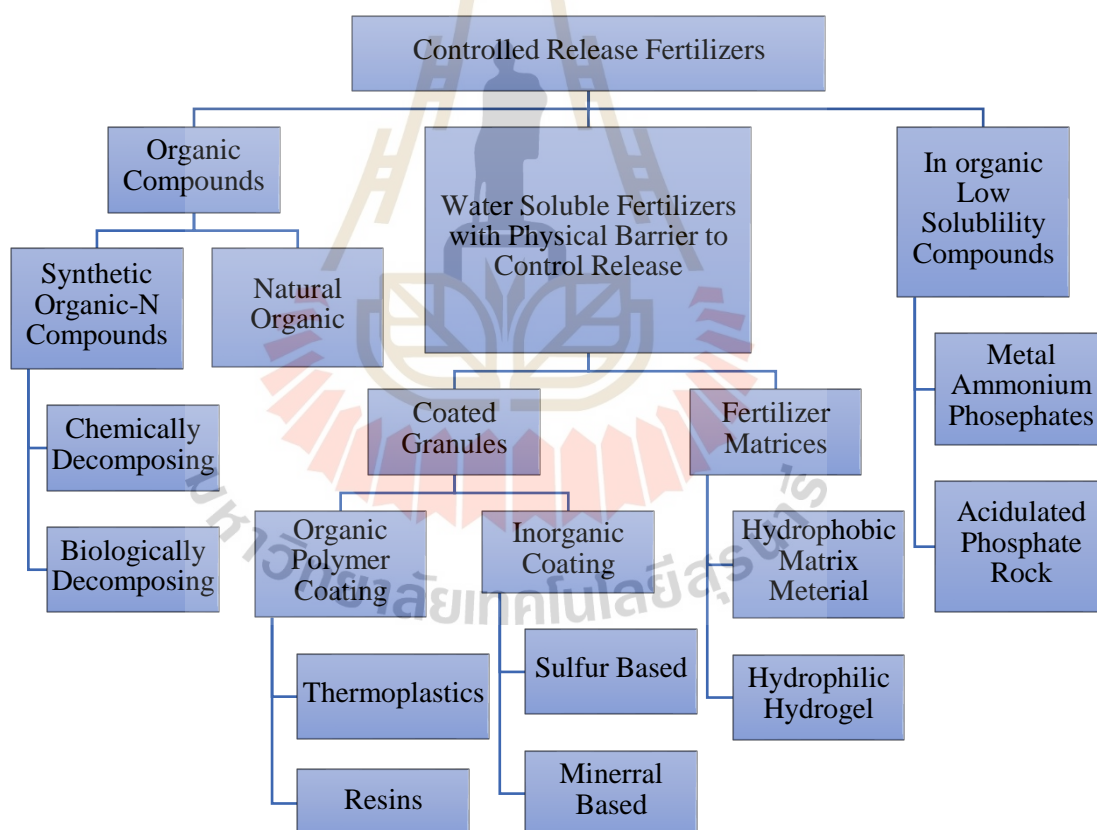
Some of the key features of chemical fertilizers are that:

- They are highly concentrated and easy to handle but they do not usually provide any organic matter.
- Nutrients are usually released quickly although there are special slow-release formulations. The most concentrated fertilizers such as urea and diammonium phosphate do not contain micronutrients. Traditional fertilizers such as single superphosphate do not contain secondary and micro-nutrients.
- Fertilizers can be formulated for specific soil and crop conditions and specific micro-nutrients can be added as required.
- They are relatively cheap per unit plant food delivered.

## 2.2 Controlled release fertilizer

Controlled release fertilizer (CRF) is a purposely designed manure that releases active fertilizing nutrients in a controlled, delayed manner in synchrony with the sequential needs of plants for nutrients. Thus, they provide enhanced nutrient use efficiency along with enhanced yields. An ideal controlled release fertilizer is coated with a natural or semi-natural, environmentally friendly macromolecule material that retards fertilizer release to such a slow pace that a single application to the soil can meet nutrient requirements for model crop growth. The terms, controlled release fertilizer (CRF) and slow release fertilizer (SRF) are generally considered analogous. Nevertheless, the terms of them can defined differences between both. In the case of SRFs, the pattern of nutrient release is nearly unpredictable and remains subject to changes in soil type and climatic conditions. To the contrary, the pattern, quantity and time of release can be predicted within limits for CRFs. However, in this study, we use

the term “Controlled release fertilizers” (CRFs) for both types. A literature review reveals that the history of CRFs' development and evolution has roots in the early 1960's. Initially, sulfur and polyethylene were used as coating materials in the preparation of SRFs. This journey eventually included numerous polymer materials, natural coating agents, multifunctional super-absorbent materials, and even nano-composites. Many of the CRFs have also been prepared on commercial scale so far. The CRFs have been classified in a diverse manner according to the literature as shown in figure. 1 (Azeem et al., 2014).



**Figure 2.1** Schematic for classification of controlled release fertilizers. (Adapted from (Azeem et al., 2014))

A comprehensive classification has been based on the opinions as portrayed in figure 1. The CRFs were classified into three major categories:

The first, organic compounds that are further sub-divided to natural organic compounds (animal manure, sewage sludge etc.) and synthetically produced organic-nitrogen, low solubility compounds. The latter group generally includes condensation products from urea and acetaldehyde. These compounds are further subdivided into biologically decomposing compounds, e.g. urea formaldehyde (UF), and chemically decomposing compounds such as isobutylidene-diurea (IBDU) or urea acetaldehyde/cyclo diurea (CDU).

The second major category includes renowned water-soluble fertilizers with physical barriers that control nutrient release. These appear either as granules/cores coated with a hydrophobic polymer, or as a matrix of active fertilizer nutrients dispersed on a continuum via hydrophobic material that encumbers fertilizer dissolution. However, controlled release matrices are less common compared to coated CRFs, which is why this paper is focused on controlled release coated fertilizer that contain only urea. Coated granular CRFs are subcategorized to those coated with organic polymer materials (e.g. thermoplastics, resins etc.) and those coated with inorganic materials (including sulfur and other minerals). The controlled release matrix material can be either hydrophobic e.g. polyolefin, rubber etc., or gel forming polymers sometimes referred to as a hydrogel. A hydrogel is hydrophilic and the dissolution of fertilizer dispersed through hydrogel material impeded by its ability to retain high amounts of water (swelling).

Lastly, inorganic low solubility compounds that include ammonium metal phosphates e.g.  $\text{NH}_4\text{KPO}_4$  and  $\text{NH}_4\text{MgPO}_4$ , and partially acidulated phosphate rock (PAPR).

A classification of CRFs can also be based on the mode of control release, i.e. diffusion, erosion or chemical reaction, swelling and osmosis. However, The CRFs is classified as two major types: those coated with low solubility compounds and those coated with water soluble materials.

Phosphates are materials containing oxoanions of phosphorus (V), ranging from the simple orthophosphate group  $\text{PO}_4^{3-}$  through ring and chain anions to infinite networks. Oxoanions of phosphorus in lower oxidation states such as phosphite,  $\text{HPO}_4^{3-}$  are also known. Many solid phosphates have been prepared or are found as minerals. Their diversity results from variations in the phosphate species, the large number of cations to which they may be coordinated, and the presence of other anions or molecules, notably  $\text{H}_2\text{O}$ . Their chemistry and properties are similar to those of solid silicates (Attfield, 2001).

Solid phosphates are conveniently classified according to the anions they contain. Orthophosphates contain isolated phosphate tetrahedrons, but these can also be linked through P–O–P bridges to give a range of condensed phosphate anions.

The orthophosphate (often shortened to “phosphate”) group,  $\text{PO}_4^{3-}$ , is the most common phosphorus oxoanion. All four oxygen atoms are usually coordinated to cations in solid orthophosphates leading to strongly bonded, extended structures. The acid orthophosphate anions hydrogen phosphate,  $\text{HPO}_4^{2-}$ , and dihydrogen phosphate,  $\text{H}_2\text{PO}_4^-$ , are also found in many materials. Almost every metallic element forms an orthophosphate, and a range of oxidation states is stabilized for transition elements,

e.g., from  $V^{II}$  to  $V^V$  in  $NaV^{II}V^{III}_2(PO_4)_3$ ,  $V^{III}PO_4$ ,  $V^{IV}O(H_2PO_4)$ , and  $V^VOPO_4$ . Mixed anion orthophosphates are sometimes found, e.g.,  $Ca_2(PO_4)F$ ,  $Fe_2(PO_4)O$ ,  $LiMn(PO_4)(OH)$ , and  $Ca_5(PO_4)_2(SiO_2)$ . Solid solutions in which the orthophosphate group is partially substituted by orthoarsenate, vanadate, and silicate groups further extend the range of possible phases.

The diphosphate anion,  $P_2O_7^{4-}$ , consists of two phosphate tetrahedrons linked through a common oxygen atom. This bridging oxygen does not coordinate even to highly charged cations. Diphosphates are also known as “pyrophosphates” as they often result from thermal treatment of orthophosphates. Many diphosphates are known and variations in composition and structure are similar to those for the orthophosphates.

Linking phosphate tetrahedrons into chains through two vertices results in polyphosphate anions,  $P_nO_{3n+1}^{(n+2)-}$ , also known as oligophosphates. Finite chains containing up to six tetrahedrons have been found in the solid state. They become less common with increasing  $n$ . Cyclophosphates (cyclopolyphosphates),  $P_nO_{3n}^{n-}$ , contain rings of up to 12 tetrahedrons, but those with three, four, and six units are most common. Infinite chain catenaphosphates,  $(PO_3^-)_n$ , are formed at high temperatures. Polyphosphates sometimes adopt layered structures which can intercalate molecules in the interlamellar spaces, e.g., organic amines are intercalated by the triphosphates  $MH_2P_3O_{10} \cdot 2H_2O$  ( $M=Al, Cr, Mn, Fe$ ).

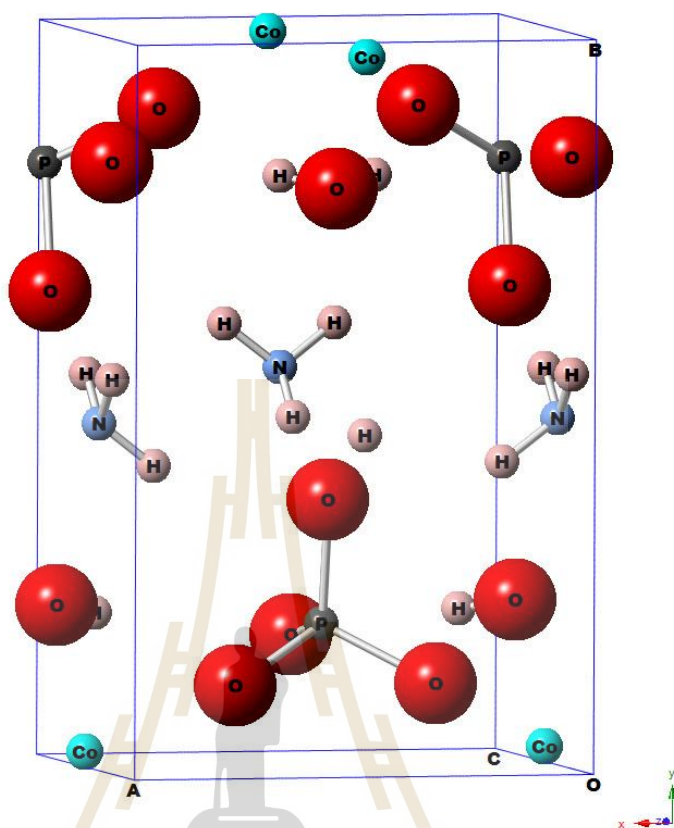
These contain two- and three-connected phosphate tetrahedrons and have stoichiometries  $P_nO_{3n-1}^{(n-2)-}$ , where  $n = 4, 5, 6, \text{ and } 8$ . The unique cage phosphate anion  $P_8O_{23}^{6-}$  is the only example of a molecular ultraphosphate anion. The other species form infinite framework anions in which charge-compensating cations reside. Ultraphosphates are anhydrous, as the P–O–P bridges between three-connected

phosphate tetrahedrons are susceptible to hydrolysis. The lanthanide ultraphosphates  $MP_5O_{14}$  are notable laser materials.

### 2.3 Ammonium/transition metal phosphates

Ammonium/transition metal phosphates  $NH_4MPO_4 \cdot H_2O$  (M)  $Mn^{2+}$ ,  $Fe^{2+}$ ,  $Co^{2+}$ ,  $Ni^{2+}$ ,  $Cu^{2+}$ ,  $Zn^{2+}$ ) have been investigated for over 50 years and have been widely applied as fertilizers, pigments for paint finishes for protection of metal, and fire retardants in paints or plastics (Yuan et al., 2008). Ammonium phosphates of general formula  $NH_4M(II)PO_4 \cdot H_2O$  were first described in 1864 by Debray (Debray, 1864). They are a good source for macro- and micronutrients (P, N, Fe, Mn, Co, Cu, Zn) required by plants (Bridger, Salutsky and Starostka, 1962). Also, they show good flammability retarding performance both in the gas phase and in the condensed phase as a combined flame retardant. Recently, more attention has been paid to potential applications in ionic conductivity and catalyst and ionic exchange of these dittmarite-type compounds with a layered or tunnel structure (Lapina, 1968, Yuan et al., 2008).

The  $NH_4MPO_4 \cdot H_2O$  (M)  $Mn^{2+}$ ,  $Fe^{2+}$ ,  $Co^{2+}$ ,  $Ni^{2+}$ ,  $Cu^{2+}$ ,  $Zn^{2+}$ ) have orthorhombic structure and has many space groups such as  $PZ1/a$ ,  $Pmnm$  and  $Pmm2_1$  (Yuan et al., 2008, Wenwei, Yanjin, Xuehang, Sen and Shushu, 2009). The figure 2.2 show representation of structure of  $NH_4CoPO_4 \cdot H_2O$ .



**Figure 2.2** The structure of  $\text{NH}_4\text{CoPO}_4 \cdot \text{H}_2\text{O}$  (Adapted from ICSD 28-0044).

## 2.4 Preparation of ammonium transition metal phosphates

Normally, the nanostructures can be synthesized by various techniques such as sol-gel, hydrothermal, solid-state reaction and co-precipitation methods. The growth rates of the size and morphology can be determined by intermolecular interactions of atoms in the compound such as solvent, the permanence of compound, type of materials and degree of supersaturating (Byrappa et al., 2007, Pang et al., 2012). Recently, many researchers studied the synthesis of ammonium metal phosphate to obtain the desired shape/structure and investigated the properties of them. The solid-state reaction method has been employed to synthesize ammonium metal phosphates. For example,  $\text{NH}_4\text{FePO}_4 \cdot \text{H}_2\text{O}$  nano-plates with thickness of 40–50 nm were synthesized via solid-

state reaction at low temperature and its thermochemistry properties are reported in Yuan et al. (2008). The single phase  $\text{NH}_4\text{NiPO}_4 \cdot 6\text{H}_2\text{O}$  was synthesized by solid-state reaction at room temperature. It can be seen that the  $\text{NH}_4\text{NiPO}_4 \cdot 6\text{H}_2\text{O}$  sample illustrated uniform polyhedral grains, which contains particles having a distribution of small particles (100-200 nm) and large particles ( $> 200$ -800 nm) (Wu, Li, Wu, Liao and Cao, 2010). Yuan et al. (2008) reported that the solid-state reaction at low temperature can be used to prepare the ammonium/transition metal phosphate monohydrate  $\text{NH}_4\text{MPO}_4 \cdot \text{H}_2\text{O}$  ( $\text{M} = \text{Mn}^{2+}, \text{Co}^{2+}, \text{Ni}^{2+}, \text{Cu}^{2+}$ ) compounds, and the thermochemistry properties of them were investigated in this research (Yuan et al., 2008). Likewise, the solid-state reaction method was used to synthesize the  $\text{NH}_4\text{MnPO}_4 \cdot \text{H}_2\text{O}$  particles with layered structure (Wenwei, Yanjin, Xuehang, Sen and Shushu, 2009). In addition, many researchers reported the synthesis of ammonium metal phosphate by hydrothermal method. Barros et al. (2006) reported that the  $\text{NH}_4\text{FePO}_4 \cdot \text{H}_2\text{O}$  was prepared by the hydrothermal method to be applied on soils to prevent iron deficiencies. It is found that the synthetic material had a microplate size of approximately 10 micrometers. The  $\text{NH}_4[\text{Co}_{1-x}\text{Ni}_x\text{PO}_4] \cdot \text{H}_2\text{O}$  ( $x = 0, 0.34, 0.59, 0.7, 1$ ) microplate was prepared by the hydrothermal method which exhibit the antiferromagnetic behavior with ordering temperatures from 5.5 K ( $x = 0.00$ ) up to 13.2 K ( $x = 1.00$ ) as reported by Torre-Fernández et al. (2013). The Co/Ni ammonium phosphate hydrates  $\text{NH}_4[\text{Co}_{1-x}\text{Ni}_x\text{PO}_4] \cdot \text{H}_2\text{O}$ , where  $x = 0.00, 0.25, 0.50, 0.75, \text{ and } 1.00$ ) nanocrystallites were synthesized by a facile hydrothermal method. The results display the largest specific surface area,  $8.39 \text{ m}^2 \text{ g}^{-1}$ , and total pore volume,  $0.069 \text{ cm}^3 \text{ g}^{-1}$ , in the  $x = 0.50$  sample leading to a good electrochemical properties (Wannasen, Chanlek, Maensiri and Swatsitang, 2019). In

the same way, the hydrothermal method was used to synthesize the ammonium/transition metal phosphates such as 3D flower-like  $\text{NH}_4\text{NiPO}_4$  (Wang, Jian, Xiao and Huang, 2018),  $\text{NH}_4\text{CuPO}_4 \cdot \text{H}_2\text{O}$  powder (Karaphun, Chirawatkul, Maensiri and Swatsitang, 2018),  $\text{NH}_4\text{CuPO}_4 \cdot \text{H}_2\text{O}$  microbundles (Wang et al., 2014), and  $\text{NH}_4\text{NiPO}_4 \cdot \text{H}_2\text{O}/\text{Ni}$  foam materials (Chen et al., 2016). Moreover, the precipitation and co-precipitation method were employed to synthesize ammonium metal phosphates such as  $\text{NH}_4\text{MnPO}_4 \cdot \text{H}_2\text{O}$  (Sronsri, Noisong and Danvirutai, 2014),  $\text{NH}_4\text{CoPO}_4 \cdot \text{H}_2\text{O}$  (Pang et al., 2013). The  $\text{NH}_4\text{CoPO}_4 \cdot \text{H}_2\text{O}$  nano-microparticles with the size ranging from 200-4000 nm can be achieved by a simple co-precipitation method in ethylene glycol solvent (Pang et al., 2012). The synthesis method, morphologies, and interesting properties of ammonium metal phosphate are summarized in Table 2.1.

Among these methods, the precipitation method is commonly used to prepare the nanomaterials where the size and shape can be controlled by varying the amount and type of solvent. Hence, the precipitation method is selected for synthesis of the  $\text{NH}_4\text{MPO}_4 \cdot \text{H}_2\text{O}$  ( $M = \text{Mg}, \text{Co}, \text{Fe}, \text{Mn}, \text{Ni}, \text{Zn}, \text{Cu}$ ) in this research.

**Table 2.1** Summary of ammonium metal phosphate prepared by different synthesis methods.

Material	Synthesis method	Morphologies	Interest properties	References
NH <sub>4</sub> FePO <sub>4</sub> ·H <sub>2</sub> O	Solid-state reaction	Nano-plates 40–50 nm	Standard molar formation enthalpy at 298.15 K is $\Delta_f H_m^\circ [\text{NH}_4\text{FePO}_4\cdot\text{H}_2\text{O}(\text{s})] = -1774.92 \pm 0.39 \text{ kJ mol}^{-1}$ .	(Yuan et al., 2008)
NH <sub>4</sub> NiPO <sub>4</sub> ·6H <sub>2</sub> O	Solid-state reaction	Platelets 100-800 nm	NH <sub>4</sub> NiPO <sub>4</sub> ·6H <sub>2</sub> O is thermodynamically more stable than NH <sub>4</sub> NiPO <sub>4</sub> ·H <sub>2</sub> O at room temperature.	(Wu et al., 2010)
NH <sub>4</sub> MPO <sub>4</sub> ·H <sub>2</sub> O (M = Mn <sup>2+</sup> , Co <sup>2+</sup> , Ni <sup>2+</sup> , Cu <sup>2+</sup> )	Solid-state reaction	-	The Standard formation enthalpies of these phosphates increase with a decrease in the ionic radius of 3d-transition metal.	(Yuan et al., 2008)
NH <sub>4</sub> MnPO <sub>4</sub> ·H <sub>2</sub> O	Solid-state reaction	Platelets	The compound has ferrimagnetic properties.	(Wenwei et al., 2009)

**Table 2.1** Summary of ammonium metal phosphate prepared by different synthesis methods (Continued).

Material	Synthesis method	Morphologies	Interest properties	References
$\text{NH}_4\text{FePO}_4\cdot\text{H}_2\text{O}$	Hydrothermal	Microplates	Increasing of the $\text{NH}_4\text{FePO}_4\cdot\text{H}_2\text{O}$ (AIP) on soil leads to a less efficient metabolism, probably due microbial competition for the nitrogen source provided by the AIP and for the carbon source.	(Barros et al., 2006)
$\text{NH}_4[\text{Co}_{1-x}\text{Ni}_x\text{PO}_4]\cdot\text{H}_2\text{O}$ (x = 0, 0.34, 0.59, 0.7, 1)	Hydrothermal	Microplates	The compound Show antiferromagnetic behaviour, with ordering temperatures from 5.5 K (x= 0) up to 13.2 K (x = 1)	(Torre-Fernández et al., 2013)
$\text{NH}_4[\text{Co}_{1-x}\text{Ni}_x\text{PO}_4]\cdot\text{H}_2\text{O}$	Hydrothermal	Microplates	At x=0.05, highest specific capacitance , 540 F g <sup>-1</sup> at 0.5 A g <sup>-1</sup>	(Wannasen et al., 2019).
$\text{NH}_4\text{NiPO}_4$	Hydrothermal	3D flower-like	Show excellent electrochemical properties	(Wang et al., 2018)

**Table 2.1** Summary of Ammonium metal phosphate prepared by different synthesis methods (Continued).

Material	Synthesis method	Morphologies	Intertest properties	References
$\text{NH}_4\text{CuPO}_4 \cdot \text{H}_2\text{O}$	Hydrothermal	Particle sizes of 0.186 to 0.563 $\mu\text{m}$	The highest $C_{\text{sc}} = 297.521 \text{ F g}^{-1}$ at $1 \text{ A g}^{-1}$ with a good cycling stability of 94.04% after 1000 cycle.	(Karaphun et al., 2018)
$\text{NH}_4\text{CuPO}_4 \cdot \text{H}_2\text{O}$	Hydrothermal	Microbundles composed of many microrods (~50 nm)	$\text{NH}_4\text{CuPO}_4 \cdot \text{H}_2\text{O}$ microbundle electrodes show $C_{\text{sc}}$ of $662 \text{ F g}^{-1}$ at $1.5 \text{ A g}^{-1}$ and $520 \text{ F g}^{-1}$ at $15 \text{ A g}^{-1}$ with excellent cycling performance of 92.7% of initial specific capacitance after 3000 cycles).	(Wang et al., 2014)
$\text{NH}_4\text{NiPO}_4 \cdot \text{H}_2\text{O}$ /Ni foam	Hydrothermal	Nanoplate 100-150 nm	Asymmetric supercapacitor, $\text{NH}_4\text{NiPO}_4 \cdot \text{H}_2\text{O}$ @PPy/Ni foam as a positive electrode and AC as a negative electrode produced a $C_{\text{sc}}$ of $133 \text{ F g}^{-1}$ at $0.5 \text{ A g}^{-1}$ .	(Chen et al., 2016)

**Table 2.1** Summary of ammonium metal phosphate prepared by different synthesis methods (Continued).

Material	Synthesis method	Morphologies	Interest properties	References
$\text{NH}_4\text{CoPO}_4 \cdot \text{H}_2\text{O}$	Nano/micromaterials	Precipitation	<p><math>\text{Co}_2\text{P}_2\text{O}_7</math> that obtained by thermal decomposition of the <math>\text{NH}_4\text{CoPO}_4 \cdot \text{H}_2\text{O}</math> nano/microstructures have a good specific capacitance (<math>367 \text{ F g}^{-1}</math>) and a good cycle life (96.2 % at <math>0.625 \text{ A g}^{-1}</math> after 3,000 cycles).</p>	(Pang et al., 2013)
$\text{NH}_4\text{CoPO}_4 \cdot \text{H}_2\text{O}$	Nano-microparticle 200-4000 nm	Co-precipitation	<p>The <math>C_{sc}</math> of <math>\text{NH}_4\text{CoPO}_4 \cdot \text{H}_2\text{O}</math> electrode is up to <math>369.4 \text{ F g}^{-1}</math> at <math>0.625 \text{ A g}^{-1}</math> and exhibits a long cycle life 99.7% of initial specific capacitance after 400 cycles.</p>	(Pang et al., 2012).

## CHAPTER III

### RESEARCH METHODOLOGY

Chapter III describes the experimental procedure of the research, which consists of synthesis, materials characterization by using various techniques, the measurement of magnetic properties and the ion releases measurement of ammonium metal phosphate  $\text{NH}_4\text{MPO}_4 \cdot \text{H}_2\text{O}$  ( $\text{M} = \text{Mg}, \text{Co}, \text{Fe}, \text{Mn}, \text{Ni}, \text{Zn}, \text{Cu}$ ).

#### 3.1 Materials

The materials used in this research are listed by

- 3.1.1 Deionized water.
- 3.1.2 Polyvinyl alcohol (PVA, Mw 89,000-98,00, Sigma-Aldrich, Germany).
- 3.1.3 Hexadecyl trimethylammonium bromide (CTAB, Sigma-Aldrich, Germany).
- 3.1.4 Sucrose. ( $\text{C}_{12}\text{H}_{22}\text{O}_{11}$ , APS, Germany)
- 3.1.5 Polyvinyl pyrrolidone (PVP, Mw 1,300,000, Sigma-Aldrich, Germany).
- 3.1.6 Nickel (II) chloride hexahydrate ( $\text{NiCl}_2 \cdot 6\text{H}_2\text{O}$ ), Sigma-Aldrich, Germany).
- 3.1.7 Copper (II) chloride dihydrate ( $\text{CuCl}_2 \cdot 2\text{H}_2\text{O}$ ), Sigma-Aldrich, Germany).

- 3.1.8 Cobalt (II) chloride hexahydrate ( $\text{CoCl}_2 \cdot 6\text{H}_2\text{O}$ ), Sigma-Aldrich, Germany).
- 3.1.9 Manganese (II) chloride tetrahydrate ( $\text{MnCl}_2 \cdot 4\text{H}_2\text{O}$ ), Sigma-Aldrich, Germany)
- 3.1.10 Magnesium (II) chloride hexahydrate ( $\text{MgCl}_2 \cdot 6\text{H}_2\text{O}$ ), Sigma-Aldrich, Germany).
- 3.1.11 Iron (II) chloride tetrahydrate ( $\text{FeCl}_2 \cdot 4\text{H}_2\text{O}$ ), Sigma-Aldrich, Germany).
- 3.1.12 Zinc (II) chloride ( $\text{ZnCl}_2$ ) Sigma-Aldrich, Germany).
- 3.1.13 Phosphoric acid solution ( $\text{H}_3\text{PO}_4$ , 85%, Sigma-Aldrich, Germany).
- 3.1.14 Ammonia solution ( $\text{NH}_4\text{OH}$ , 25%, Merck, Germany).
- 3.1.15 Beaker 250 ml.
- 3.1.16 Magnetic bar 5 cm.

## 3.2 Instrumentation

- 3.2.1 Scanning electron microscope (SEM, Carl Zeiss Auriga, USA)
- 3.2.2 Transmission electron microscope (TEM, Tecnai G2 s-twin, USA)
- 3.2.3 X-ray diffraction (XRD, Bruker D8 Advance,)
- 3.2.4 Thermogravimetric analysis and differential scanning calorimetric method (TGA-DSC, Mettler)
- 3.2.5 X-ray photoelectron spectroscopy (XPS, Beamline5, SUT-NANOTech-SLIR, Thailand)
- 3.2.6 X-ray absorption spectroscopy (XAS, Beamline5, SUT-NANOTech-SLIR, Thailand)

3.2.7 Fourier transform infrared spectroscopy (FT-IR, Tensor 27, USA)

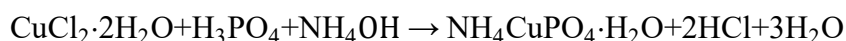
3.2.8 Ultraviolet–visible spectroscopy (UV-Vis, Cary 300, USA)

3.2.9 Inductively couple plasma optical emission spectrometer (ICP-OES Agilent technologies 7500CE, USA)

### **3.3 Synthesis of ammonium metal phosphate $\text{NH}_4\text{MPO}_4\cdot\text{H}_2\text{O}$ (M = Mg, Co, Fe, Mn, Ni, Zn, Cu).**

This work used a simple precipitation method which was a modified simple solution method (Maensiri, Masingboon, Boonchom and Seraphin, 2007) to prepare  $\text{NH}_4\text{MPO}_4\cdot\text{H}_2\text{O}$  (M = Mg, Co, Fe, Mn, Ni, Zn, Cu) at room temperature with different of surfactants such as Polyvinylpyrrolidone (PVP), polyvinyl alcohol (PVA), Sucrose and Hexadecyl trimethylammonium bromide (CTAB). In a typical procedure, 5% by weight of polymer was first mixed with 100 ml of deionized water under vigorous stirring at 300 K until the homogeneous solution was obtained. Water, PVP, PVA, Sucrose and CTAB were used as the polymer source. Nickel (II) chloride hexahydrate ( $\text{NiCl}_2\cdot 6\text{H}_2\text{O}$ ), copper (II) chloride dihydrate ( $\text{CuCl}_2\cdot 2\text{H}_2\text{O}$ ), cobalt (II) chloride hexahydrate ( $\text{CoCl}_2\cdot 6\text{H}_2\text{O}$ ), manganese (II) chloride tetrahydrate ( $\text{MnCl}_2\cdot 4\text{H}_2\text{O}$ ), magnesium (II) chloride hexahydrate ( $\text{MgCl}_2\cdot 6\text{H}_2\text{O}$ ), iron (II) chloride tetrahydrate ( $\text{FeCl}_2\cdot 4\text{H}_2\text{O}$ ) and zinc (II) chloride ( $\text{ZnCl}_2$ ) were used as the metal sources. The metal sources (20 mmol) and phosphoric acid solution (70 wt%, 3 mL) were dissolved in deionized water (50 mL) to form a clear solution. The mixed solution was precipitated by adding ammonium solution (25%) under vigorous stirring until a pH ~ 7. The precipitates were washed several times by deionized water and ethanol. After that the

samples were dried at 70 °C in air. An example of the chemical reaction involved in this process can be described as follows:



The prepared products were characterized by XRD, SEM, TEM, VSM, XAS, XPS, and ions release techniques.

### **3.4 Morphological characterization of ammonium metal phosphate**

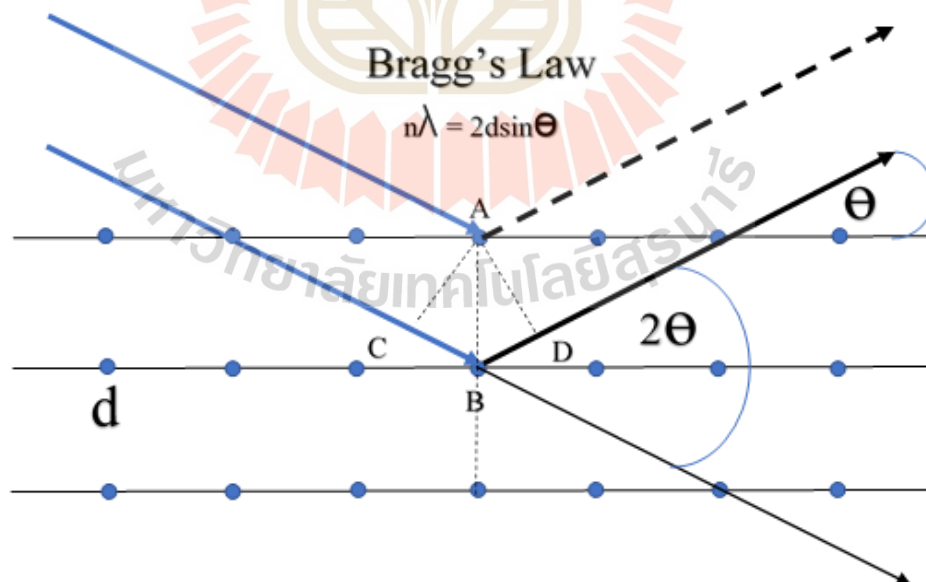
Morphology and microstructure of the synthesized ammonium metal phosphates will be investigated by SEM and TEM techniques. Scanning electron microscopy (SEM) is a powerful technique for materials examination. A high-energy beam of electrons is focused on the surface of the specimen and which then generates a variety of signals. The signals reveal information about the sample including external morphology, chemical composition, and the orientation of materials making up the sample. In this work, the samples were held on a metal stub and coated in a vacuum gold coating for 9-12 minutes before SEM analysis. FESEM JEOL JSM 7800X was employed to investigate external morphologies, such as surface, diameter size, and shape of samples. Transmission electron microscopy (TEM) is a microscopy technique which is used to observe internal morphology and particle size distribution. The high resolution images can be recorded by the transmission of electron beams through an ultra-thin specimen, magnified and focused by an objective lens. The specimen needs to be thin enough to be transparent for electrons. In this study, the sample was dispersed in ethanol and then dripped and dried on a copper grid and bright field transmission electron microscopy (BF-TEM) FEI Tecnai G2 20 200kV was used to investigate the internal microstructure.

### 3.5 X-ray diffraction (XRD)

XRD patterns will be used to analyze the phase structures and the composition of composite. The crystalline size of each composite will be calculated by Scherer's equation as follow;

$$D = \frac{K\lambda}{\beta \cos \theta}$$

Where: D is the mean size of the ordered (crystalline) domains, which may be smaller or equal to the grain size. K is a dimensionless shape factor with a value close to unity. The shape factor has typical value of 0.9, but it varies with the actual shape of the crystallite.  $\lambda$  is the X-ray wavelength.  $\beta$  is the line broadening at half the maximum intensity (FWHM) after subtracting the instrumental line broadening in radians. This quantity is also sometimes denoted as  $\Delta(2\theta)$ , which  $\theta$  is the Bragg angle.



**Figure 3.1** Diagram represents the principles of XRD.

### **3.6 Fourier transform infrared spectroscopy (FTIR)**

FTIR will be used to investigate the bonding energy of products in order to examine the samples remain in the final product. The FTIR spectrometer records the interaction of infrared radiation with a sample by measuring the frequencies at which the sample absorbs the radiation and the intensities of the absorptions. Chemical functional groups are known to absorb light at specific frequencies. Thus, the chemical structure can be determined from the frequencies recorded. In this study, FTIR spectra were analyzed using Bruker Tensor 27 with a resolution of  $4\text{ cm}^{-1}$  in the wavenumber range of  $400\text{-}4000\text{ cm}^{-1}$  and all samples were prepared without potassium bromide mixing (KBr).

### **3.7 Thermogravimetric analysis**

The thermogravimetric analysis and differential scanning calorimetry (TGA/DSC) are the techniques used to study the thermal characteristics of samples. The weight losses of the sample during heat treatment are evidence of structure deformation or decomposition that can be helpful for consideration of the proper temperature for calcination of samples.

In this work, the thermal stability and exothermic reaction of all the samples were carried out in  $\text{N}_2$  atmosphere ( $100\text{ ml}\cdot\text{min}^{-1}$ ) in the temperature range of  $25\text{-}700\text{ }^\circ\text{C}$  with a heating rate of  $10\text{ }^\circ\text{C}\cdot\text{min}^{-1}$  using Mettler TOLEDO.

### **3.8 X-ray Absorption Spectroscopy (XAS)**

X-ray absorption spectroscopy (XAS) is a widely used technique for investigation of the local structure of the material. In this technique, an x-ray is

absorbed by an atom when the energy of the x-ray is transferred to a core-level electron (K, L, or M shell) which is ejected from the atom. The atom is left in an excited state with an empty electronic level (a core hole). Any excess energy from the X-ray is given to the ejected photo-electron. XAS measures the energy dependence of the x-ray absorption coefficient  $\mu(E)$  at and above the absorption edge of a selected element. Generally,  $\mu(E)$  can be measured through transmission and fluorescence modes. In transmission mode, the X-ray flux before ( $I$ ) and after ( $I_0$ ) beam transmitted through the sample with thickness ( $t$ ) is measured. Hence,  $\mu(E)$  is defined as Equation 3.1. On the other hand, the fluorescence mode measures the incident flux ( $I_0$ ) and the fluorescence X-ray ( $I_f$ ) in equation 3.2.

$$\mu(E)t = -\ln(I/I_0) \quad 3.1$$

$$\mu(E) \propto I_f/I_0 \quad 3.2$$

In this study, X-ray absorption near-edge structure (XANES) analysis at the Mn *K*-edge, Ni *K*-edge, Co *K*-edge, Cu *K*-edge, Fe *K*-edge, Zn *K*-edge and Mg *K*-edge were performed in fluorescent mode at the Synchrotron Light Research Institute (BL 5.2 SUT-NANOTEC-SLRI XAS) of Thailand. The spectra were measured in the width range of 120 eV with an energy step of 0.2 eV in both the pre- and post-edge regions. The obtained XAS spectra were evaluated by using Athena software to study the structure of all samples.

### 3.9 X-ray photoelectron spectroscopy (XPS)

X-ray photoelectron spectroscopy (XPS), also known as electron spectroscopy for chemical analysis, is a widely used technique for determination of the elementary

composition of material. The theoretical fundamental of XPS is based on the equation proposed by Einstein to explain the photoelectric effect:

$$h\nu = E_b - E_{kin} \quad 3.3$$

where  $h\nu$  is the quantum energy,  $E_b$  is the binding energy of the electron in matter (i.e. energy required to remove an electron) and  $E_{kin}$  is the kinetic energy of the ejected electron. XPS spectra are obtained by irradiating a material with a beam of X-rays while simultaneously measuring the kinetic energy and number of electrons that escape from the material being analyzed.

In this work, XPS spectra were collected on a PHI 5000 Versa Probe II XPS system (ULVAC-PHI, Japan) with Al K $\alpha$  (1486.4 eV) radiation as the excitation source to determine the element and valence state of Mg, Co, Cu, Fe, Mn, Ni, and Zn in the NH<sub>4</sub>MPO<sub>4</sub>·H<sub>2</sub>O (M= Mg, Co, Fe, Mn, Ni, Zn, Cu) sample.

### 3.10 Magnetic properties measurement

A vibrating sample magnetometer (VSM) was used to study the magnetic properties such as diamagnetic, paramagnetic, ferromagnetic and antiferromagnetic of materials. In this technique, magnetic parameters such as magnetization ( $M$ ) and coercivity ( $H_c$ ) values are recorded as function of magnetic field ( $H$ ) providing a  $M$ - $H$  hysteresis curve. For the measurement, powder was weighed and then placed in a small sample holder which was located at the end of a sample rod mounted in an electromechanical transducer for measurement. The sample is vibrated parallel to the field direction; an electromagnet provides the magnetizing field, a vibrator mechanism to vibrate the sample in the magnetic field, and detection coils which generate signal voltage due to the changing flux emanating from the vibrating sample. The output

measurement displays the magnetic moment as function of a magnetic field or the temperature dependent of magnetization. The measurement can be made at RT and above/below RT (350 K to 50 K) in field rang of 1000 Oe to 15000 Oe.

In this work, the magnetic properties of the  $\text{NH}_4\text{MPO}_4\cdot\text{H}_2\text{O}$  (M= Mg, Co, Fe, Mn, Ni, Zn, Cu) samples are measured at RT by using a vibrating sample magnetometer (VSM; VersaLab<sup>TM</sup>, PPMS, KKU).

### **3.11 Inductively couple plasma optical emission spectrometer (ICP-OES)**

Inductively couple plasma optical emission spectrometer is one method of optical emission spectrometry. When plasma energy is given to an analysis sample from outside, the component elements (atoms) are excited. When the excited atoms return to low energy position, emission rays (spectrum rays) are released and the emission rays that correspond to the photon wavelength are measured. The element type is determined based on the position of the photon rays, and the content of each element is determined based on the rays' intensity.

To generate plasma, first, argon gas is supplied to torch coil, and high frequency electric current is applied to the work coil at the tip of the torch tube. Using the electromagnetic field created in the torch tube by the high frequency current, argon gas is ionized and plasma is generated. This plasma has high electron density and temperature (10000K) and this energy is used in the excitation-emission of the sample. Solution samples are introduced into the plasma in an atomized state through the narrow tube in the center of the torch tube (Olesik, 1991). In the torch desolvation, atomization and ionizations of the sample takes place. Due to the thermic energy taken up by the

electrons, they reach a higher "excited" state. When the electrons drop back to ground level energy is liberated as light (photons). Each element has an own characteristic emission spectrum that is measured with a spectrometer. The light intensity on the wavelength is measured and with the calibration calculated into a concentration.

### 3.12 Ion release

To evaluate the ion release of the ammonium metal phosphates, the aqueous ion release from the precipitate was examined at room temperature. The room-temperature aqueous ion release was examined in the prepared solution (0.5 g of the dried sample in 50 mL of deionized water) which was stirred continuously for 24 h. The sample was collected by filtering with a 0.22  $\mu\text{m}$  filter membrane and subjecting to high-speed centrifugation at 8,000 rpm. Finally, the  $\text{M}^{2+}$  and  $\text{P}^{5+}$  concentration in the supernatant was determined using the inductively coupled plasma atomic emission spectroscopy (ICP-OES) (Optima 2100 DV ICP-OES, Perkin Elmer Instruments, USA).

## **CHAPTER IV**

### **RESULTS AND DISCUSSION**

Chapter IV deals with the results and discussion. It is divided into two sections related to two different groups of prepared samples:  $\text{NH}_4\text{MPO}_4\cdot\text{H}_2\text{O}$  (M= Mg, Co, Fe, Mn, Ni, Zn, Cu) and effect of water, PVP, PVA, Sucrose, CTAB respectively. For each group of study, the thermogravimetric analysis (TGA) was used to observe weight loss as a function of temperature. The crystal structure was identified using X-ray diffraction (XRD), the morphologies were investigated using high resolution scanning electron microscopy (FE-SEM) and transmission electron microscopy (TEM). The chemical compositions and electronic states, samples were determined by XPS and XANES. The magnetic measurements were carried out using a VSM measurement. Finally, the metal ions concentration in the supernatant was determined by Inductively coupled plasma optical emission spectrometer (ICP-OES).

## 4.1 Structural characterization of $\text{NH}_4\text{MPO}_4\cdot\text{H}_2\text{O}$ (M = Mg, Co, Fe, Mn, Ni, Zn, Cu) samples prepared by chemical precipitation method in water solution

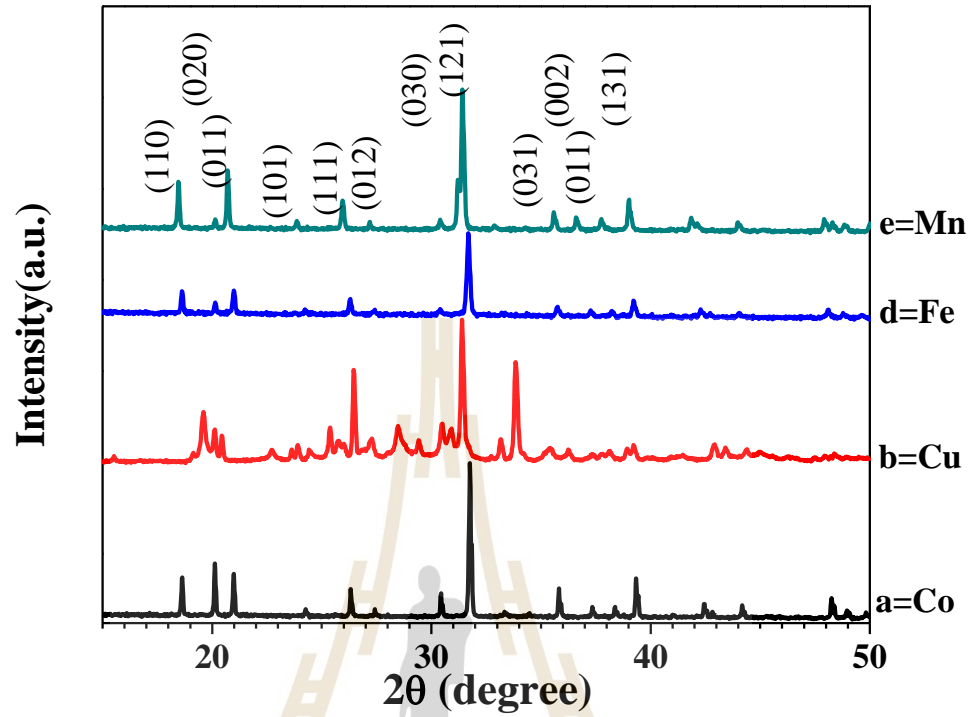
### 4.1.1 X-ray diffraction (XRD) analysis of $\text{NH}_4\text{MPO}_4\cdot\text{H}_2\text{O}$ (M= Mg, Co, Fe, Mn, Ni, Zn, Cu) samples prepared by chemical precipitation method in water

Figure 4.1 shows XRD patterns of the prepared  $\text{NH}_4\text{MPO}_4\cdot\text{H}_2\text{O}$  (M = Co, Mn, Fe, Ni) samples. These XRD patterns confirm the formation of orthorhombic structure with the  $Pmn2_1$  space group. The diffraction peaks of  $\text{NH}_4\text{MPO}_4\cdot\text{H}_2\text{O}$  (M = Co, Mn, Fe, Ni) sample mainly consist of (001), (110), (020), (011), (101), (111), (012), (030), (121), (031), (002), (011) and (131) planes, which is in good agreement with the standard data. No other impurities phases are detected in M = Co, Mn, Fe, Ni samples.

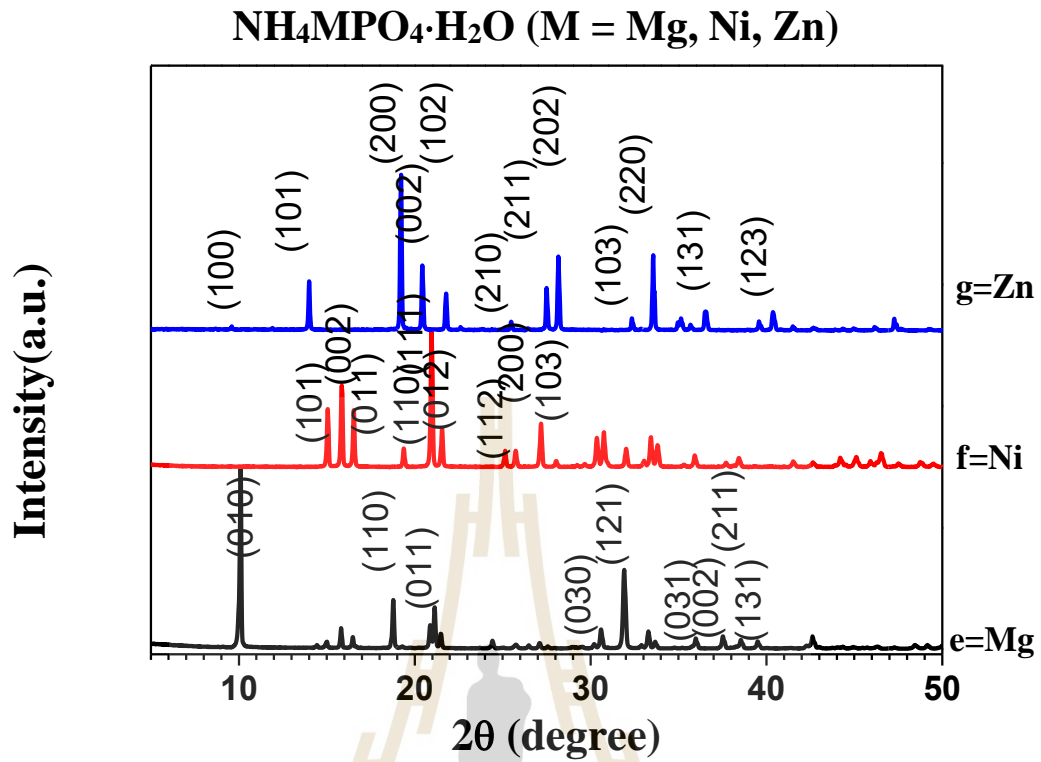
Figure 4.2 shows XRD patterns of the prepared  $\text{NH}_4\text{MPO}_4\cdot\text{H}_2\text{O}$  (M = Zn, Ni, Mg) sample. For  $\text{NH}_4\text{MgPO}_4\cdot\text{H}_2\text{O}$  sample, XRD pattern can be indexed as orthorhombic structure (JCPDS No. 036-1496) with space group of  $Pmnm$ . The diffraction peaks of  $\text{NH}_4\text{MgPO}_4\cdot\text{H}_2\text{O}$  sample mainly consist of (010), (110), (011), (030), (121), (031), (002), (211) and (131) planes, which agree well with the standard data. However, the presence of  $\text{NH}_4\text{MgPO}_4\cdot 6\text{H}_2\text{O}$  phase impurities could be detected in this sample indicating low purity phase. For  $\text{NH}_4\text{NiPO}_4\cdot\text{H}_2\text{O}$  sample, XRD pattern shows the formation of monoclinic structure with the  $P2_1$  space group (JCPDS No 089-1303) consisting of the diffraction peaks of (100), (101), (200), (002), (102), (210), (211), (202), (103), (220), (131) and (123) planes. This result is in good agreement with the standard data without detected any other phase impurities. On the other hand, the

XRD pattern of  $\text{NH}_4\text{ZnPO}_4$  sample indicates the formation of hexagonal structure with the P63 space group (JCPDS No 089-6315). The diffraction peaks of this sample mainly consist of (100), (101), (200), (002), (102), (210), (211), (202), (103), (220), (131) and (123) planes, which is in good agreement with the standard data. Note that the other phases impurities could not be detected in this sample.

As presented above, all samples show the ammonium metal phosphate structure with standard JCPDS file No. 21-0793, 089-1303, 045-2404, 050-0554, 086-1866, and 036-1496 for  $\text{NH}_4\text{MPO}_4 \cdot \text{H}_2\text{O}$  where  $M = \text{Co}, \text{Cu}, \text{Fe}, \text{Mn}, \text{Ni}, \text{and Mg}$  samples, respectively. The unit cell parameters ( $a$ ,  $b$ , and  $c$ ), cell volume ( $V$ ), expected profile residual ( $R_{exp}$ ), profile residual ( $R_p$ ), weighted profile residual ( $R_{wp}$ ), goodness of fit (GOF) values of all  $\text{NH}_4\text{MPO}_4 \cdot \text{H}_2\text{O}$  ( $M = \text{Co}, \text{Cu}, \text{Fe}, \text{Mn}, \text{Ni}, \text{and Mg}$ ) samples were calculated by Rietveld refinement unit cell analysis (TOPAS software) and the values of these parameters are summarized in Table 4.1.

**$\text{NH}_4\text{MPO}_4 \cdot \text{H}_2\text{O}$  (M = Co, Cu, Fe, Mn)**

**Figure 4.1** XRD patterns of the prepared  $\text{NH}_4\text{MPO}_4 \cdot \text{H}_2\text{O}$  (M = Co, Cu, Fe, Mn) powder.



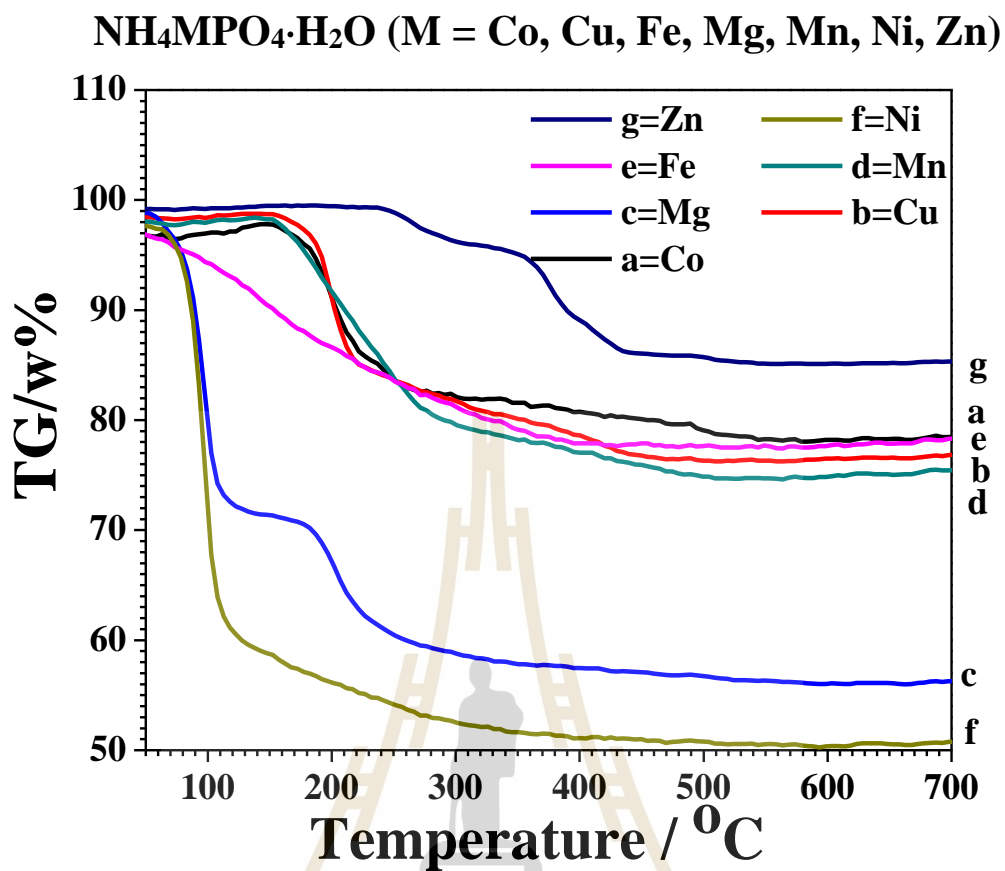
**Figure 4.2** XRD patterns of the prepared  $\text{NH}_4\text{MPO}_4 \cdot \text{H}_2\text{O}$  (M =Zn, Ni, Mg) powder.

**Table 4.1** Lattice parameter (a, b, and c),  $\beta$  angle, cell volume (V), Rietveld refinement parameters ( $R_p$ ,  $R_{exp}$ ,  $R_{wp}$  GOF) and specific magnetization of the  $NH_4MPO_4 \cdot H_2O$  (M= Mg, Co, Fe, Mn, Ni, Zn, Cu) powder prepared by chemical precipitation method.

Parameter	$NH_4MPO_4 \cdot H_2O$ (M= Mg, Co, Fe, Mn, Ni, Zn, Cu) samples						
	Co	Cu	Fe	Mg	Mn	Ni	Zn
Lattice parameters ( $\text{\AA}$ )							
a	5.62	7.41	5.57	5.61	5.72	6.92	10.69
b	8.77	7.53	8.82	8.76	8.81	6.10	10.69
c	4.80	8.66	4.88	4.79	4.90	11.17	8.71
Cell volume ( $10^6 \text{pm}^3$ )	236.10	482.55	240.52	236.00	247.78	472.23	862.12
$R_p$ (%)	5.28	8.24	2.81	8.49	2.85	5.27	4.67
$R_{exp}$ (%)	2.36	2.47	1.86	4.25	2.23	2.72	2.46
$R_{wp}$ (%)	8.51	11.86	4.45	11.36	4.02	7.04	6.66
GOF (%)	3.60	4.79	2.39	2.67	1.80	2.59	2.70
M at 10kOe (emu/g)	14.98	2.14	17.52	-1.56	26.17	4.83	-0.69

#### 4.1.2 Thermo gravimetric analysis (TGA) of the $\text{NH}_4\text{MPO}_4\cdot\text{H}_2\text{O}$ (M = Mg, Co, Fe, Mn, Ni, Zn, Cu)

Figure 4.3 and 4.4 show the TG/DSC curves of the  $\text{NH}_4\text{MPO}_4\cdot\text{H}_2\text{O}$  (M = Mg, Co, Fe, Mn, Ni, Zn, Cu) samples obtained at a heating rate of  $5\text{ }^\circ\text{C}/\text{min}^{-1}$  at temperature below  $700\text{ }^\circ\text{C}$  in  $\text{N}_2$  atmosphere. As shown in Figure 4.3, the weight loss of all samples continuously decreases from room temperature and stable at about  $450\text{ }^\circ\text{C}$ . This decrease could be attributed to the evaporation of water molecules. Furthermore, the M = Zn sample exhibits a high rate of the weight loss which possibly due to it does not have  $\text{H}_2\text{O}$  content in the  $\text{NH}_4\text{ZnPO}_4$  structure. Figure 4.4 shows thermal decomposition of all samples which occurs in three well-defined steps. In the first step at temperature of  $50 - 300\text{ }^\circ\text{C}$ , the strong endothermic DSC peaks can be attributed to a water molecule and ammonia eliminated from  $\text{NH}_4\text{MPO}_4\cdot\text{H}_2\text{O}$  (M = Mg, Co, Fe, Mn, Ni, Cu) and the formation of  $\text{MHPO}_4$  (Pysiak, Prodan, Samuskevich, Pacewska and Shkorik, 1993). The second decomposition step at temperature of  $500 - 700\text{ }^\circ\text{C}$  is attributed to the dehydration of  $\text{MHPO}_4$  (Pang et al., 2012, Karaphun et al., 2018). The exothermic DSC peak of the third decomposition step at  $700\text{ }^\circ\text{C}$  is related to the formation of new phase  $\text{M}_2\text{P}_2\text{O}_7$ .



**Figure 4.3** TG-DTG curves of the  $\text{NH}_4\text{MPO}_4 \cdot \text{H}_2\text{O}$  (M = Co, Cu, Mg, Mn, Fe, Ni and Zn) powder performed at a heating rate of  $5\text{ }^\circ\text{C min}^{-1}$  in  $\text{N}_2$  atmosphere.

$\text{NH}_4\text{MPO}_4 \cdot \text{H}_2\text{O}$  M = Co, Cu, Fe, Mg, Mn, Ni, Zn

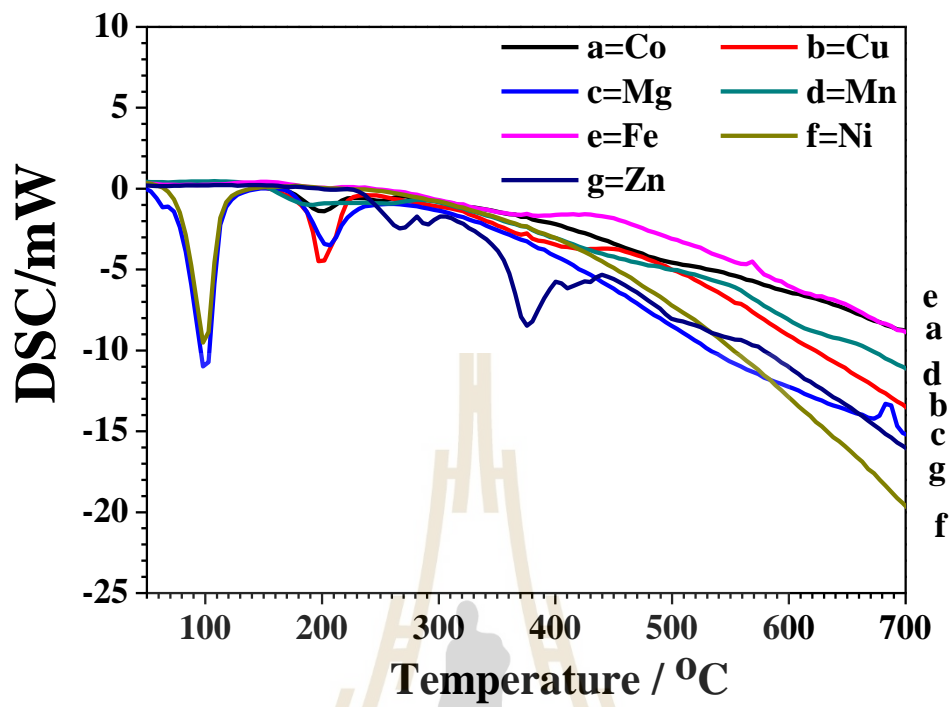
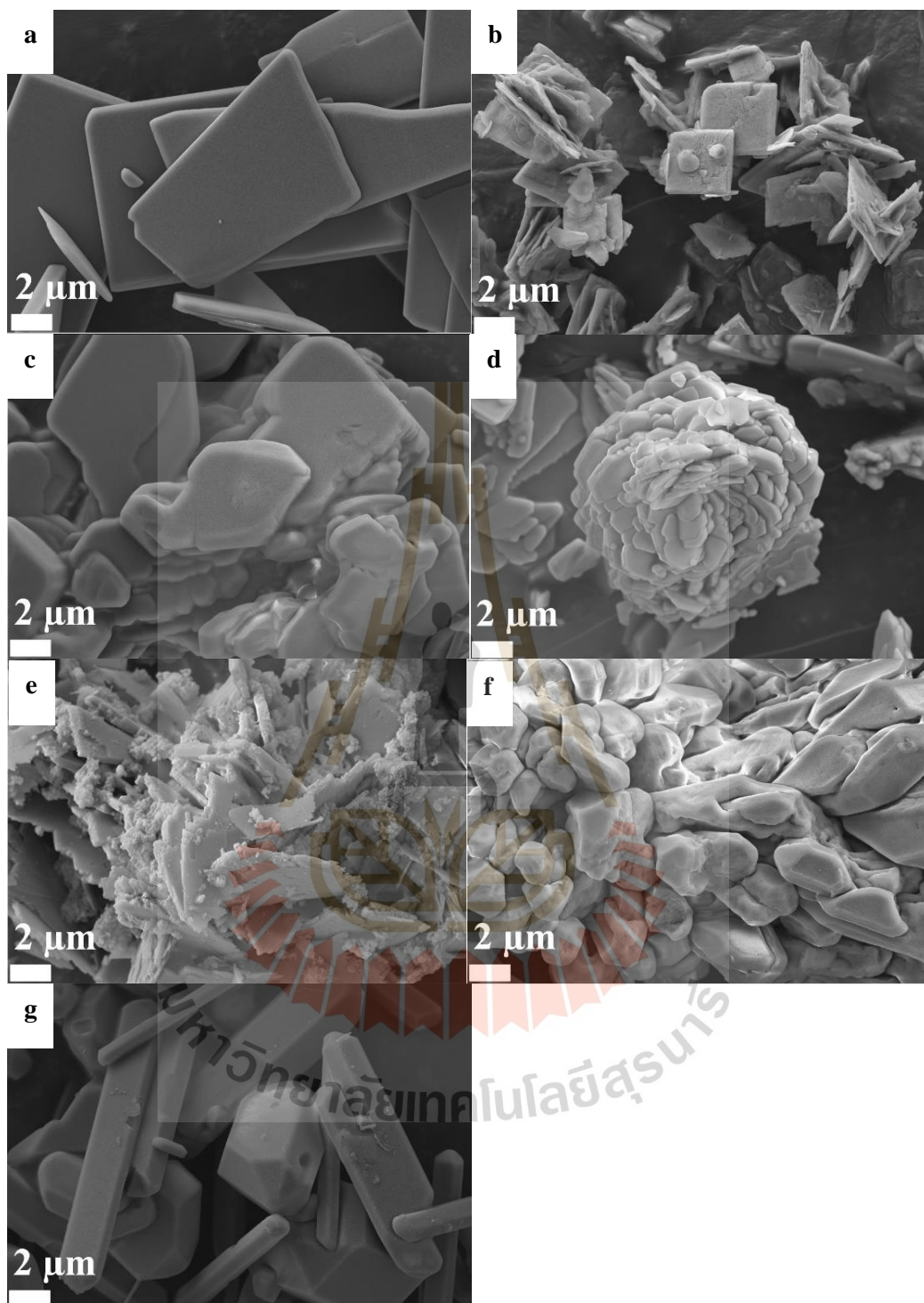


Figure 4.4 shows the DSC curves of the prepared samples, when heated at a rate of 5 °C/min from ambient temperature to 700 °C.

### 4.1.3 Morphology of $\text{NH}_4\text{MPO}_4\cdot\text{H}_2\text{O}$ powder (M = Mg, Co, Fe, Mn, Ni, Zn, Cu) by SEM

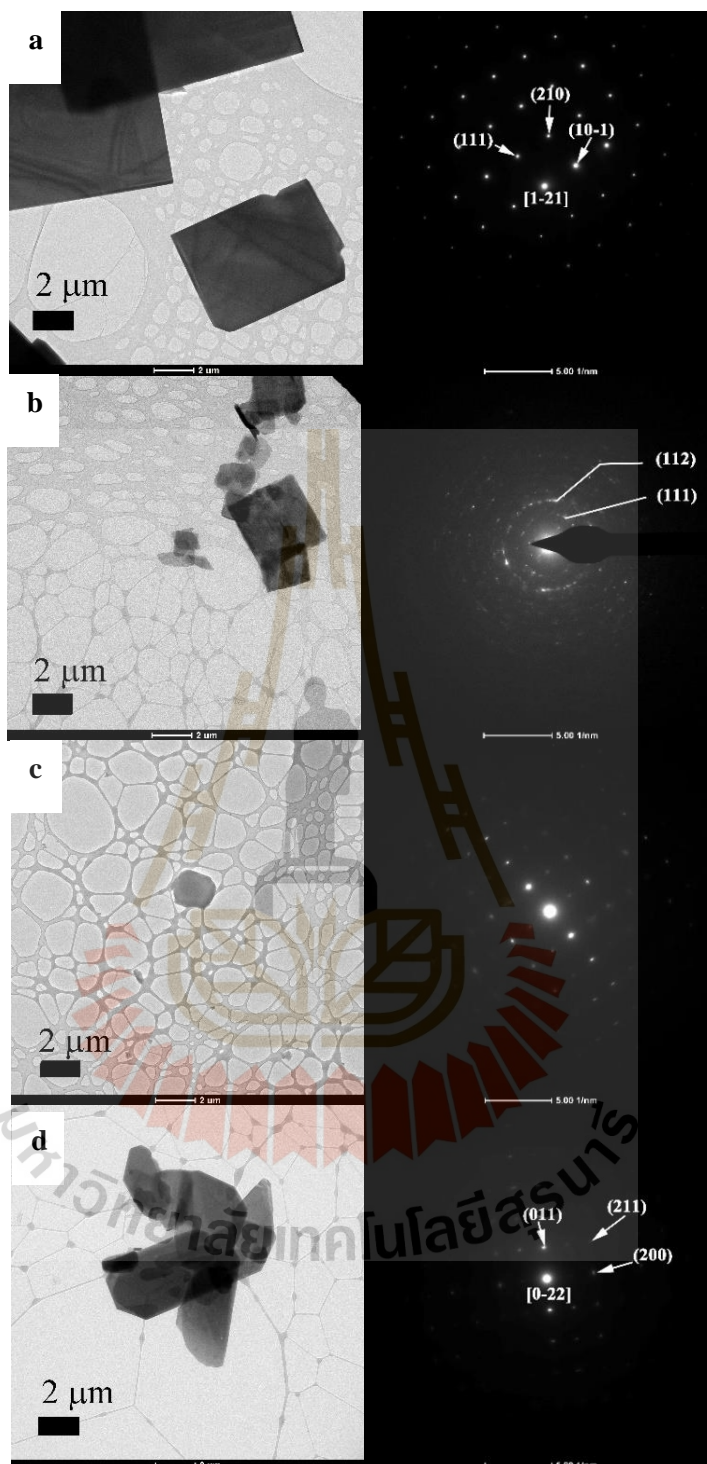
Figure 4.5 shows the SEM image of  $\text{NH}_4\text{MPO}_4\cdot\text{H}_2\text{O}$  powder with M = Mg, Co, Fe, Mn, Ni, Zn, Cu. The size and shape of as-prepared  $\text{NH}_4\text{MPO}_4\cdot\text{H}_2\text{O}$  were examined by scanning electron microscopy Figure 4(a) 4(b) 4(c) 4(e) shows SEM images of  $\text{NH}_4\text{CoPO}_4\cdot\text{H}_2\text{O}$ ,  $\text{NH}_4\text{CuPO}_4\cdot\text{H}_2\text{O}$ ,  $\text{NH}_4\text{MgPO}_4\cdot\text{H}_2\text{O}$  and  $\text{NH}_4\text{FePO}_4\cdot\text{H}_2\text{O}$  samples. SEM images of all sample almost completely consists of oblong plate structures, which are uniform with a width of 3–5  $\mu\text{m}$  and a length of 5–10  $\mu\text{m}$ . Figure 4(d) 4(f) show the detailed morphology and structure of the of  $\text{NH}_4\text{MnPO}_4\cdot\text{H}_2\text{O}$  and  $\text{NH}_4\text{NiPO}_4\cdot\text{H}_2\text{O}$  samples prepared chemical precipitation. The SEM images of  $\text{NH}_4\text{MnPO}_4\cdot\text{H}_2\text{O}$  evidenced the obtained all of particles were micro flower and nearly sphere morphology with the size about 10  $\mu\text{m}$ . The SEM images of  $\text{NH}_4\text{NiPO}_4\cdot\text{H}_2\text{O}$  evidenced the obtained all of particles were micro nearly sphere morphology with the size about 10  $\mu\text{m}$ . Figure 4(g) show the detailed morphology and structure of the of  $\text{NH}_4\text{ZnPO}_4$  samples prepared chemical precipitation. The SEM images evidenced the obtained all of particles were micro particle morphology and micro rod with the size about 10  $\mu\text{m}$ .



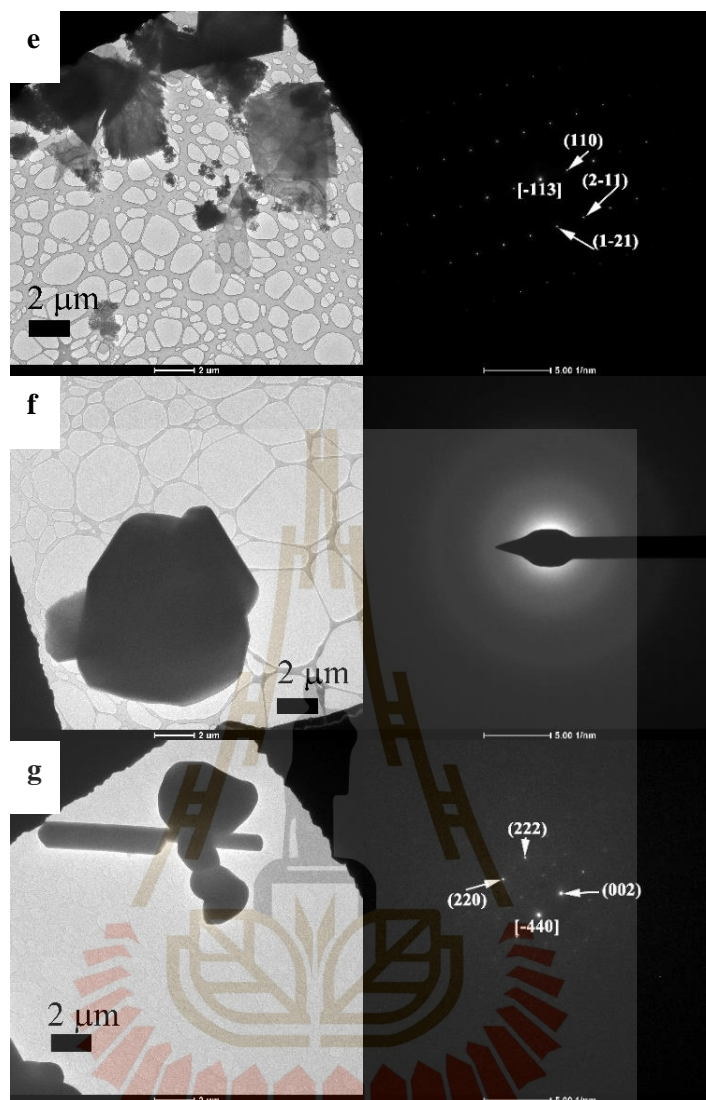
**Figure 4.5** SEM image of  $\text{NH}_4\text{MPO}_4 \cdot \text{H}_2\text{O}$  powder with M = (a) Co (b) Cu (c) Mg (d) Mn (e) Fe (f) Ni and (g) Zn.

#### 4.1.4 Morphology of $\text{NH}_4\text{MPO}_4\cdot\text{H}_2\text{O}$ powder (M = Mg, Co, Fe, Mn, Ni, Zn, Cu) by TEM

Figure 4.6(a) shows the TEM images of Bright field TEM images and with corresponding selected areas of electron diffraction (SAED) patterns of the  $\text{NH}_4\text{CoPO}_4\cdot\text{H}_2\text{O}$  powder. The TEM bright field images show that the micro plates sizes obtained were about 5–10  $\mu\text{m}$ . The SAED patterns shows lattice fringes and spot patterns of  $\text{NH}_4\text{CoPO}_4\cdot\text{H}_2\text{O}$  orthorhombic structure without secondary phase for all samples, which correspond to the XRD results. Figure 4.6(b) shows the morphology and structure of the  $\text{NH}_4\text{CuPO}_4\cdot\text{H}_2\text{O}$  powder. The TEM images evidenced that all of the plates were micro plate with the size about 5  $\mu\text{m}$ . The SAED patterns of the plates show spotty patterns which indicate the sample is single crystalline structure. Figure 4.6(c) shows the morphology and structure of the  $\text{NH}_4\text{MgPO}_4\cdot\text{H}_2\text{O}$  powder. The TEM bright field images show that the micro plates sizes obtained were about 1  $\mu\text{m}$ . Figure 4.6(d) shows the morphology and structure of the  $\text{NH}_4\text{MnPO}_4\cdot\text{H}_2\text{O}$ . The TEM images evidenced that all of the plates were micro plate with the size about 2 to 5  $\mu\text{m}$ . The SAED patterns show lattice fringe and spot pattern of  $\text{NH}_4\text{MnPO}_4\cdot\text{H}_2\text{O}$  orthorhombic structure without secondary phase for all samples, which correspond to XRD results. Figure 4.7(e) show the morphology and structure of the of  $\text{NH}_4\text{FePO}_4\cdot\text{H}_2\text{O}$ . The TEM images evidenced that all of the plates were micro plate and amorphous morphology with the size about 1  $\mu\text{m}$ . The SAED patterns of the plates show spotty patterns of  $\text{NH}_4\text{FePO}_4\cdot\text{H}_2\text{O}$  orthorhombic structure which indicate the sample is single crystalline structure.



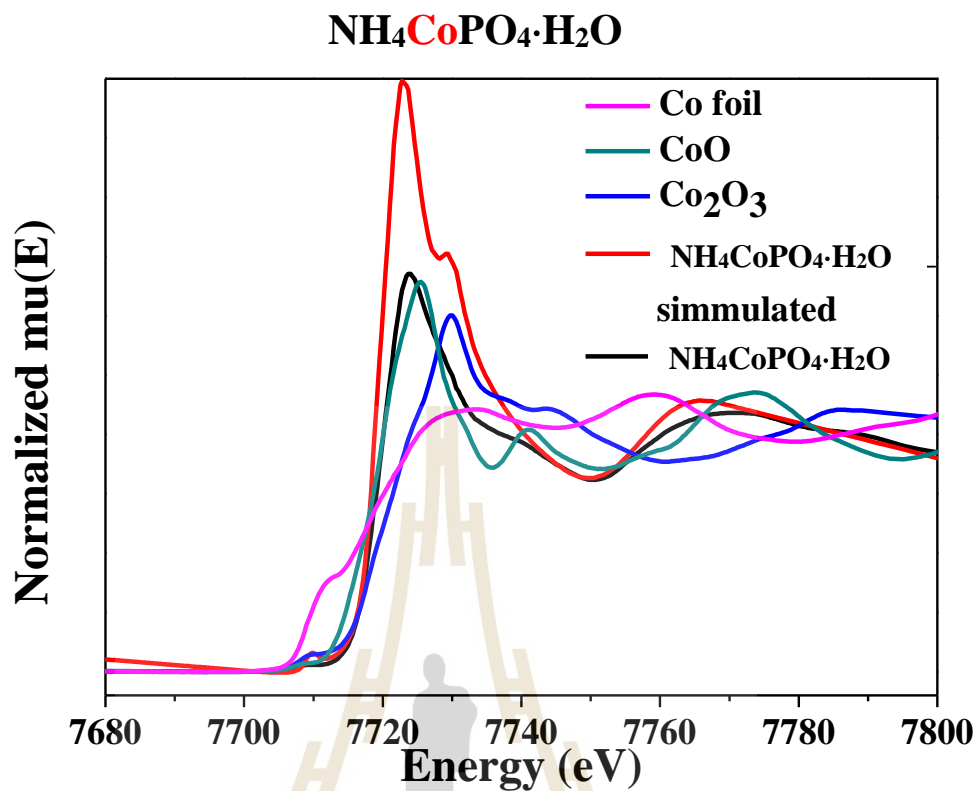
**Figure 4.6** TEM images with corresponding selected-area electron diffraction (SAED) patterns of the  $\text{NH}_4\text{MPO}_4 \cdot \text{H}_2\text{O}$  powder with  $M =$  (a) Co (b) Cu (c) Mg (d) Mn.



**Figure 4.7** TEM images with corresponding selected-area electron diffraction (SAED) patterns of the  $\text{NH}_4\text{MPO}_4 \cdot \text{H}_2\text{O}$  powder with  $M = \text{Fe}$  (e)  $\text{Ni}$  (f) and  $\text{Zn}$  (g).

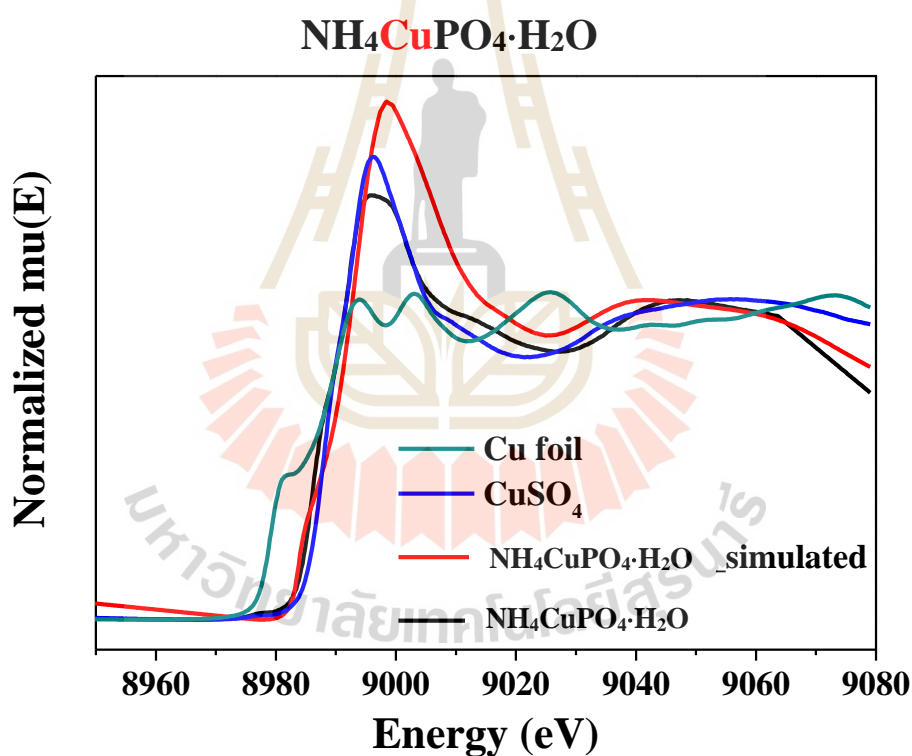
#### 4.1.5 X-ray absorption spectroscopy study of the $\text{NH}_4\text{MPO}_4\cdot\text{H}_2\text{O}$ powder (M = Mg, Co, Fe, Mn, Ni, Zn, Cu)

The X-ray absorption near-edge structure (XANES) spectra of the  $\text{NH}_4\text{CoPO}_4\cdot\text{H}_2\text{O}$  was measured at Co K-edge at energy range of 7650-7800 eV to examine the chemical states of cobalt element in the samples. The XANES technique is used to distinguish the chemical species and oxidation states of Co in the samples. The energy edges were evaluated using Athena software, Figure 4.8 shows the normalized Co K-edge XANES spectra of the  $\text{NH}_4\text{CoPO}_4\cdot\text{H}_2\text{O}$  particles, which were compared with the standard compounds CoO ( $\text{Co}^{2+}$ ) and  $\text{Co}_2\text{O}_3$  ( $\text{Co}^{3+}$ ). The results indicated that the spectra feature of all samples show quite similar feature. In general, the edge and pre-edge energy positions of XANES spectra related to the valence state of the absorbing atom in the sample and shifted to higher energy when oxidation state of the absorbing atom increase. The edge energy positions of samples were 7720.04 eV. The edge energy positions of samples match with the edge energy positions of  $\text{Co}_2\text{O}_3$  ( $E_0 = 7722.33$  eV) and CoO ( $E_0 = 7719.86$  eV) standard samples. These results can be implied that Co ions in all samples have a  $\text{Co}^{2+}$  and  $\text{Co}^{3+}$  in the structure.



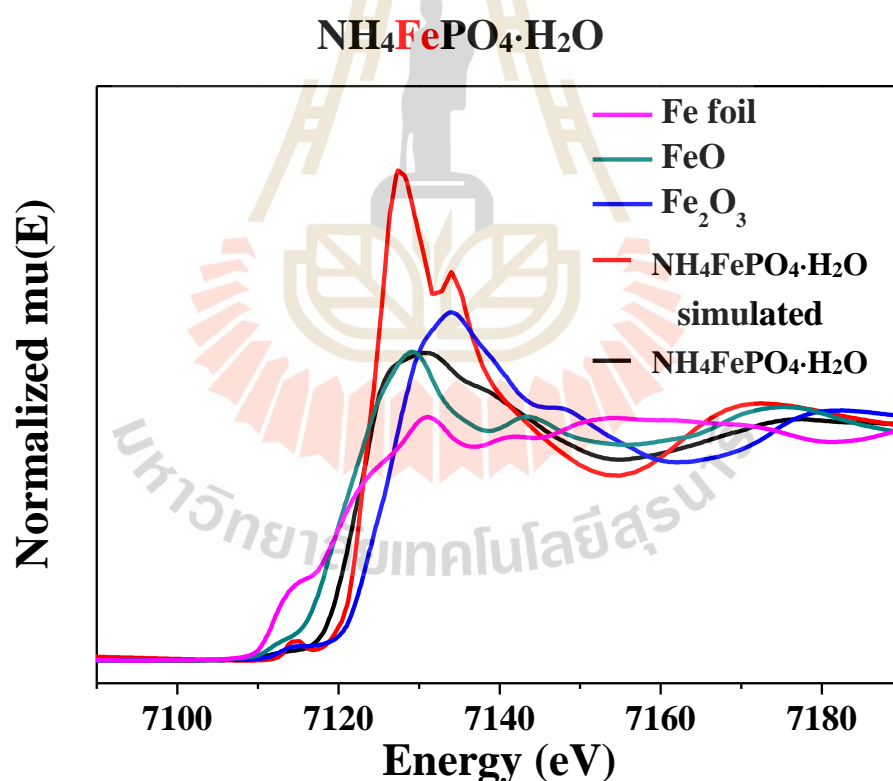
**Figure 4.8** XANES spectra at the Co K absorption edge for Co foil, CoO and Co<sub>2</sub>O<sub>3</sub> standard and XANES spectra of the NH<sub>4</sub>CoPO<sub>4</sub>·H<sub>2</sub>O.

The XANES spectra of  $\text{NH}_4\text{CuPO}_4\cdot\text{H}_2\text{O}$  at Cu K-edge were measured at energy range of 8950-9080 eV to examine the oxidation states of copper element in the samples. Figure 4.9 shows the normalized Cu K-edge XANES spectrum of the  $\text{NH}_4\text{CuPO}_4\cdot\text{H}_2\text{O}$  sample, which was compared with the standard compounds of Cu and  $\text{Cu}^{2+}$ . The edge energy positions of samples were at 8986.11 eV, which were between the edge energy positions of Cu foil ( $E_0 = 8979.18$  eV) and  $\text{CuSO}_4$  ( $E_0 = 8987.73$  eV) standard samples. These results can be implied that Cu ions in all samples have mixing of Cu and  $\text{Cu}^{2+}$  in the structure.



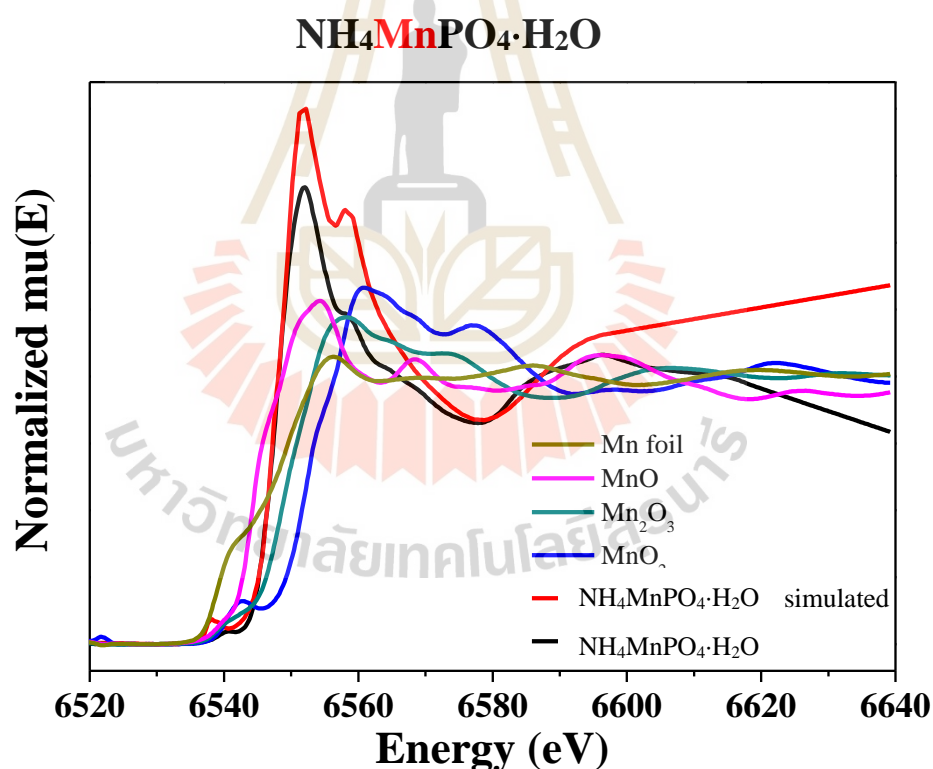
**Figure 4.9** XANES spectra at the Cu K absorption edge for Cu foil and  $\text{CuCl}_2$  standard and XANES spectra of the  $\text{NH}_4\text{CuPO}_4\cdot\text{H}_2\text{O}$ .

Figure 4.10 shows the normalized Fe K-edge XANES spectrum of the  $\text{NH}_4\text{FePO}_4\cdot\text{H}_2\text{O}$  sample, which was compared with the standard compounds of Fe,  $\text{Fe}^{2+}$  and  $\text{Fe}^{3+}$ . The XANES spectra of  $\text{NH}_4\text{FePO}_4\cdot\text{H}_2\text{O}$  at Fe K-edge was measured at energy range of 7080-7200 eV to examine the chemical states of iron element in the samples. The edge energy positions of samples were found at 7122.35 eV, which were between the edge energy positions of FeO ( $E_0 = 7122.14$  eV) and  $\text{Fe}_2\text{O}_3$  ( $E_0 = 7126.53$  eV) standard samples. These results can be concluded that Fe ions in all samples have a  $\text{Fe}^{+2}$  and  $\text{Fe}^{3+}$  in the structure.



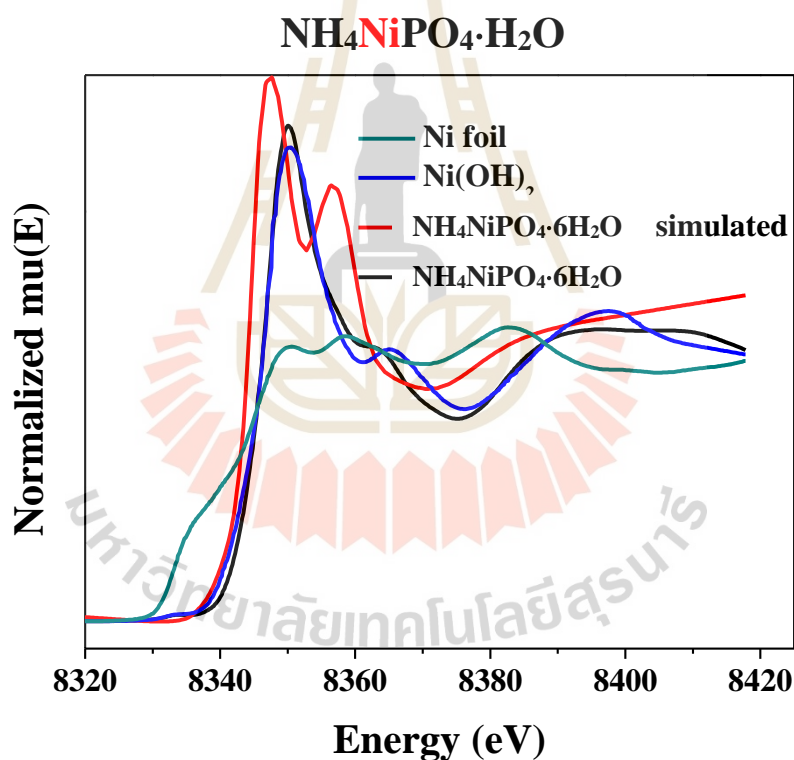
**Figure 4.10** XANES spectra at the Fe K absorption edge for Fe foil, FeO and  $\text{Fe}_2\text{O}_3$  standard and XANES spectra of the  $\text{NH}_4\text{FePO}_4\cdot\text{H}_2\text{O}$ .

The XANES spectra of Mn K-edge XANES were measured at energy range 6500-6640 eV to examine the oxidation states of iron element in the samples. Figure 4.11 shows the normalized Mn K-edge XANES spectrum of the  $\text{NH}_4\text{MnPO}_4\cdot\text{H}_2\text{O}$  sample, which was compared with the standard compounds of  $\text{Mn}^{2+}$ ,  $\text{Mn}^{3+}$  and  $\text{Mn}^{4+}$ . The edge energy positions of samples were at 6547.45 eV, which lied between the edge energy positions of MnO ( $E_0 = 6544.20$  eV),  $\text{Mn}_2\text{O}_3$  ( $E_0 = 6548.42$  eV) and  $\text{MnO}_2$  ( $E_0=76552.61$  eV) standard samples. These results can be implied that Mn ions in all samples have  $\text{Mn}^{+2}$  and  $\text{Mn}^{3+}$  in the structure.



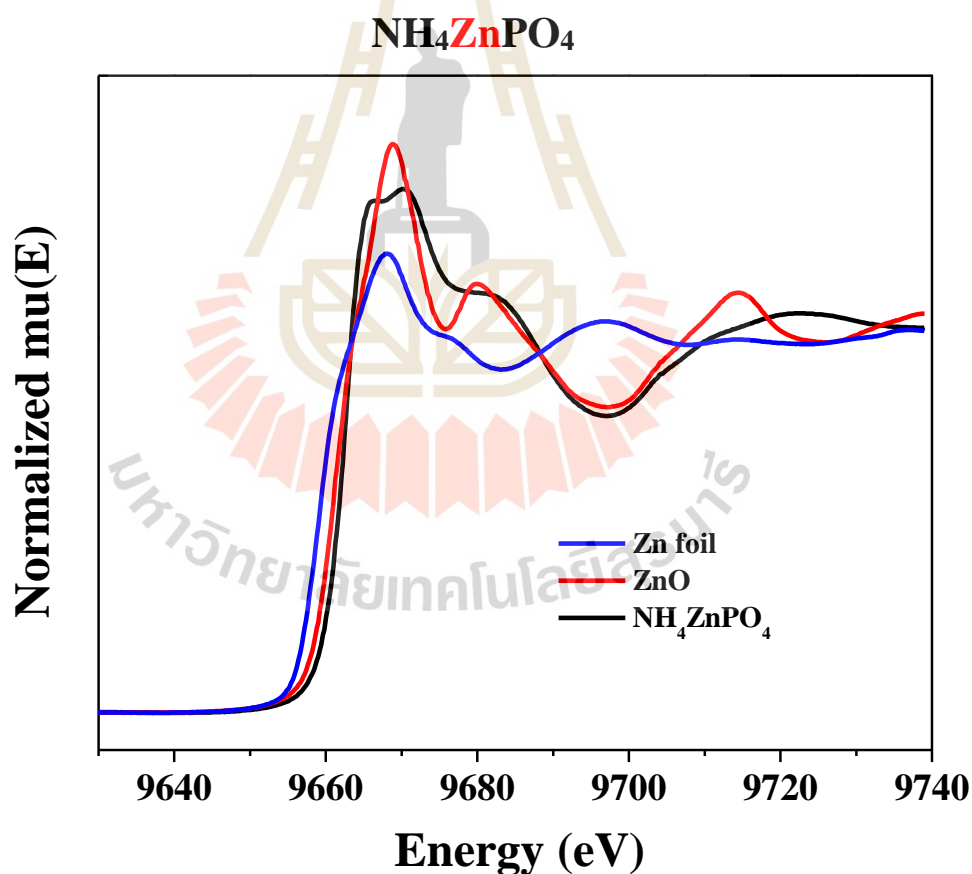
**Figure 4.11** XANES spectra at the Mn K absorption edge for Mn foil, MnO,  $\text{Fe}_2\text{O}_3$  and MnO standard and XANES spectra of the  $\text{NH}_4\text{MnPO}_4\cdot\text{H}_2\text{O}$ .

Figure 4.12 shows the normalized Ni K-edge XANES spectrum of the  $\text{NH}_4\text{NiPO}_4 \cdot \text{H}_2\text{O}$  sample, which was compared with the standard compounds of Ni and  $\text{Ni}^{2+}$ . The XANES spectrum of Ni K-edge XANES was measured at energy range 8300-8420 eV to examine the oxidation states of iron element in the samples. The edge energy positions of samples were found at 8346.1 eV, which lied on the edge energy positions of  $\text{Ni}(\text{OH})_2$  ( $E_0 = 8346.00\text{eV}$ ) standard samples. These results can be concluded that Ni ions in all samples are  $\text{Ni}^{+2}$  in the structure.



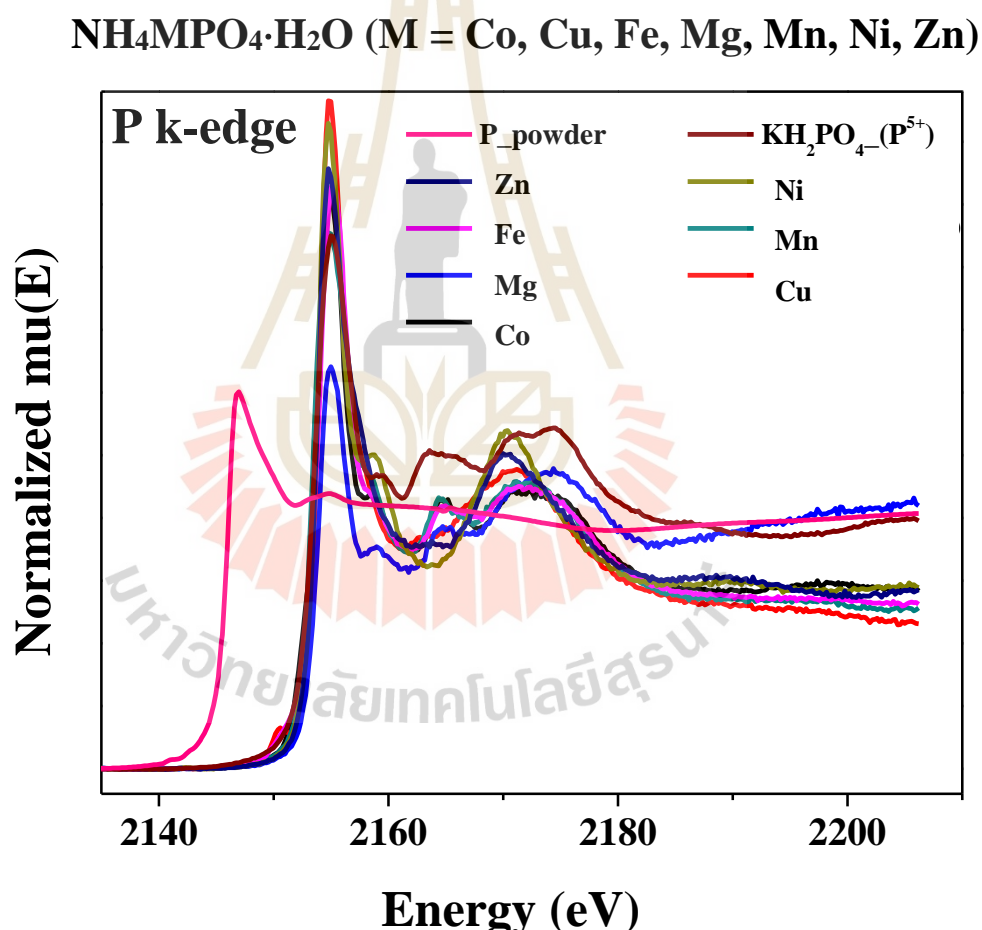
**Figure 4.12** XANES spectra at the Ni K absorption edge for Ni foil and  $\text{NiO}$  standard and XANES spectra of the  $\text{NH}_4\text{NiPO}_4 \cdot 6\text{H}_2\text{O}$ .

The XANES spectrum of  $\text{NH}_4\text{ZnPO}_4$  of Zn K-edge XANES was measured at energy range 9600-9760 eV to examine the oxidation states of iron element in the samples. Figure 4.13 shows the normalized Zn K-edge XANES spectrum of the  $\text{NH}_4\text{ZnPO}_4$  sample, which was compared with the standard compounds of Zn and  $\text{Zn}^{2+}$ . The edge energy positions of samples were 9662.60 eV, which lied on the edge energy positions of ZnO ( $E_0 = 9662.69$  eV) standard samples. These results can be implied that Zn ions in all samples have a  $\text{Zn}^{+2}$  in the structure.



**Figure 4.13** XANES spectra at the Zn K absorption edge for Zn foil and ZnO standard and XANES spectra of the  $\text{NH}_4\text{ZnPO}_4$ .

Figure 4.14 shows the normalized P K-edge XANES spectra of the  $\text{H}_4\text{MPO}_4 \cdot \text{H}_2\text{O}$  ( $\text{M} = \text{Mg}, \text{Co}, \text{Fe}, \text{Mn}, \text{Ni}, \text{Zn}, \text{Cu}$ ) particles, which was compared with the standard compounds of  $\text{P}^{0+}$  and  $\text{P}^{5+}$ . The results indicated that the spectra feature of all samples show quite similar feature. The edge energy positions of samples match with edge energy positions of  $\text{KH}_2\text{PO}_4$  standard samples. These results can be concluded that P ions in all samples have a  $\text{P}^{5+}$  in the structure.



**Figure 4.14** XANES spectra at the P K absorption edge for P powder and  $\text{KH}_2\text{PO}_4$  standard and XANES spectra of  $\text{NH}_4\text{MPO}_4 \cdot \text{H}_2\text{O}$  ( $\text{M} = \text{Mg}, \text{Co}, \text{Fe}, \text{Mn}, \text{Ni}, \text{Zn}, \text{Cu}$ ).

#### 4.1.6 X-Ray Photoelectron spectroscopy study of the $\text{NH}_4\text{MPO}_4\cdot\text{H}_2\text{O}$ powder (M = Mg, Co, Fe, Mn, Ni, Zn, Cu)

The chemical compositions and oxidation states were studied by XPS. XPS survey spectra of  $\text{NH}_4\text{MPO}_4\cdot\text{H}_2\text{O}$  powders (M = Mg, Co, Fe, Mn, Ni, Zn, Cu) are shown in Figure 4.15. Figure 4.15 shows main binding energy peaks indicating the presence of C, N, O, P, Mg, Co, Fe, Mn, Ni, Zn, Cu observed at approximately 284.8, 400.5, 530.7, 133.04, 780.1, 932.3, 710, 641.01, 856, 1022 eV in  $\text{NH}_4\text{MPO}_4\cdot\text{H}_2\text{O}$  powders. The result indicates that  $\text{NH}_4\text{MPO}_4\cdot\text{H}_2\text{O}$  powders still have  $\text{NH}_4\text{MPO}_4\cdot\text{H}_2\text{O}$  in sample. However, the addition binding energy peak of Mg, Co, Fe, Mn, Ni, Zn, Cu increase observed in the XPS survey spectra of prepared  $\text{NH}_4\text{MPO}_4\cdot\text{H}_2\text{O}$ . These indicated simple method for generated structure  $\text{NH}_4\text{MPO}_4\cdot\text{H}_2\text{O}$  sample which is consistent with the XRD results.

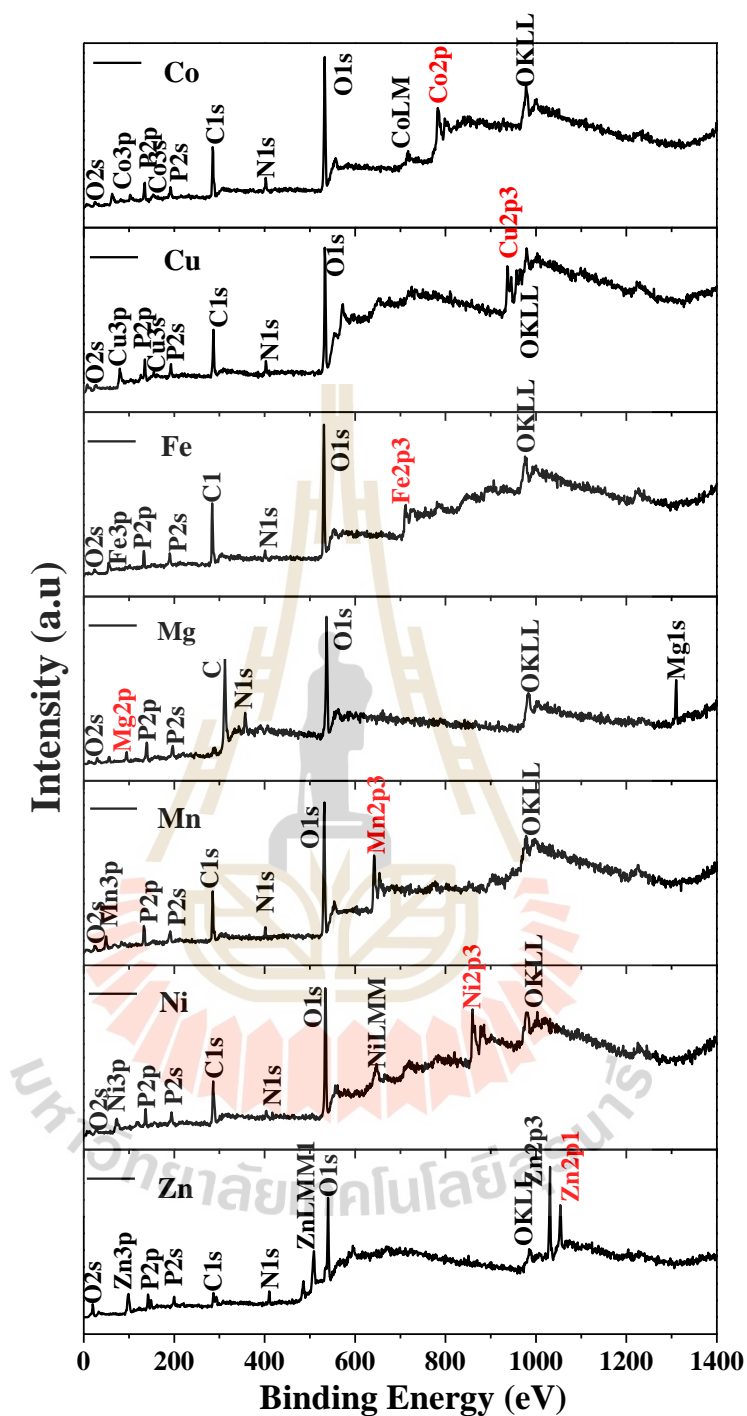
The high resolution XPS spectra of N 1s peaks of  $\text{NH}_4\text{MPO}_4\cdot\text{H}_2\text{O}$  are shown in Figure 4.16. Peaks fit of both N and NH are observed in sample  $\text{NH}_4\text{MPO}_4\cdot\text{H}_2\text{O}$  powders (M = Co, Fe, Mn, Ni, Cu). This result indicates that  $\text{NH}_4\text{MPO}_4\cdot\text{H}_2\text{O}$  powder (M = Co, Fe, Mn, Ni, Cu) suitable for fertilizer application. In the case of  $\text{NH}_4\text{MPO}_4\cdot\text{H}_2\text{O}$  powders (M = Mg and Zn) not exhibited N peak that mean the fertilizer may also be unsuitable.

The XPS spectra in the Co 2p, Cu 2p, Fe 2p, Mg 2s, Mn 2p, and Zn 2p regions of  $\text{NH}_4\text{MPO}_4\cdot\text{H}_2\text{O}$  powders (M = Mg, Co, Fe, Mn, Ni, Zn, Cu) are shown in Figure 4.17. The spectra show the presences of  $\text{Co}^{2+}$  ( $2p_{3/2}$  BE = 781.23 eV)  $\text{Co}^{3+}$  ( $2p_{3/2}$  BE = 783.56 eV) states in  $\text{NH}_4\text{CoPO}_4\cdot\text{H}_2\text{O}$ ,  $\text{Cu}^{1+}$  ( $2p_{3/2}$  BE = 933.40 eV,  $2p_{1/2}$  BE = 953.20 eV)  $\text{Cu}^{2+}$  ( $2p_{3/2}$  BE = 936.22 eV,  $2p_{1/2}$  BE = 956.02 eV) states in  $\text{NH}_4\text{CuPO}_4\cdot\text{H}_2\text{O}$ ,  $\text{Fe}^{2+}$

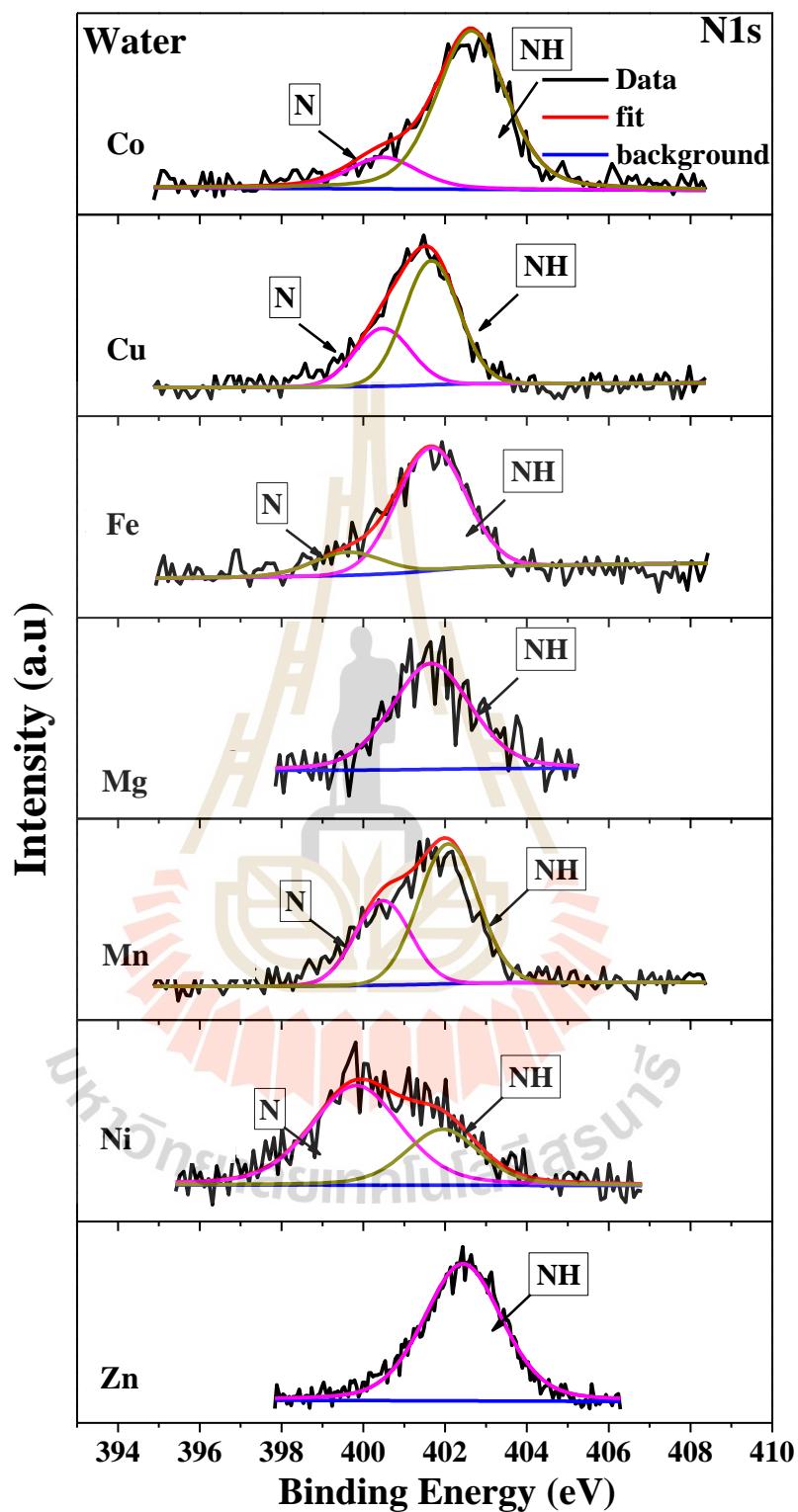
( $2p_{3/2}$  BE = 710.09 eV,  $2p_{1/2}$  BE = 724.10 eV) and  $Fe^{3+}$  ( $2p_{3/2}$  BE = 711.95 eV,  $2p_{1/2}$  BE = 726.50 eV) states in  $NH_4FePO_4 \cdot H_2O$ ,  $Mg^{2+}$  ( $2s$  BE = 89.32 eV) states in  $NH_4MgPO_4 \cdot H_2O$ ,  $Mn^{3+}$  ( $2p_{3/2}$  BE = 641.42 eV,  $2p_{1/2}$  BE = 653.02 eV)  $Mn^{4+}$  ( $2p_{3/2}$  BE = 642.85 eV,  $2p_{1/2}$  BE = 654.45 eV) states in  $NH_4MnPO_4 \cdot H_2O$ ,  $Ni^{2+}$  ( $2p_{3/2}$  BE = 856.83 eV,  $2p_{1/2}$  BE = 874.43 eV) states in  $NH_4NiPO_4 \cdot H_2O$  and  $Zn^{2+}$  ( $2p_{3/2}$  BE = 1022 eV) state in the  $NH_4ZnPO_4$ . These transition metal of  $Co^{2+}$ ,  $Co^{3+}$ ,  $Cu^{1+}$ ,  $Cu^{2+}$ ,  $Fe^{2+}$ ,  $Fe^{3+}$ ,  $Mn^{3+}$ ,  $Mn^{4+}$ ,  $Ni^{2+}$  lead to the introduction of magnetism in  $NH_4MPO_4 \cdot H_2O$  powders. We believed that transition metal is a originate of magnetic properties observed in the samples.

The XPS spectra of P 2p region of  $NH_4MPO_4 \cdot H_2O$  powder (M = Mg, Co, Fe, Mn, Ni, Zn, Cu) are shown in Figure 4.18. The strong peak of P 2p are observed in sample  $NH_4MPO_4 \cdot H_2O$  powder (M = Co, Cu, Fe, Mn, Ni, Cu, Zn). This result indicates that rich of P in the sample, which P is the element that plants need.

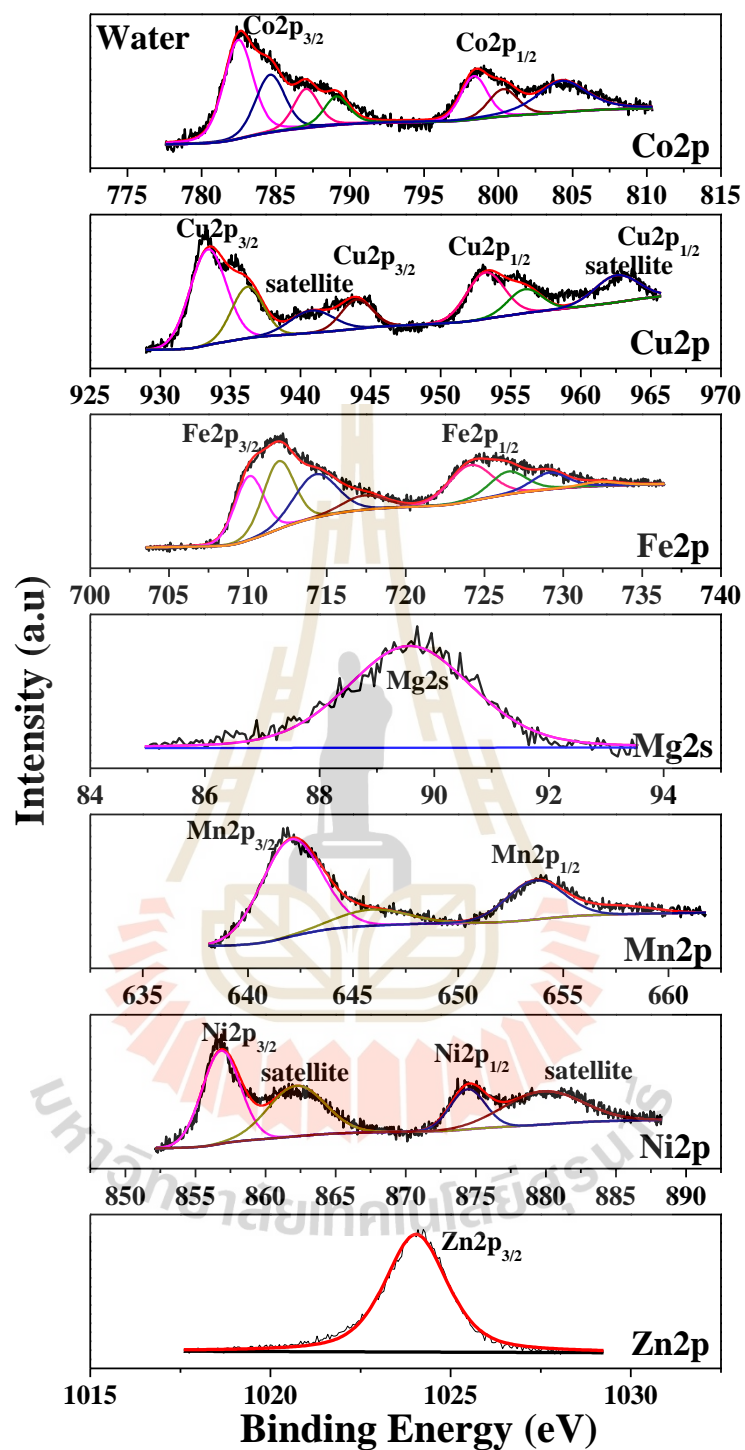
The XPS spectra of O 1s region of  $NH_4MPO_4 \cdot H_2O$  powders (M = Mg, Co, Fe, Mn, Ni, Zn, Cu) are shown in Figure 4.19. The O1s peaks of all samples can be divided into three peaks at approximately ~529 eV, ~531 eV, and ~533 eV. The binding energy at ~529.9 eV has corresponded to  $O^{2-}$  ions on the metal oxide structure. The binding energy at ~531.1 eV can be attributed to  $O^{2-}$  ions in the lattice structure. The binding energy at ~533.2 eV can be assigned to the bound oxygen, such as hydroxyl group on the surface (Caglar and Yakuphanoglu, 2012). The observation of the hydroxyl group in the O 1s XPS spectra supports the results obtained from XRD results because the hydroxyl group can be created  $H_2O$  in structure. This observed  $H_2O$  is the origin of fertilizer release in samples.



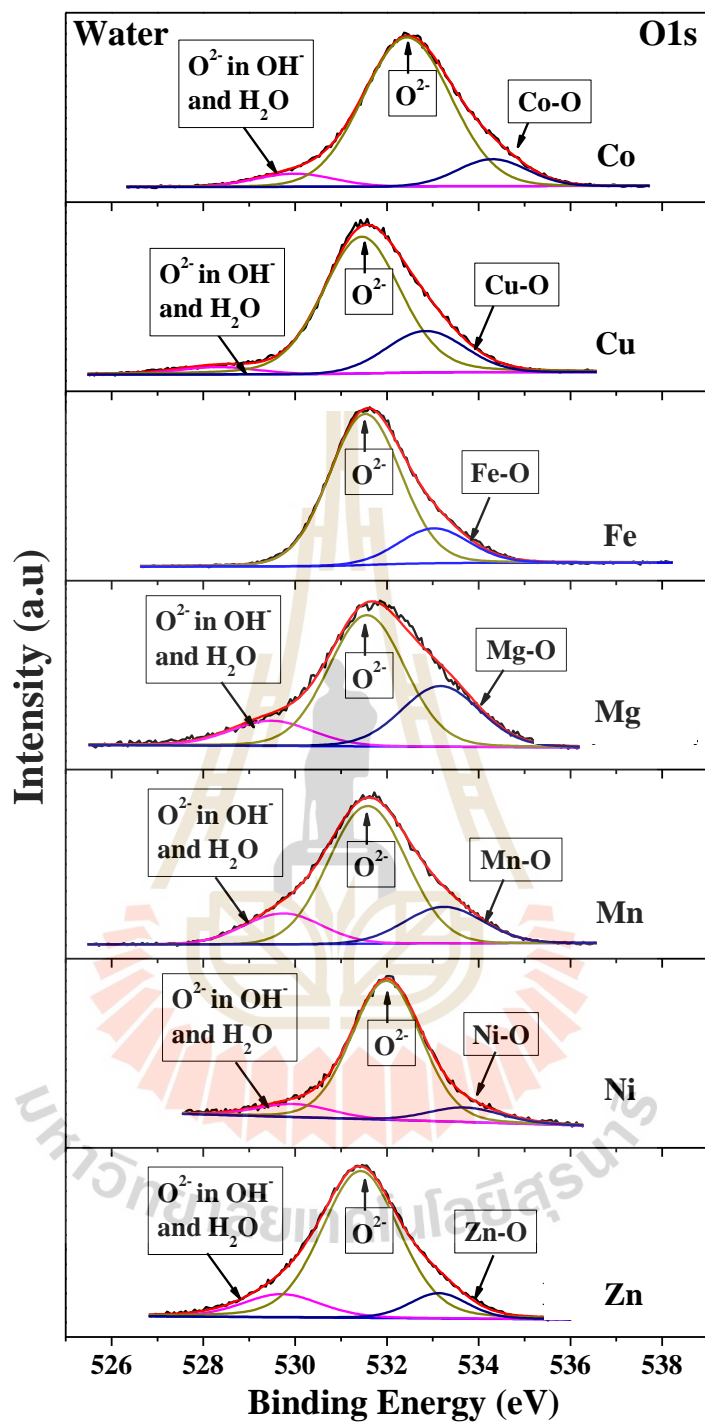
**Figure 4.15** XPS spectra of  $\text{NH}_4\text{MPO}_4 \cdot \text{H}_2\text{O}$  (M = Mg, Co, Fe, Mn, Ni, Zn, Cu) samples with the survey scan mode.



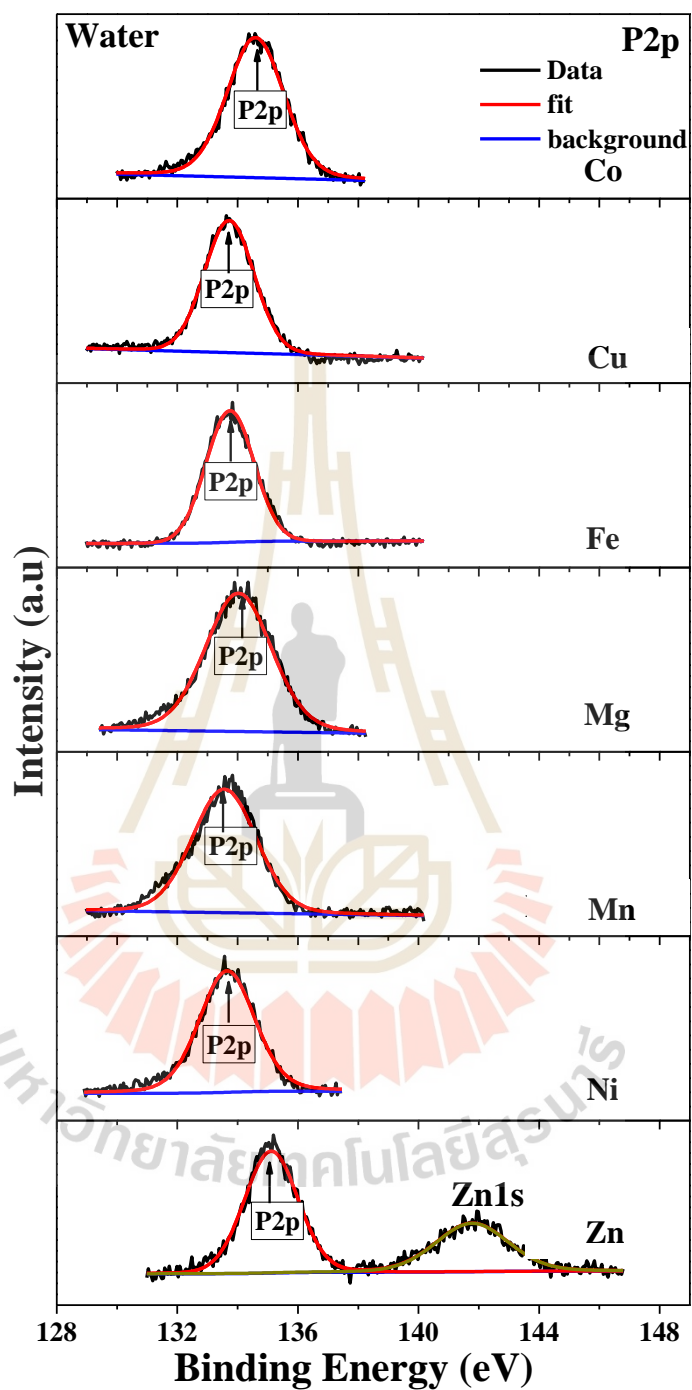
**Figure 4.16** Curve-fitting for N1s and XPS spectra of  $\text{NH}_4\text{MPO}_4\cdot\text{H}_2\text{O}$  (M = Mg, Co, Fe, Mn, Ni, Zn, Cu) samples.



**Figure 4.17** Curve-fitting for Co2p, Cu2p, Fe2p, Mg2s, Mn2p, Ni2p, Zn2p and XPS spectra of  $\text{NH}_4\text{MPO}_4 \cdot \text{H}_2\text{O}$  (M = Mg, Co, Fe, Mn, Ni, Zn, Cu) samples.



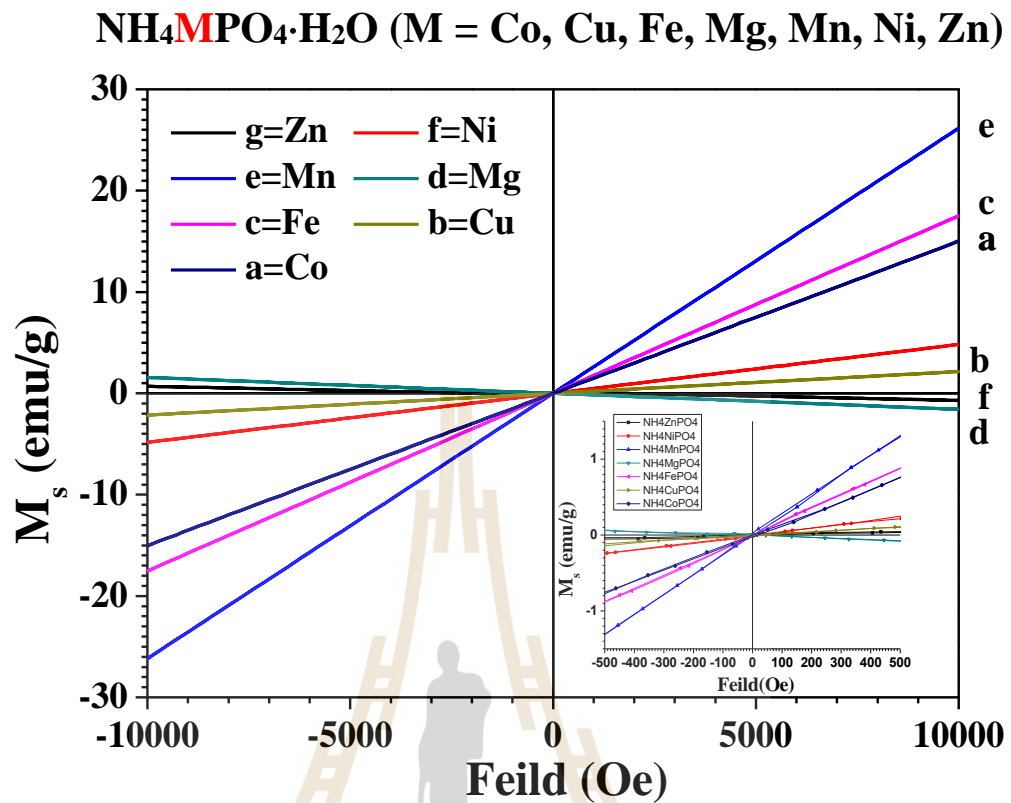
**Figure 4.18** Curve-fitting for O1s and XPS spectra of  $\text{NH}_4\text{MPO}_4 \cdot \text{H}_2\text{O}$  ( $M = \text{Mg, Co, Fe, Mn, Ni, Zn, Cu}$ ) samples.



**Figure 4.19** Curve-fitting for P2p and XPS spectra of  $\text{NH}_4\text{MPO}_4\cdot\text{H}_2\text{O}$  ( $M = \text{Mg}, \text{Co}, \text{Fe}, \text{Mn}, \text{Ni}, \text{Zn}, \text{Cu}$ ) samples.

#### 4.1.7 The magnetic properties of the $\text{NH}_4\text{MPO}_4\cdot\text{H}_2\text{O}$ (M = Mg, Co, Fe, Mn, Ni, Zn, Cu) samples

The magnetic properties of the samples were obtained by VSM measurement at room temperature as shown in Figure 4.20. The coercivity ( $H_c$ ) of all the prepared  $\text{NH}_4\text{MPO}_4\cdot\text{H}_2\text{O}$  (M = Co, Fe, Mn, Ni, Cu,) samples was close to 0 Oe, implying antiferromagnetic behaviour (López-Quintela and Rivas, 1993, Bica, 1999, Rezlescu, Rezlescu, Popa and Rezlescu, 1999). For  $\text{NH}_4\text{MgPO}_4\cdot\text{H}_2\text{O}$  and  $\text{NH}_4\text{ZnPO}_4$ , magnetization values decrease with increasing external magnetic field then show diamagnetic behaviour. The magnetization values at 10kOe were obtained to be 14.98, 2.14, 17.52, 26.17 and 4.83 emu/g for the prepared  $\text{NH}_4\text{MPO}_4\cdot\text{H}_2\text{O}$  (M = Co, Cu, Fe, Mn, Ni) samples, respectively. Clearly, the results indicate that the magnetization value depends on the oxidation state transition metals in the structure correspond to XPS and XAS results. These occurrences of antiferromagnetism can be described by a superexchange mechanism, concerning the transfer of an electron between neighbouring  $\text{M}^{2+}\text{-O-M}^{2+}$  ions (Touaiher et al., 2001, Koo and Whangbo, 2008).

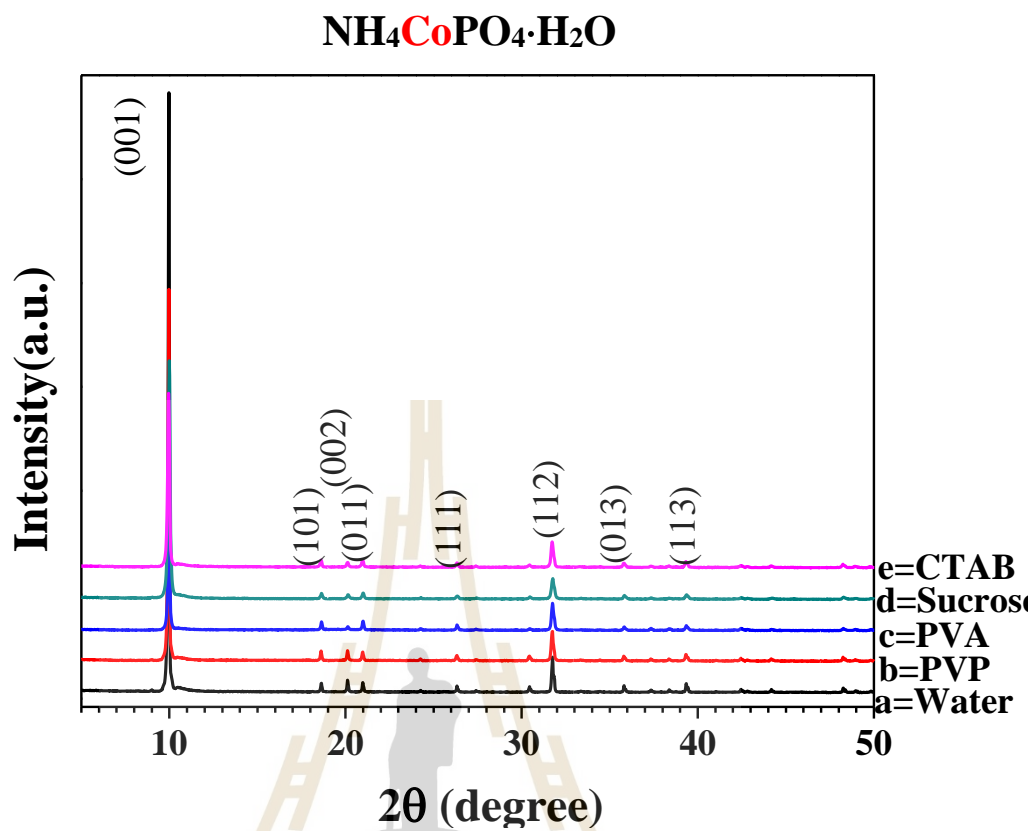


**Figure 4.20** The specific magnetization as a function of field, measured at 20 °C of the  $\text{NH}_4\text{MPO}_4 \cdot \text{H}_2\text{O}$  (M= Mg, Co, Fe, Mn, Ni, Zn, Cu) powder.

## 4.2 Effect of solvent on $\text{NH}_4\text{MPO}_4\cdot\text{H}_2\text{O}$ (M= Mg, Co, Fe, Mn, Ni, Zn, Cu) structures

### 4.2.1 X-ray diffraction (XRD) analysis of $\text{NH}_4\text{MPO}_4\cdot\text{H}_2\text{O}$ (M= Mg, Co, Fe, Mn, Ni, Zn, Cu) samples within water, PVP, PVA, Sucrose and CTAB solution

Figure 4.21 shows XRD patterns of the prepared samples. The XRD patterns confirm the formation orthorhombic structure within space group  $Pmn2_1$  for the  $\text{NH}_4\text{CoPO}_4\cdot\text{H}_2\text{O}$  sample. The diffraction peaks for  $\text{NH}_4\text{CoPO}_4\cdot\text{H}_2\text{O}$  sample mainly consist of (001), (101), (002), (011), (111), (112), (013) and (113) planes, which corresponds to the standard data (JCPDS NO.21-0793). The prepared samples have orthorhombic without the presence of any other phase impurities. The unit-cell parameters (a, b, and c), cell volume (V), expected profile residual ( $R_{exp}$ ), profile residual ( $R_p$ ), weighted profile residual ( $R_{wp}$ ), goodness of fit (GOF) values of all  $\text{NH}_4\text{CoPO}_4\cdot\text{H}_2\text{O}$  samples were calculated by Rietveld refinement unit cell analysis using TOPAS software and the values of these parameters are summarized in Table 4.2. From the XRD result, the medium solution such as water, PVP, PVA, Sucrose and CTAB cannot change phase structure.

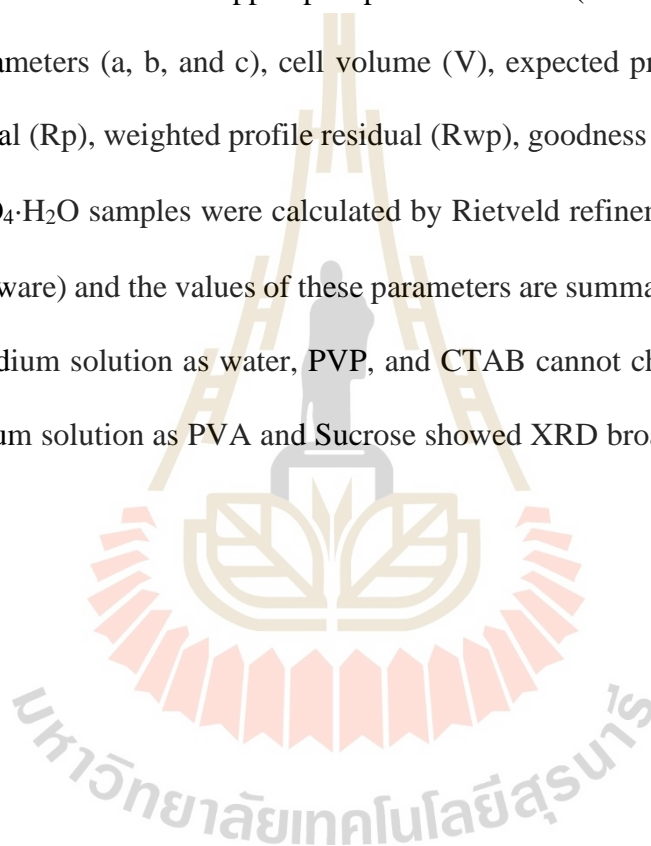


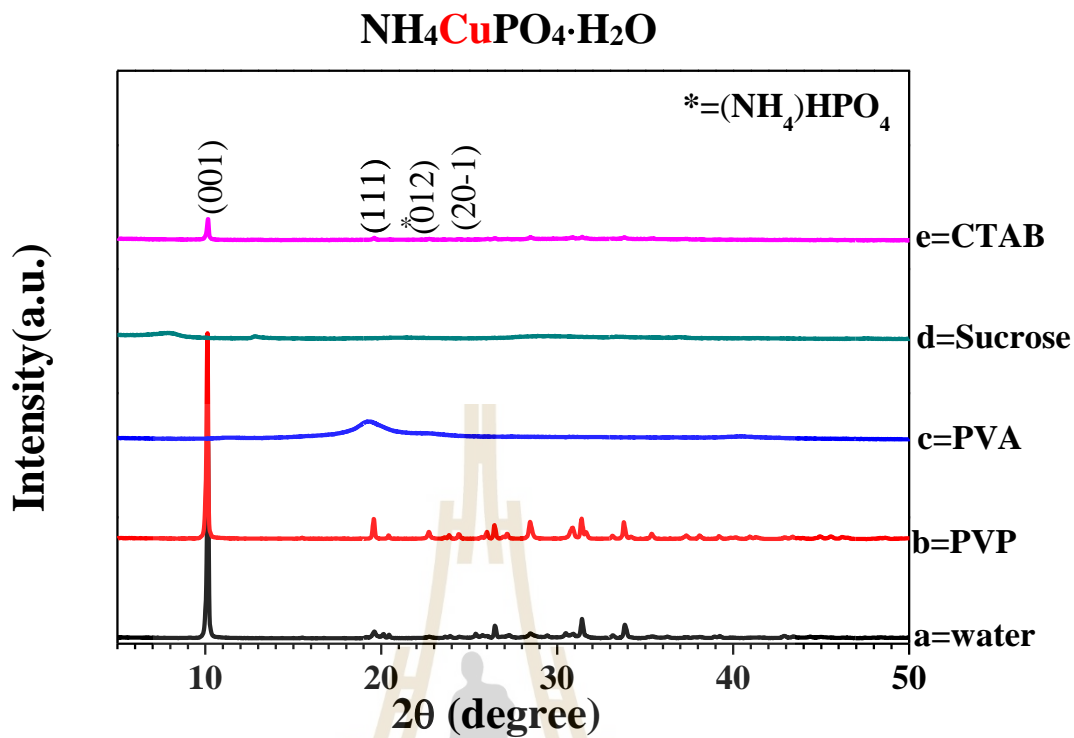
**Figure 4.21** XRD pattern of  $\text{NH}_4\text{CoPO}_4 \cdot \text{H}_2\text{O}$  powder prepared by chemical precipitation method with (a) water (b) PVP (c) PVA (d) Sucrose and (e) CTAB.

**Table 4.2** Lattice parameter (a, b, and c),  $\beta$  angle, cell volume (V), Rietveld refinement parameters ( $R_p$ ,  $R_{exp}$ ,  $R_{wp}$  and GOF) of the  $NH_4CoPO_4 \cdot H_2O$  powders prepared by chemical precipitation method and different medium condition (Water, PVP, PVA, Sucrose and CTAB).

Parameter	$NH_4CoPO_4 \cdot H_2O$ samples				
	Water	PVP	PVA	Sucrose	CTAB
Lattice parameters ( $\text{\AA}$ )					
a	5.62	5.63	5.63	5.63	5.63
b	8.77	8.77	8.78	8.77	8.78
c	4.80	4.80	4.80	4.81	4.80
Cell volume ( $10^6 \text{pm}^3$ )	236.10	237.33	237.48	237.38	237.40
Space group	Pmn21	Pmn21	Pmn21	Pmn21	Pmn21
$R_p$ (%)	5.28	4.29	3.35	3.45	3.45
$R_{exp}$ (%)	2.36	2.39	2.57	2.48	2.42
$R_{wp}$ (%)	8.51	6.43	4.48	4.81	4.93
GOF (%)	3.60	2.69	1.75	1.94	2.04

Figure 4.22 shows XRD patterns of the prepared all samples. The XRD patterns reveal the formation monoclinic structure within space group P21 for  $\text{NH}_4\text{CuPO}_4\cdot\text{H}_2\text{O}$  sample. The diffraction peaks for  $\text{NH}_4\text{CuPO}_4\cdot\text{H}_2\text{O}$  sample mainly consist of (001), (111), (012), and (20-1) planes, which correspond to the standard data. The prepared samples have monoclinic without the presence of any other phase impurities. The ammonium copper phosphate structure (JCPDS NO.89-1303). The unit-cell parameters (a, b, and c), cell volume (V), expected profile residual ( $R_{\text{exp}}$ ), profile residual ( $R_p$ ), weighted profile residual ( $R_{\text{wp}}$ ), goodness of fit (GOF) values of all  $\text{NH}_4\text{CuPO}_4\cdot\text{H}_2\text{O}$  samples were calculated by Rietveld refinement unit cell analysis (TOPAS software) and the values of these parameters are summarized in Table 4.3. By using the medium solution as water, PVP, and CTAB cannot change phase structure. For the medium solution as PVA and Sucrose showed XRD broad peak of amorphous structure.



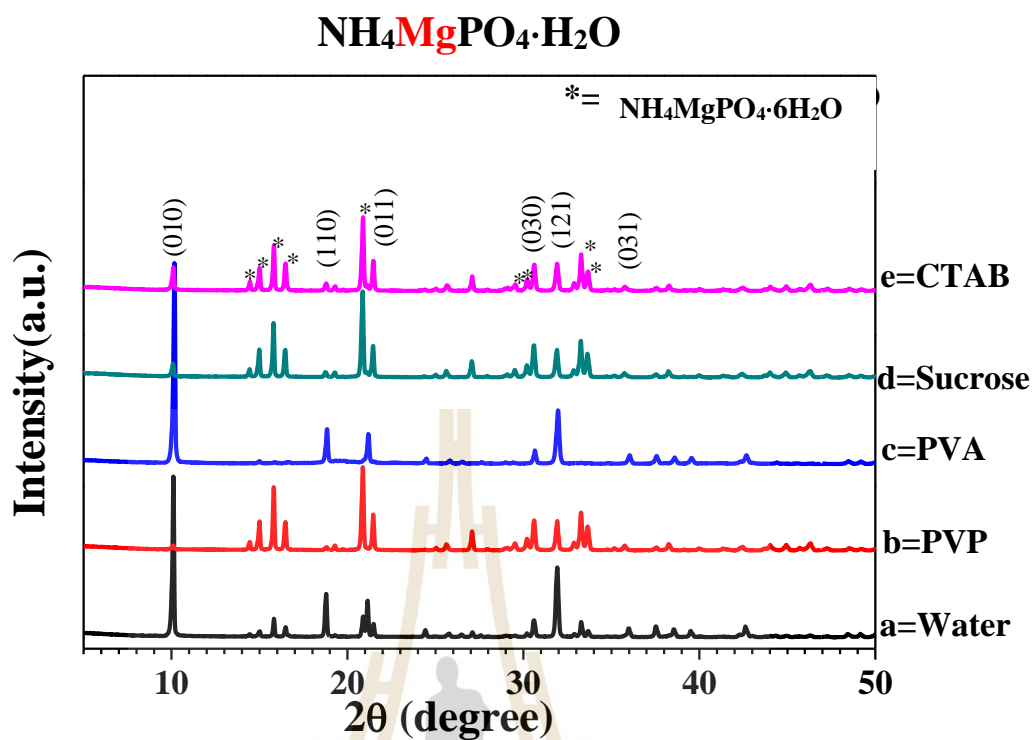


**Figure 4.22** XRD pattern of NH<sub>4</sub>CuPO<sub>4</sub>·H<sub>2</sub>O powder prepared by chemical precipitation method with (a) water (b) PVP (c) PVA (d) Sucrose and (e) CTAB.

**Table 4.3** Lattice parameter (a, b, and c),  $\beta$  angle, cell volume (V), Rietveld refinement parameters ( $R_p$ ,  $R_{exp}$ ,  $R_{wp}$  and GOF) of the  $NH_4CuPO_4 \cdot H_2O$  powder prepared by chemical precipitation method and different medium condition (Water, PVP, PVA, Sucrose and CTAB).

Parameter	$NH_4CuPO_4 \cdot H_2O$ samples				
	Water	PVP	PVA	Sucrose	CTAB
Lattice parameters ( $\text{\AA}$ )					
a	7.42	7.28	-	-	7.46
b	7.53	7.52	-	-	7.54
c	8.66	8.70	-	-	8.66
Beta	94.44	94.09	-	-	92.66
Cell volume ( $10^6 \text{pm}^3$ )	482.56	475.19	-	-	486.17
Space group	P121/a1	P121/a1	-	-	P121/a1
$R_p$ (%)	8.24	12.21	-	-	3.00
$R_{exp}$ (%)	2.47	2.42	-	-	2.33
$R_{wp}$ (%)	11.86	19.20	-	-	4.07
GOF (%)	4.79	7.92	-	-	1.75

Figure 4.23 shows XRD patterns of the prepared all samples. The XRD patterns reveal the formation orthorhombic structure within space group Pmmn for the  $\text{NH}_4\text{MgPO}_4\cdot\text{H}_2\text{O}$  samples. The diffraction peaks the  $\text{NH}_4\text{MgPO}_4\cdot\text{H}_2\text{O}$  samples mainly consist of (010), (110), (011), (030), (121) and (031) planes, which correspond to the standard data. The prepared samples have orthorhombic and the presence of other phase impurities as  $\text{NH}_4\text{MgPO}_4\cdot 6\text{H}_2\text{O}$ . The ammonium magnesium phosphate structure (JCPDS NO.36-1491). The unit-cell parameters (a, b, and c), cell volume (V), expected profile residual ( $R_{\text{exp}}$ ), profile residual ( $R_p$ ), weighted profile residual ( $R_{\text{wp}}$ ), goodness of fit (GOF) values of all  $\text{NH}_4\text{MgPO}_4\cdot\text{H}_2\text{O}$  samples were calculated by Rietveld refinement unit cell analysis (TOPAS software) and the values of these parameters are summarized in Table 4.4. By using the medium solution as water, PVP, PVA, Sucrose and CTAB can change phase structure to the  $\text{NH}_4\text{MgPO}_4\cdot 6\text{H}_2\text{O}$ . Table 4.5 reveals calculated percentage of  $\text{NH}_4\text{MgPO}_4\cdot\text{H}_2\text{O}$  structure as water (75.26%), PVP (3.25%), PVA (87.51%), Sucrose (8.61%) and CTAB (9.15%).

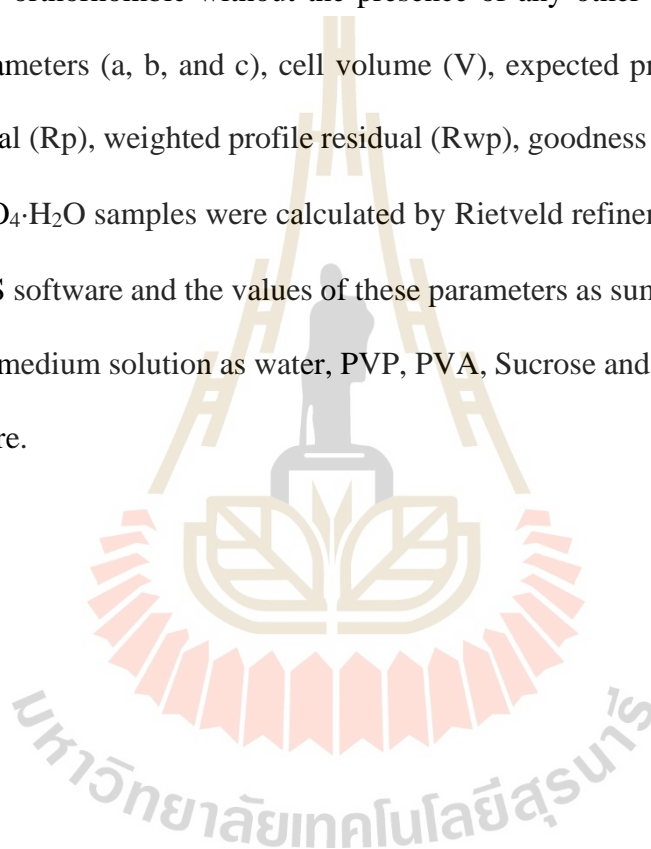


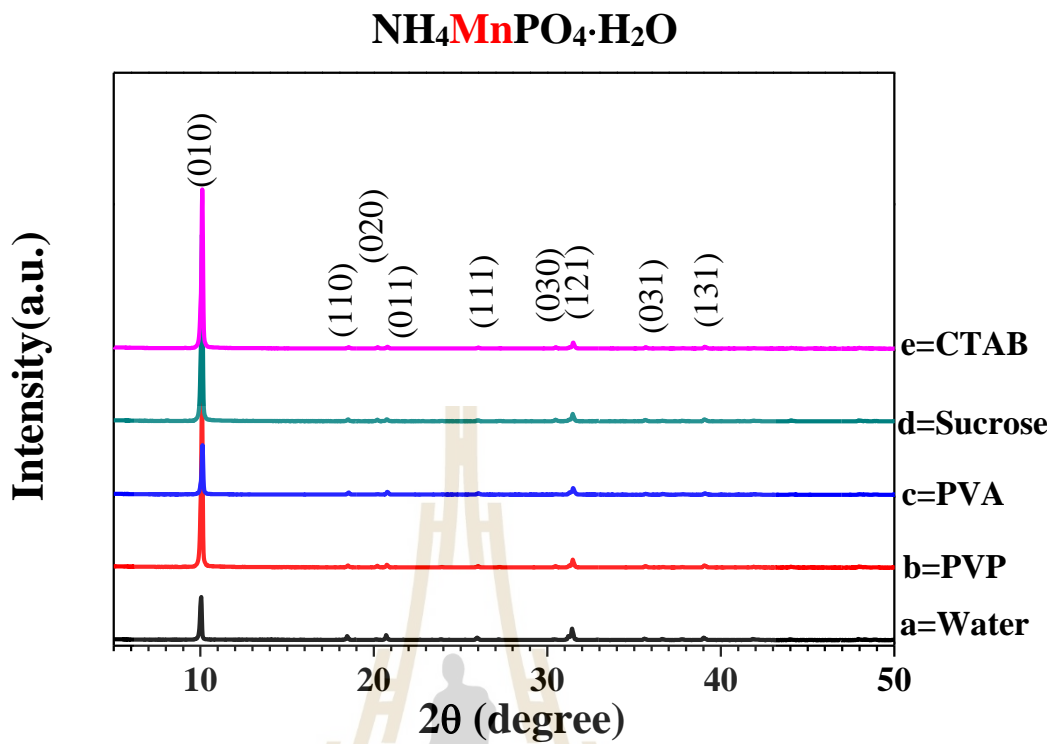
**Figure 4.23** XRD pattern of NH<sub>4</sub>MgPO<sub>4</sub>·H<sub>2</sub>O powder prepared by chemical precipitation method with (a) water (b) PVP (c) PVA (d) Sucrose and (e) CTAB.

**Table 4.4** Lattice parameters (a, b, and c), cell volume (V), Rietveld refinement parameters ( $R_p$ ,  $R_{exp}$ ,  $R_{wp}$  and GOF) of the  $NH_4MgPO_4 \cdot H_2O$  powder with different medium condition (Water, PVP, PVA, Sucrose and CTAB).

Parameter	$NH_4MgPO_4 \cdot H_2O$ samples				
	Water	PVP	PVA	Sucrose	CTAB
Struvite (%)	24.74	96.75	12.49	91.39	90.85
Lattice parameters (Å)					
a	6.95	6.95	6.87	6.95	6.95
b	6.14	6.14	6.10	6.14	6.14
c	11.21	11.21	11.46	11.22	11.22
Cell volume ( $10^6 pm^3$ )	478.09	478.79	480.14	478.98	478.81
Space group	Pmn21	Pmn21	Pmn21	Pmn21	Pmn21
Dittmarite (%)	75.26	3.25	87.51	8.61	9.15
Lattice parameters (Å)					
a	5.61	5.61	5.62	5.62	5.62
b	8.77	8.77	8.77	8.77	8.77
c	4.79	4.85	4.80	4.80	4.79
Cell volume ( $10^6 pm^3$ )	236.00	238.47	236.51	236.25	236.13
Space group	Pm21n	Pm21n	Pm21n	Pm21n	Pm21n
$R_p$ (%)	8.49	8.93	9.02	8.85	8.90
$R_{exp}$ (%)	4.25	4.04	4.12	3.99	4.08
$R_{wp}$ (%)	11.36	11.31	11.82	11.05	11.79
GOF (%)	2.67	2.80	2.87	2.77	2.89

Figure 4.24 shows the XRD patterns of the prepared all samples. The XRD patterns confirm the formation orthorhombic structure within space group Pmnm for the  $\text{NH}_4\text{MnPO}_4 \cdot \text{H}_2\text{O}$  sample. The diffraction peaks for  $\text{NH}_4\text{MnPO}_4 \cdot \text{H}_2\text{O}$  sample mainly consists of (010), (110), (020), (011), (111), (030), (121), (031) and (131) planes, which conform to the standard data (JCPDS NO.50-0554). The prepared samples have orthorhombic without the presence of any other phase impurities. The unit-cell parameters (a, b, and c), cell volume (V), expected profile residual (R<sub>exp</sub>), profile residual (R<sub>p</sub>), weighted profile residual (R<sub>wp</sub>), goodness of fit (GOF) values of all  $\text{NH}_4\text{MnPO}_4 \cdot \text{H}_2\text{O}$  samples were calculated by Rietveld refinement unit cell analysis using TOPAS software and the values of these parameters as summarized in Table 4.5. By using the medium solution as water, PVP, PVA, Sucrose and CTAB cannot change phase structure.



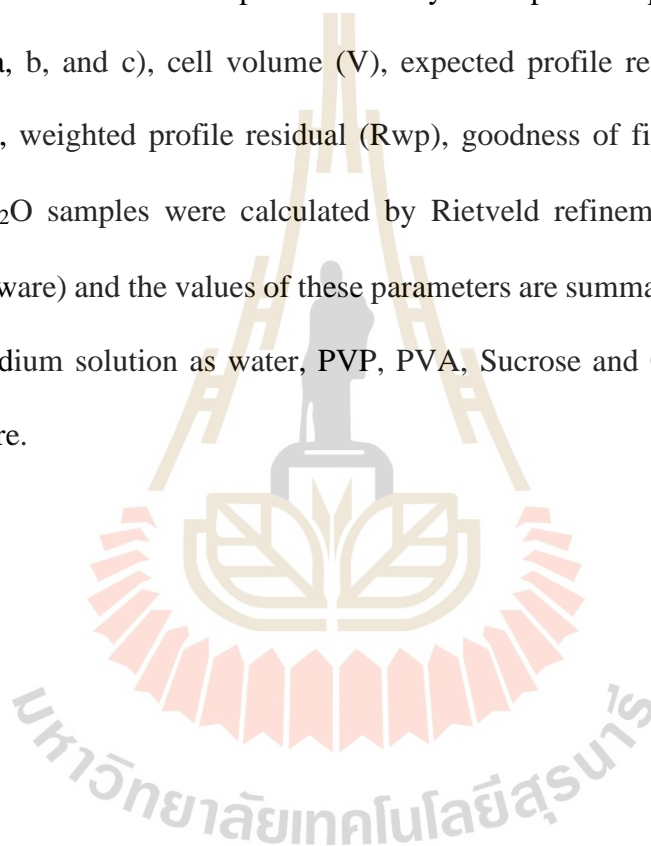


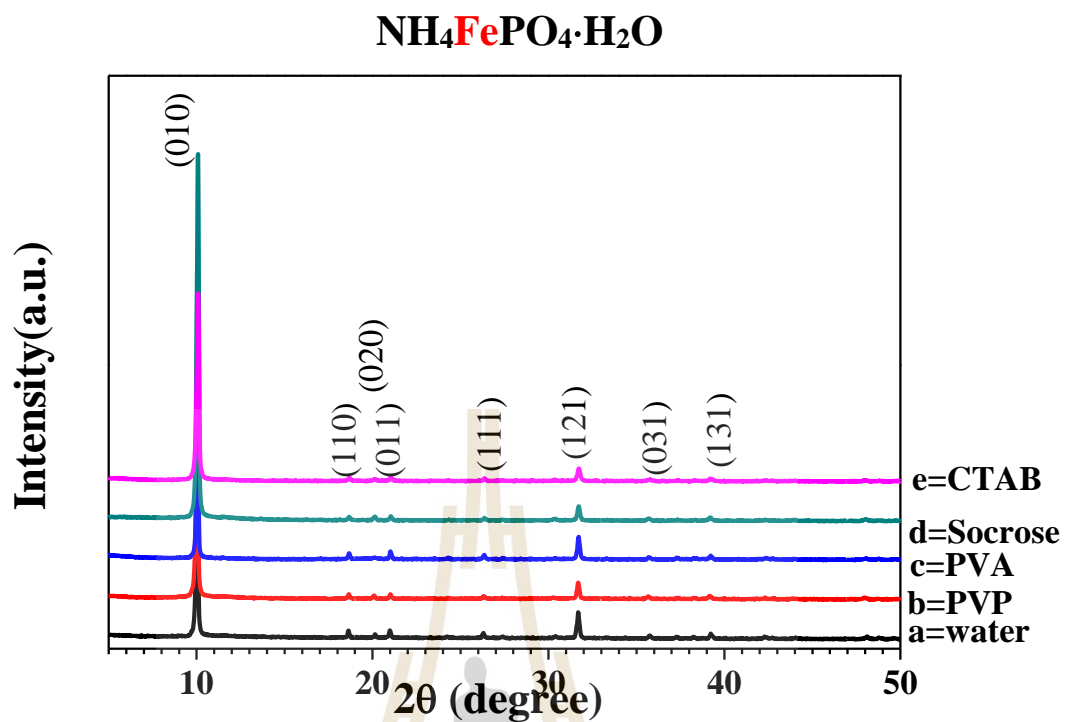
**Figure 4.24** XRD pattern of  $\text{NH}_4\text{MnPO}_4\cdot\text{H}_2\text{O}$  powders prepared by chemical precipitation method with (a) water (b) PVP (c) PVA (d) Sucrose and (e) CTAB.

**Table 4.5** Lattice parameters (a, b, and c), cell volume (V), Rietveld refinement parameters ( $R_p$ ,  $R_{exp}$ ,  $R_{wp}$  and GOF) of the  $NH_4MnPO_4 \cdot H_2O$  powder prepared by chemical precipitation method and different medium condition (Water, PVP, PVA, Sucrose and CTAB).

Parameter	$NH_4MnPO_4 \cdot H_2O$ samples				
	Water	PVP	PVA	Sucrose	CTAB
Lattice parameters (Å)					
a	5.73	5.73	5.73	5.73	5.73
b	8.82	8.80	8.81	8.82	8.81
c	4.90	4.91	4.91	4.90	4.91
Cell volume ( $10^6 pm^3$ )	247.78	247.62	248.12	248.36	247.66
Space group	Pmnm	Pmnm	Pmnm	Pmnm	Pmnm
$R_p$ (%)	2.85	3.99	3.00	5.81	4.07
$R_{exp}$ (%)	2.23	2.35	2.64	2.32	2.52
$R_{wp}$ (%)	4.02	5.71	3.94	8.39	5.69
GOF (%)	1.80	2.43	1.49	3.61	2.25

Figure 4.25 shows XRD patterns of the prepared all samples. The XRD patterns show the formation orthorhombic structure within space group Pmmn for  $\text{NH}_4\text{FePO}_4\cdot\text{H}_2\text{O}$  sample. The diffraction peaks for  $\text{NH}_4\text{FePO}_4\cdot\text{H}_2\text{O}$  sample mainly consists of (010), (110), (020), (011), (111), (030), (121), (031) and (131) planes, which is in agreement with the standard data (JCPDS NO.45-0424). The prepared samples have orthorhombic without the presence of any other phase impurities. The unit-cell parameters (a, b, and c), cell volume (V), expected profile residual ( $R_{\text{exp}}$ ), profile residual ( $R_{\text{p}}$ ), weighted profile residual ( $R_{\text{wp}}$ ), goodness of fit (GOF) values of all  $\text{NH}_4\text{FePO}_4\cdot\text{H}_2\text{O}$  samples were calculated by Rietveld refinement unit cell analysis (TOPAS software) and the values of these parameters are summarized in Table 4.6. By using the medium solution as water, PVP, PVA, Sucrose and CTAB cannot change phase structure.



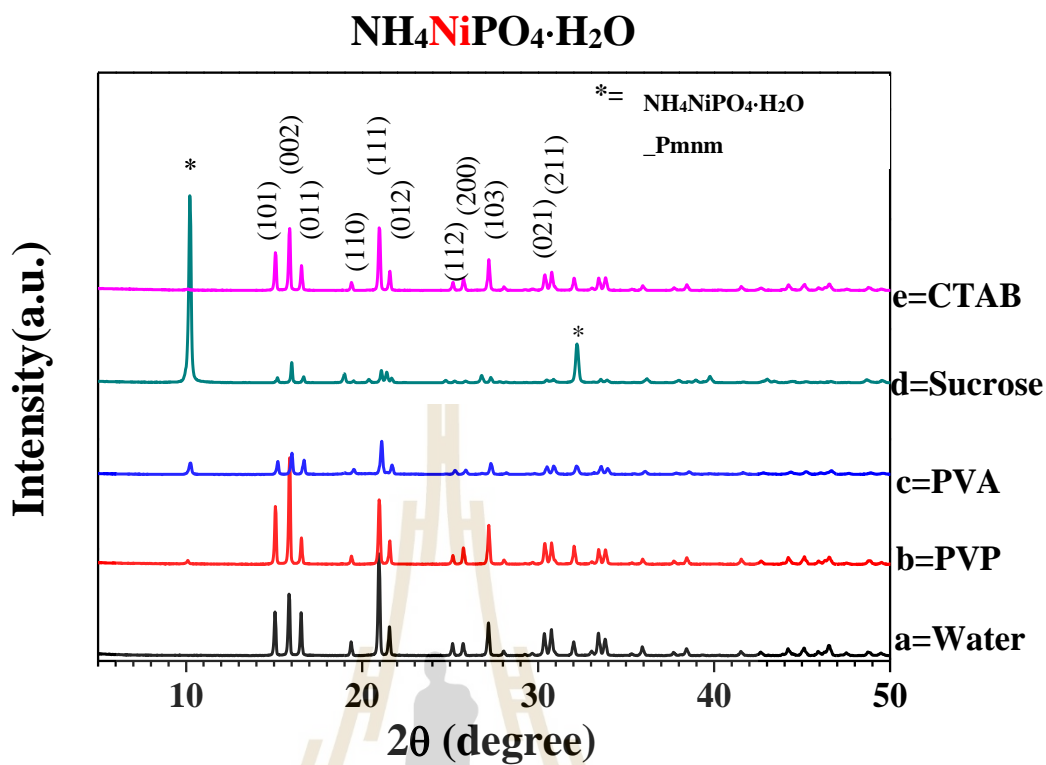


**Figure 4.25** XRD pattern of NH<sub>4</sub>FePO<sub>4</sub>·H<sub>2</sub>O powders prepared by chemical precipitation method with (a) water (b) PVP (c) PVA (d) Sucrose and (e) CTAB.

**Table 4.6** Lattice parameters (a, b, and c), cell volume (V), Rietveld refinement parameters ( $R_p$ ,  $R_{exp}$ ,  $R_{wp}$  and GOF) of the  $NH_4FePO_4 \cdot H_2O$  powder prepared by chemical precipitation method and different medium condition (Water, PVP, PVA, Sucrose and CTAB).

Parameter	$NH_4FePO_4 \cdot H_2O$ samples				
	Water	PVP	PVA	Sucrose	CTAB
Lattice parameters ( $\text{\AA}$ )					
a	5.57	5.66	5.66	5.66	5.65
b	8.82	8.87	8.83	8.85	8.83
c	4.89	4.82	4.83	4.83	4.83
Cell volume ( $10^6 \text{pm}^3$ )	240.52	241.84	241.27	241.76	240.87
Space group	Pmn21	Pmn21	Pmn21	Pmn21	Pmn21
$R_p$ (%)	2.81	2.37	2.14	3.23	2.77
$R_{exp}$ (%)	1.86	1.93	2.00	2.08	2.21
$R_{wp}$ (%)	4.45	3.25	2.84	4.47	3.81
GOF (%)	2.39	1.69	1.42	2.15	1.72

Figure 4.26 shows the XRD patterns of the prepared all samples. The XRD patterns confirm the formation orthorhombic structure within space group Pmn21 for  $\text{NH}_4\text{NiPO}_4 \cdot 6\text{H}_2\text{O}$  sample. The diffraction peaks for  $\text{NH}_4\text{NiPO}_4 \cdot 6\text{H}_2\text{O}$  sample mainly consists of (101), (002), (011), (110), (111), (012), (112), (200), (103), (021) and (211) planes, which conform with the standard data (JCPDS NO.86-1866). The prepared samples have orthorhombic and the presence of other phase impurities as  $\text{NH}_4\text{NiPO}_4 \cdot \text{H}_2\text{O}$ . The unit-cell parameters (a, b, and c), cell volume (V), expected profile residual ( $R_{\text{exp}}$ ), profile residual ( $R_p$ ), weighted profile residual ( $R_{\text{wp}}$ ), goodness of fit (GOF) values of all  $\text{NH}_4\text{NiPO}_4 \cdot 6\text{H}_2\text{O}$  samples were calculated by Rietveld refinement unit cell analysis (TOPAS software) and the values of these parameters are summarized in Table 4.7. By using of the medium solution as PVP, PVA, Sucrose and CTAB can change phase structure to  $\text{NH}_4\text{NiPO}_4 \cdot \text{H}_2\text{O}$ . From table 4.5 showed calculate percentage of  $\text{NH}_4\text{NiPO}_4 \cdot 6\text{H}_2\text{O}$  structure as water (100%), PVP (97.43%), PVA (86.77%), Sucrose (24.00%) and CTAB (97.22%).

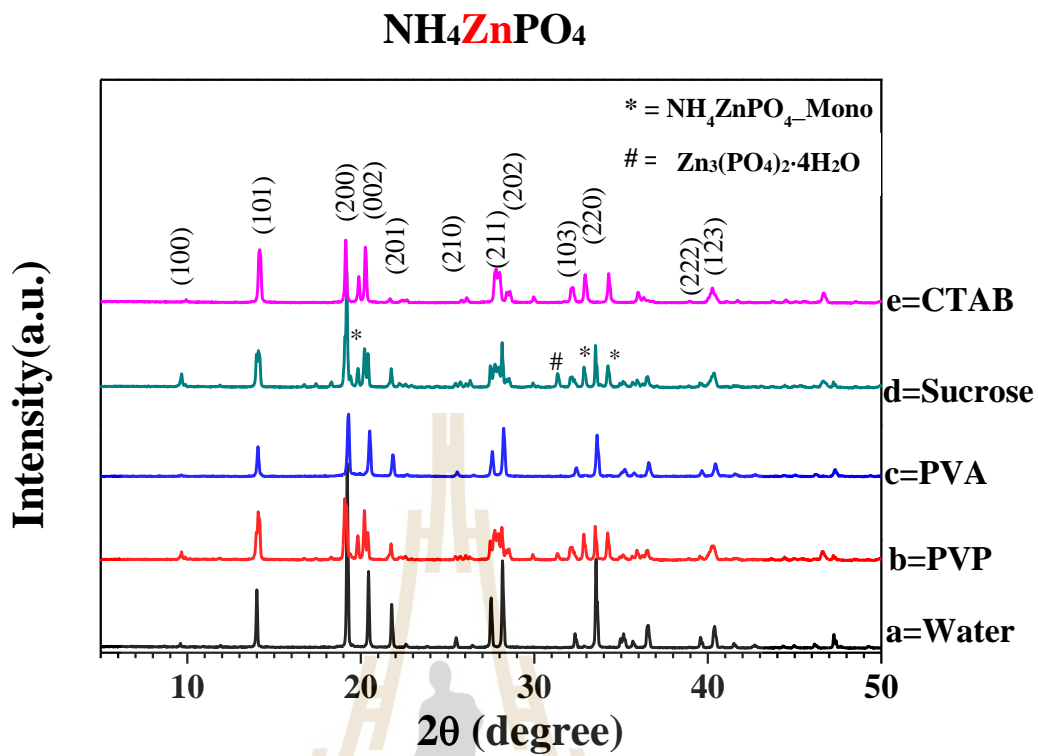


**Figure 4.26** XRD pattern of  $\text{NH}_4\text{NiPO}_4 \cdot 6\text{H}_2\text{O}$  powders prepared by chemical precipitation method with (a) water (b) PVP (c) PVA (d) Sucrose and (e) CTAB.

**Table 4.7** Lattice parameters (a, b, and c), cell volume (V), Rietveld refinement parameters ( $R_p$ ,  $R_{exp}$ ,  $R_{wp}$  and GOF) of the  $NH_4NiPO_4 \cdot 6H_2O$  powders prepared by chemical precipitation method with water, PVP, PVA, Sucrose and CTAB).

Parameter	$NH_4NiPO_4 \cdot 6H_2O$ samples				
	Water	PVP	PVA	Sucrose	CTAB
$NH_4NiPO_4 \cdot 6H_2O$ (%)	100	97.43	86.77	24.00	97.22
Lattice parameters (Å)					
a	6.92	6.92	6.92	6.92	6.92
b	6.11	6.11	6.11	6.11	6.11
c	11.57	11.17	11.18	11.17	11.17
Cell volume ( $10^6 pm^3$ )	472.23	4723.8	472.69	472.52	472.19
Space group	Pmn21	Pmn21	Pmn21	Pmn21	Pmn21
$NH_4NiPO_4 \cdot H_2O$ (%)	0	2.57	13.23	76.00	2.78
Lattice parameters (Å)					
a	-	5.59	5.57	5.57	5.62
b	-	8.77	8.77	8.77	8.78
c	-	4.73	4.75	4.75	4.68
Cell volume ( $10^6 pm^3$ )	-	232.32	232.21	232.36	231.05
Space group	Pmnm	Pmnm	Pmnm	Pmnm	Pmnm
$R_p$ (%)	5.27	5.63	6.38	5.74	6.91
$R_{exp}$ (%)	2.72	2.82	4.08	3.67	3.33
$R_{wp}$ (%)	7.04	7.38	8.14	7.40	9.16
GOF (%)	2.59	2.62	2.00	2.02	2.75

Figure 4.27 shows XRD patterns of the prepared all samples. These XRD patterns shows the formation hexagonal structure within space group  $Pm\bar{n}2_1$  for  $NH_4ZnPO_4$  sample. The diffraction peaks for  $NH_4ZnPO_4$  sample mainly consists of (100), (101), (200), (002), (201), (210), (211), (202), (103), (220), (222) and (123) planes, which is in agreement with the standard data. The prepared samples have hexagonal and the presence of other phase impurities as  $NH_4ZnPO_4$  monoclinic structure. The ammonium magnesium phosphate structure (JCPDS NO.89-6315). The unit-cell parameters (a, b, and c), cell volume (V), expected profile residual ( $R_{exp}$ ), profile residual ( $R_p$ ), weighted profile residual ( $R_{wp}$ ), goodness of fit (GOF) values of all  $NH_4ZnPO_4$  samples were calculated by Rietveld refinement unit cell analysis (TOPAS software) and the values of these parameters are summarized in Table 4.8. Using of the medium solution as PVP, Sucrose and CTAB can change phase structure to  $NH_4ZnPO_4$  monoclinic structure. For CTAB condition showed XRD pattern only  $NH_4ZnPO_4$  monoclinic structure.



**Figure 4.27** XRD pattern of NH<sub>4</sub>ZnPO<sub>4</sub> powders prepared by chemical precipitation method with (a) water (b) PVP (c) PVA (d) Sucrose and (e) CTAB.

**Table 4.8** Lattice parameters (a, b, and c),  $\beta$  angle, cell volume (V), Rietveld refinement parameters ( $R_p$ ,  $R_{exp}$ ,  $R_{wp}$  and GOF) of the  $NH_4ZnPO_4$  powders prepared by chemical precipitation method and different medium condition (Water, PVP, PVA, Sucrose and CTAB).

Parameter	$NH_4ZnPO_4$ samples				
	Water	PVP	PVA	Sucrose	CTAB
Lattice parameters ( $\text{\AA}$ )					
a	10.67	10.69	10.69	10.69	8.79
b	10.67	10.69	10.69	10.69	5.45
c	8.71	8.71	8.71	8.71	8.96
beta (°)	90	90	90	90	90.34
Cell volume ( $10^6\text{pm}^3$ )	862.13	861.96	862.40	861.76	429.16
Space group	P63	P63	P63	P63	P21
$R_p$ (%)	4.67	3.84	3.77	4.39	3.03
$R_{exp}$ (%)	2.46	2.27	2.77	2.28	2.56
$R_{wp}$ (%)	6.66	5.94	5.03	6.02	3.88
GOF (%)	2.70	2.62	1.82	2.64	1.51

#### 4.2.2 Morphology of $\text{NH}_4\text{MPO}_4\cdot\text{H}_2\text{O}$ powder (M = Mg, Co, Fe, Mn, Ni, Zn, Cu) by SEM

Figure 4.28 shows the SEM image of the  $\text{NH}_4\text{CoPO}_4\cdot\text{H}_2\text{O}$  powder prepared with water, PVP, PVA, Sucrose and CTAB solution. The size and shape of the prepared  $\text{NH}_4\text{CoPO}_4\cdot\text{H}_2\text{O}$  were examined. Figure 4.28(a), (b), (c), (d) and (e) show SEM images of water, PVP, PVA, Sucrose and CTAB solution samples. SEM images of all samples almost completely consist of oblong plate structures, which are uniform with a width of 3–5  $\mu\text{m}$  and a length of 5–10  $\mu\text{m}$ . Figure 4.28(c) and (d) show the detailed morphology and size about 3–5  $\mu\text{m}$ . The PVA and Sucrose can reduce size of the  $\text{NH}_4\text{CoPO}_4\cdot\text{H}_2\text{O}$  but cannot reduce size to nanoparticle.

The SEM image of the  $\text{NH}_4\text{CuPO}_4\cdot\text{H}_2\text{O}$  powders prepared with water, PVP, PVA, Sucrose and CTAB solution as revealed in Figure 4.29. The size and shape of the prepared  $\text{NH}_4\text{CuPO}_4\cdot\text{H}_2\text{O}$  were examined. Figure 4.29(a) and (b) show SEM images of water and PVP solution samples almost completely consists of oblong plate structures, which are uniform with a width of 3  $\mu\text{m}$  and a length of 4  $\mu\text{m}$ . Figure 4.29(c), (d) and (f) show the detailed morphology and size about 50-100 nm.

Figure 4.30 shows the SEM image of the  $\text{NH}_4\text{MgPO}_4\cdot\text{H}_2\text{O}$  powders prepared with water, PVP, PVA and CTAB solution. Figure 4.30(a) and (b) show SEM images of water and PVP solution samples almost completely consists of oblong plate structures, which are uniform with a width of 3  $\mu\text{m}$  and a length of 4  $\mu\text{m}$ . Figure 4.30(c), (d) and (f) show the detailed morphology and size about 50-100 nm. The PVA, Sucrose and CTAB can reduce size of the  $\text{NH}_4\text{MgPO}_4\cdot\text{H}_2\text{O}$  to nanoparticle.

Figure 4.31 shows the SEM image of the  $\text{NH}_4\text{MnPO}_4\cdot\text{H}_2\text{O}$  powders prepared with water, PVP, PVA and CTAB solution. Figure 4.31(a) and (b) show SEM images of water and PVA solution samples that almost completely consists of oblong plate agglomerate like flower structures, which are uniform with a size of  $10\ \mu\text{m}$ . Figure 4.31(b), (c), (d) and (f) show the detailed morphology and size about  $1\text{--}10\ \mu\text{m}$ . The PVP, PVA, Sucrose and CTAB can reduce size of the  $\text{NH}_4\text{MnPO}_4\cdot\text{H}_2\text{O}$ .

Figure 4.32 shows the SEM image of the  $\text{NH}_4\text{FePO}_4\cdot\text{H}_2\text{O}$  powders prepared with water, PVP, PVA, Sucrose and CTAB solution. Figure 4.32(a), (b), (c), (d) and (e) show SEM images of water, PVP, PVA, Sucrose and CTAB solution samples. SEM images of all sample almost completely consists of oblong plate and include nanoparticle structures, which are uniform with a width of  $3\text{--}5\ \mu\text{m}$  and a length of  $5\text{--}10\ \mu\text{m}$ . Figure 4.28(c) show the detailed morphology size and about  $3\text{--}5\ \mu\text{m}$  and without nanoparticles. The water, PVP, PVA, Sucrose and CTAB solution cannot reduce size of the  $\text{NH}_4\text{FePO}_4\cdot\text{H}_2\text{O}$  but this cannot reduce size microplate to nanoparticle.

Figure 4.33 shows the SEM image of the  $\text{NH}_4\text{NiPO}_4\cdot\text{H}_2\text{O}$  powders prepared with water, PVP, PVA and CTAB solution. The size and shape of the prepared  $\text{NH}_4\text{NiPO}_4\cdot\text{H}_2\text{O}$  were examined by scanning electron microscopy Figure 4.33(a), (b), (c) and (d) shows SEM images of water, PVP, PVA and CTAB solution samples. SEM images of all sample almost completely consists of microparticles for morphology and size about  $2\text{--}5\ \mu\text{m}$ . The PVP, PVA and CTAB solution can change morphology to microplate particles but cannot reduce size to nanoparticle.

Figure 4.34 shows the SEM image of the  $\text{NH}_4\text{ZnPO}_4$  powders prepared with water, PVP, PVA and CTAB solution. Figure 4.32(a), (b), (c), (d) and (e) shows

SEM images of water, PVP, PVA, sucrose and CTAB solution samples. SEM images of all sample almost completely consists of microparticles for morphology and size about 0.4–10  $\mu\text{m}$ . The PVP, PVA sucrose and CTAB solution can change morphology of the  $\text{NH}_4\text{ZnPO}_4$  size to nanoparticle. This confirms that the ammonium zinc phosphate has different morphologies and sizes, which is in good agreement with XRD results. It can be seen in figure 3(a) that the micro-rods, which are obtained by using non-surfactant of water, formed due to their self-assembly (Harrison, Sobolev and Phillips, 2001). Although, the ion concentration profiles in water have defined by the speciation diagrams of phosphoric acid ( $\text{H}_3\text{PO}_4$ ) and ammonia solution. The chemical reaction of ammonium zinc phosphate has been represented by the following equation.

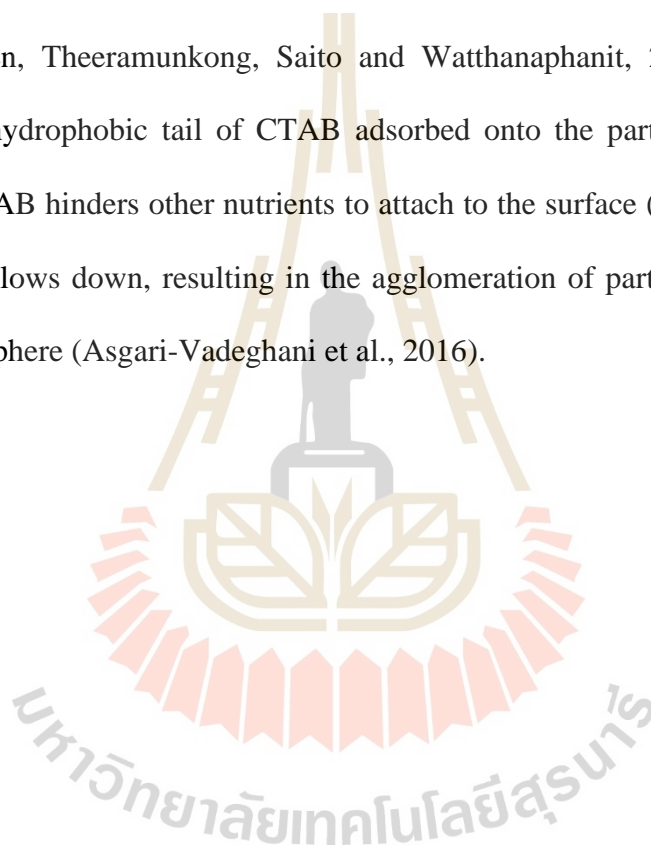


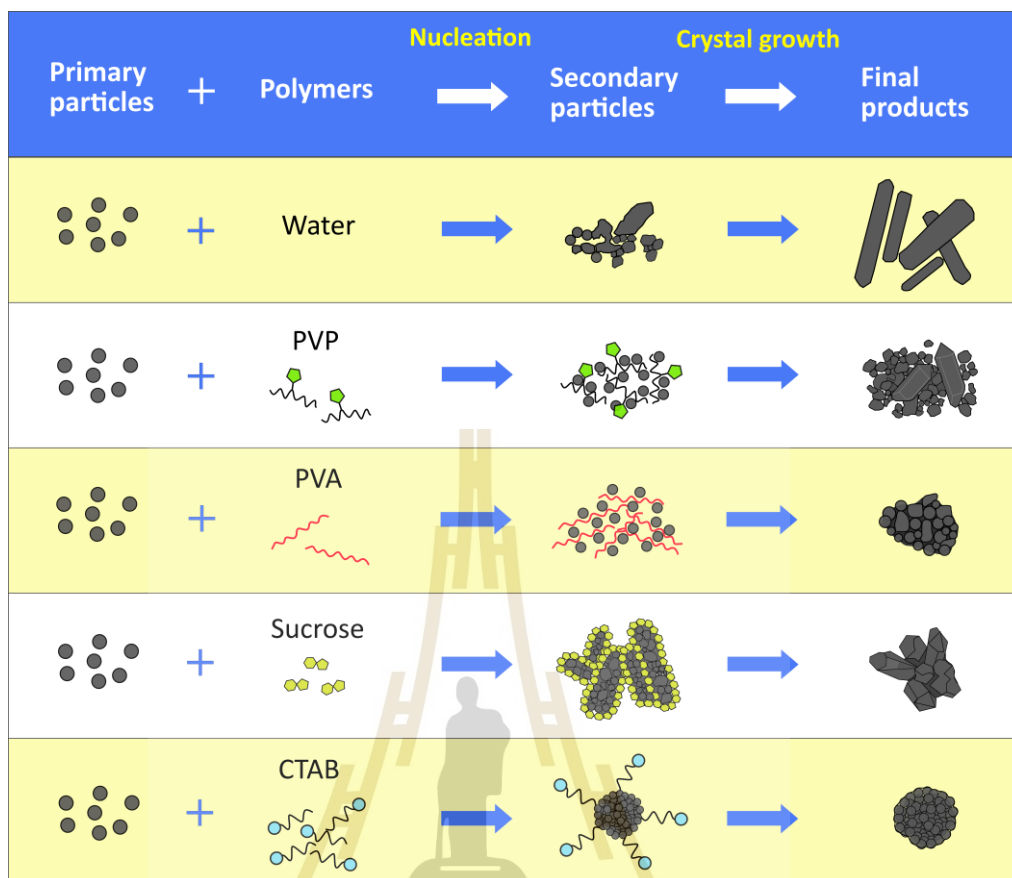
During the precipitation process, the morphology such as particle size not only depends on the chemical reaction of the compound but also other experimental conditions such as surfactants and solvents. Therefore, we also synthesized  $\text{NH}_4\text{ZnPO}_4$  powders in water without any surfactant and template materials for comparison, and it is found that the product has normal morphology. Therefore, it predicates that the surfactant shows as the template of the  $\text{NH}_4\text{ZnPO}_4$  powders with various morphologies. The morphologies of the prepared  $\text{NH}_4\text{ZnPO}_4$  particles are controlled by the relative growth rate of different crystal facets (Li, Liu and Shen, 2011). Moreover, the rare earth orthophosphate with hexagonal phase shows a high anisotropic structure, which strongly influences their morphologies evolution (Yan and Gu, 2009). However, the phosphates with the monoclinic structure have less anisotropic and decrease the tendency to grow along a random direction (Amghouz et al., 2014). Then, the use of

PVP, PVA, sucrose and CTAB solution can change the morphology of the  $\text{NH}_4\text{ZnPO}_4$  to the nanoparticle size.

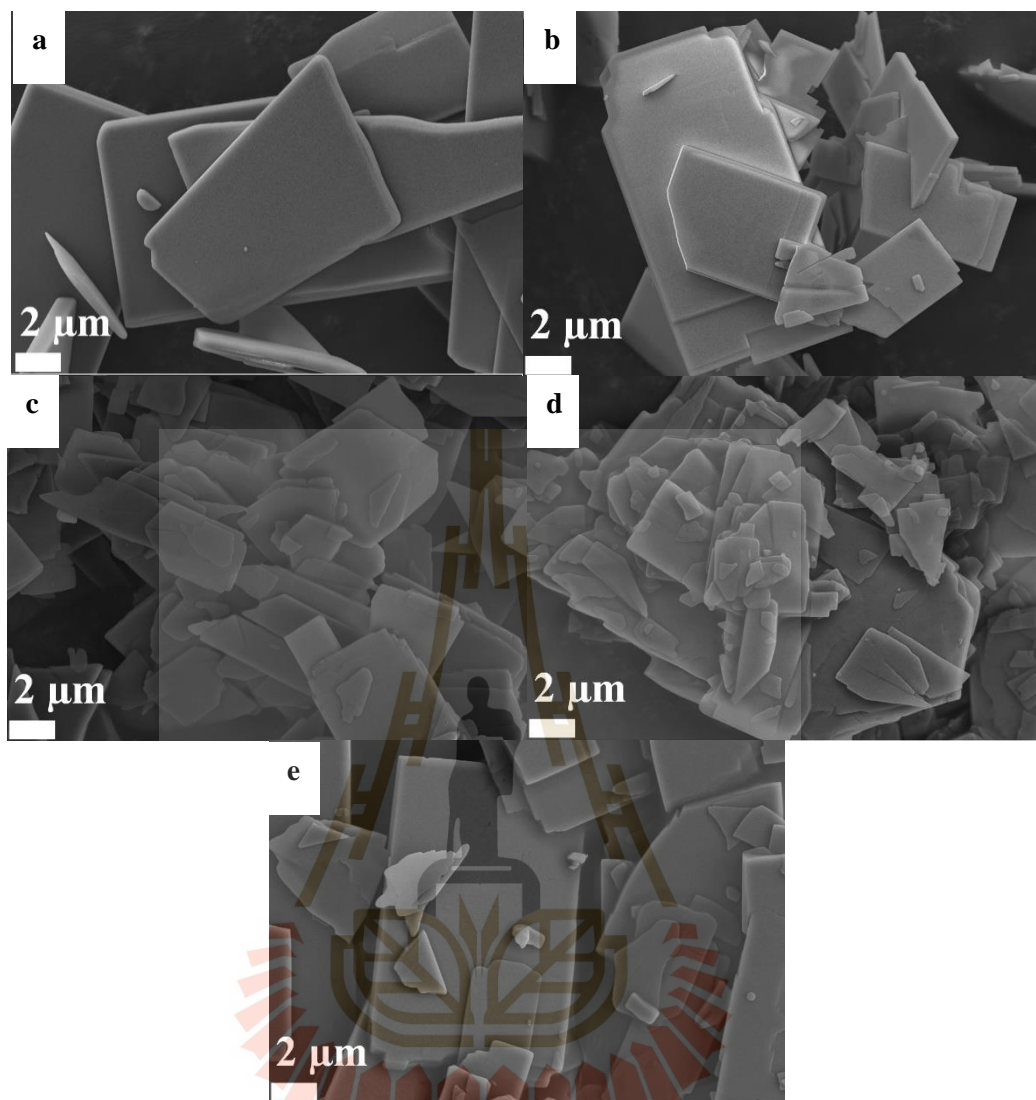
The possible formation of  $\text{NH}_4\text{ZnPO}_4$  structures by using water and polymers sources of PVP, PVA, sucrose and CTAB is proposed in figure 4.28 In generally, the formation of particles is related to the following two process of nucleation and crystal growth (Thanh, Maclean and Mahiddine, 2014, Chen, Wang, Zheng, Fang and Meng, 2018). The nucleation process consists of the formation of stable nuclei and the growth of the critical nuclei resulting in the larger crystal formed in the crystal growth process (Patel and Anderson, 2013, Jiang et al., 2014, Wang et al., 2014). In the absence of surfactant as seen in figure 4, the secondary particles resulting from the aggregation of the primary particles self-assembles into the micro-rods. It is well-known that the growth of the particles was related to the adsorption of surfactants onto particular crystallographic facets of the growing crystal (Zhu, Wang, Meng, Qin and Diao, 2012). By adding the surfactants of PVP, PVA, sucrose and CTAB into the nucleation process, these surfactants can affect the surface energy and thus control the nucleation rate (Jiang, Xie, Jiang, Wei and Chen, 2013). The slower nucleation rate results in the larger particle size. When nonionic surfactant of PVP is added, the agglomeration of the particles together with micro-rods like shape was observed. These results may possibly explain due to the high PVP concentration. The following explanations are (Zhu et al., 2012) : (i) the adsorption of PVP was not enough for the effective coverage of  $\text{NH}_4\text{ZnPO}_4$  phase, resulting in the agglomeration of the particles and (ii) the continuous self-assembly of those particles, resulting in micro-rod like shape. For PVA, a polymer chain of PVA adsorbed onto the particles surface through non-covalent bonding of hydroxyl groups. The adsorbed PVA form a multilayer coating

around the particles as a water protecting agent, resulting in the smaller particle size and less agglomeration (Kyrychenko, Pasko and Kalugin, 2017). In case of sucrose, the multiple hydroxyl groups of a large molecular size of non-reducing sucrose adsorbed onto certain crystal planes as a coating agent to form steric hinderance and thus sucrose may possibly transformed to glucose and gluconic acid that coated on the particles surface resulting in a decrease of particle size (Sun et al., 2009, Treesukkasem, Chokradjaroen, Theeramunkong, Saito and Watthanaphanit, 2019). In contrast to CTAB, the hydrophobic tail of CTAB adsorbed onto the particles surface and the adsorbed CTAB hinders other nutrients to attach to the surface (Pan et al., 2011). The growth rate slows down, resulting in the agglomeration of particles forming as bulk products of sphere (Asgari-Vadeghani et al., 2016).

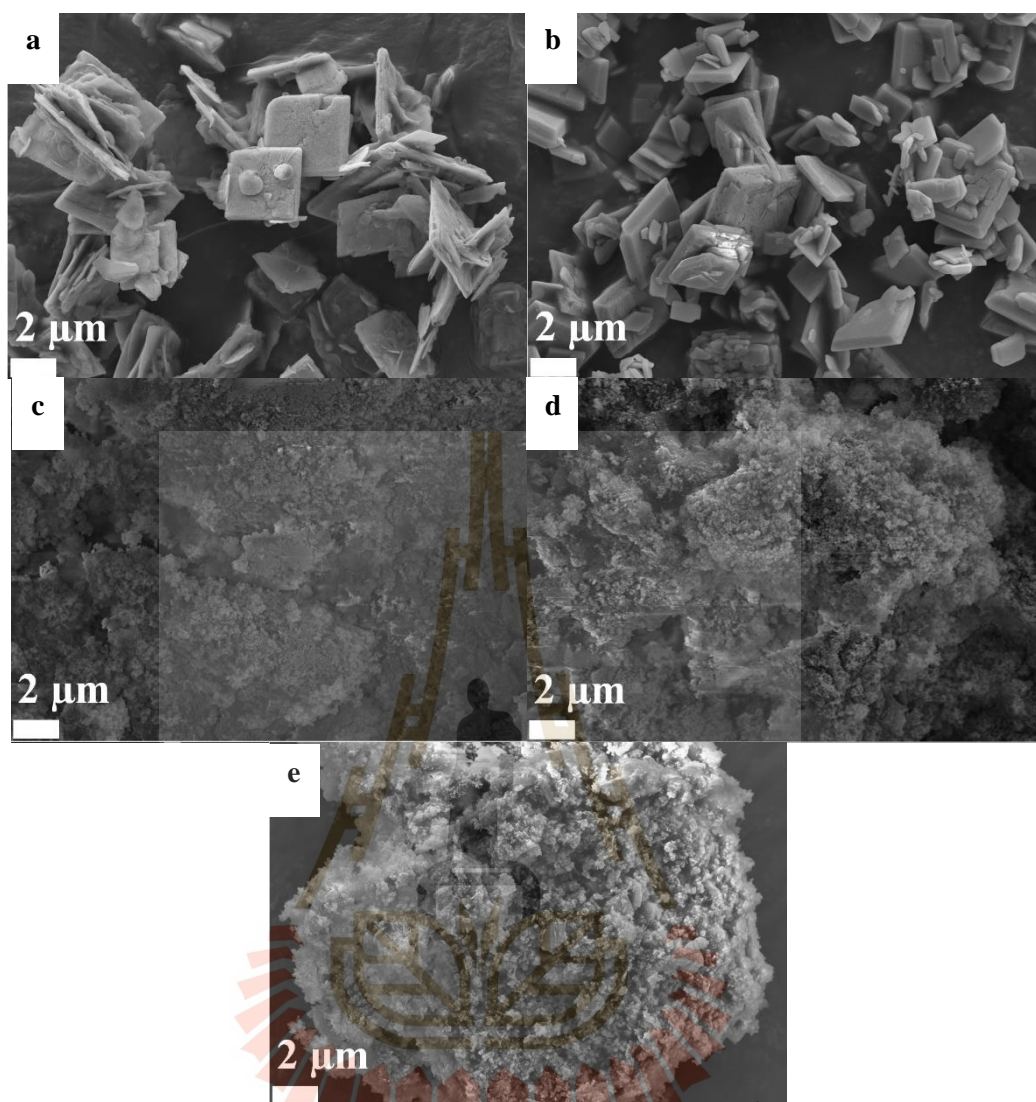




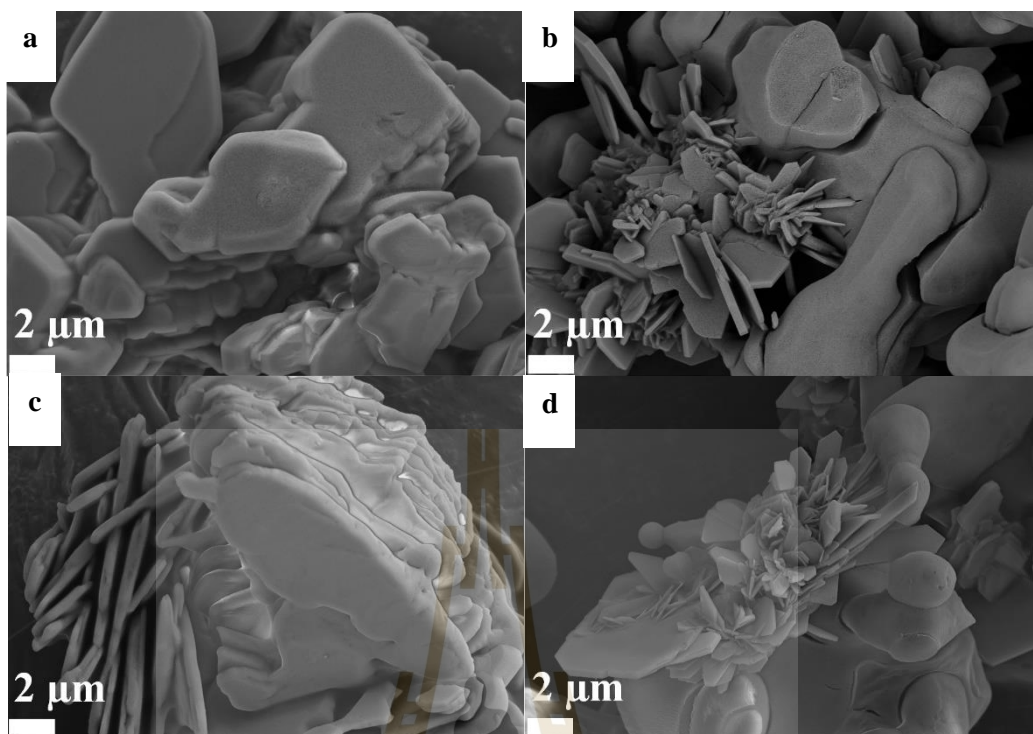
**Figure 4. 28** The possible formation mechanism of  $\text{NH}_4\text{ZnPO}_4$  microstructures prepared by using water and polymer sources of PVP, PVA, sucrose and CTAB.



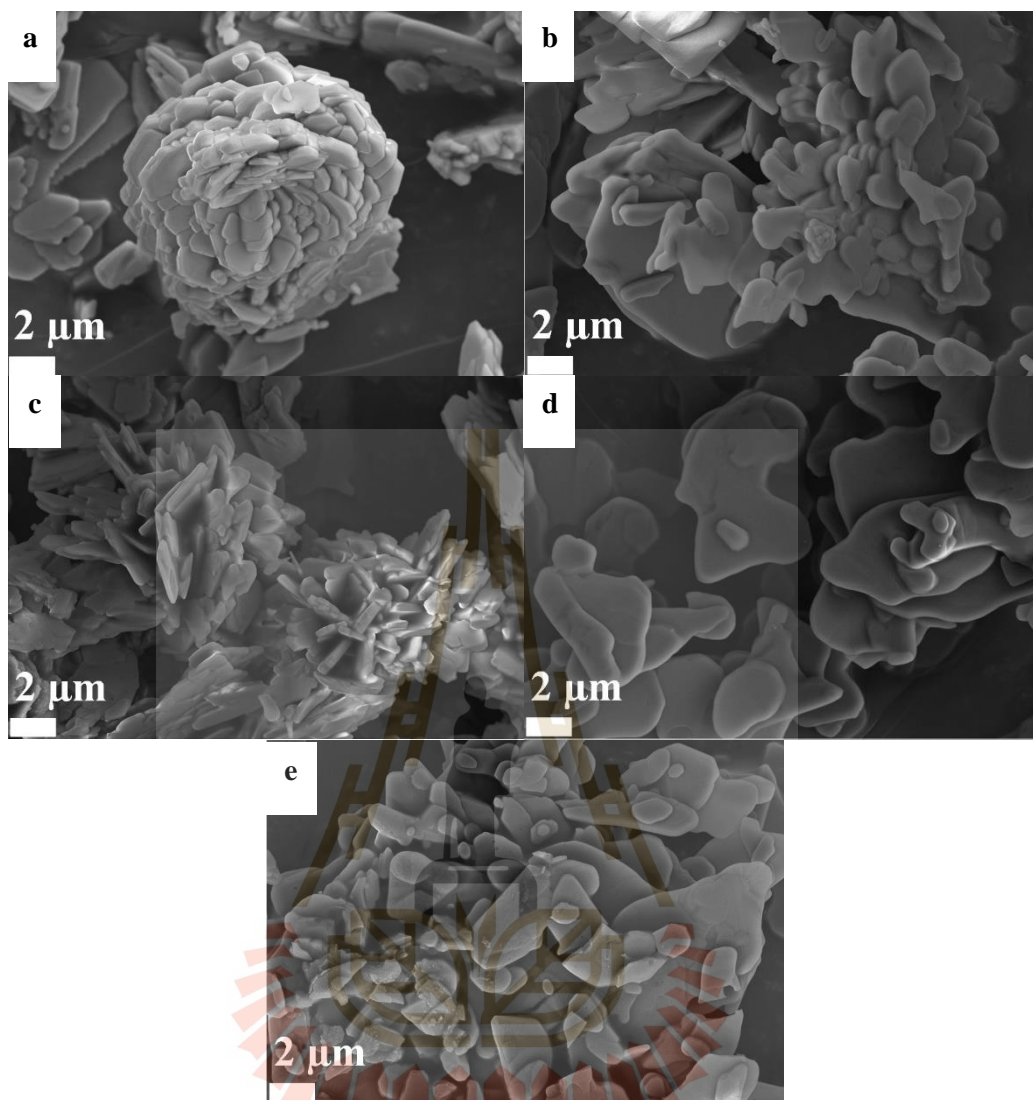
**Figure 4.29** SEM image of  $\text{NH}_4\text{CoPO}_4 \cdot \text{H}_2\text{O}$  powders prepared by chemical precipitation method with (a) water (b) PVP (c) PVA (d) Sucrose and (e) CTAB.



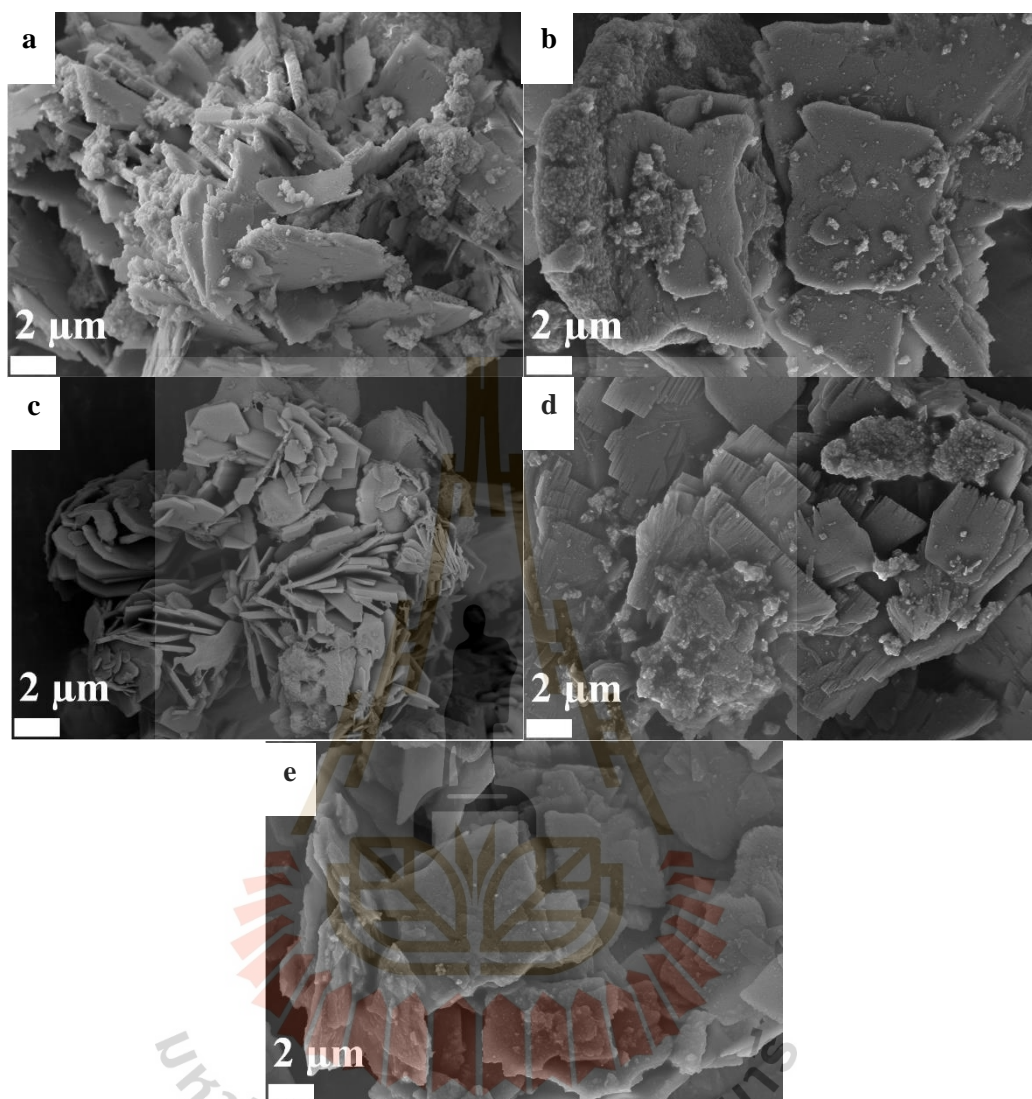
**Figure 4.30** SEM image of  $\text{NH}_4\text{CuPO}_4\cdot\text{H}_2\text{O}$  powders prepared by chemical precipitation method with (a) water (b) PVP (c) PVA (d) Sucrose and (e) CTAB.



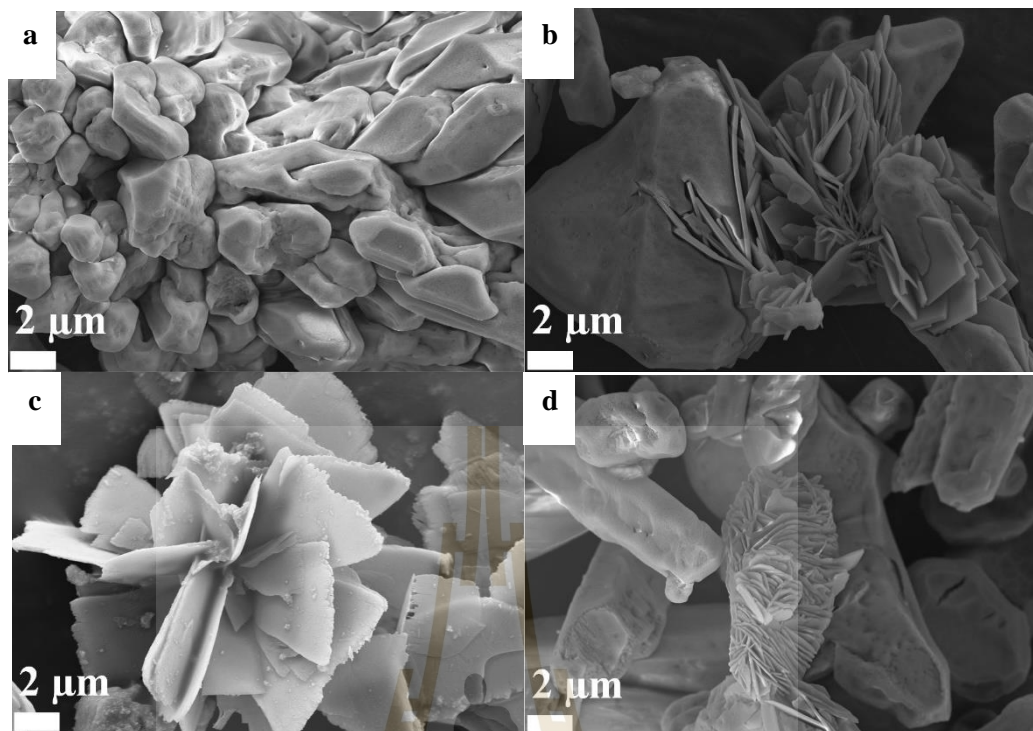
**Figure 4.31** SEM image of  $\text{NH}_4\text{MgPO}_4 \cdot \text{H}_2\text{O}$  powders prepared by chemical precipitation method with (a) water (b) PVP (c) PVA and (d) CTAB.



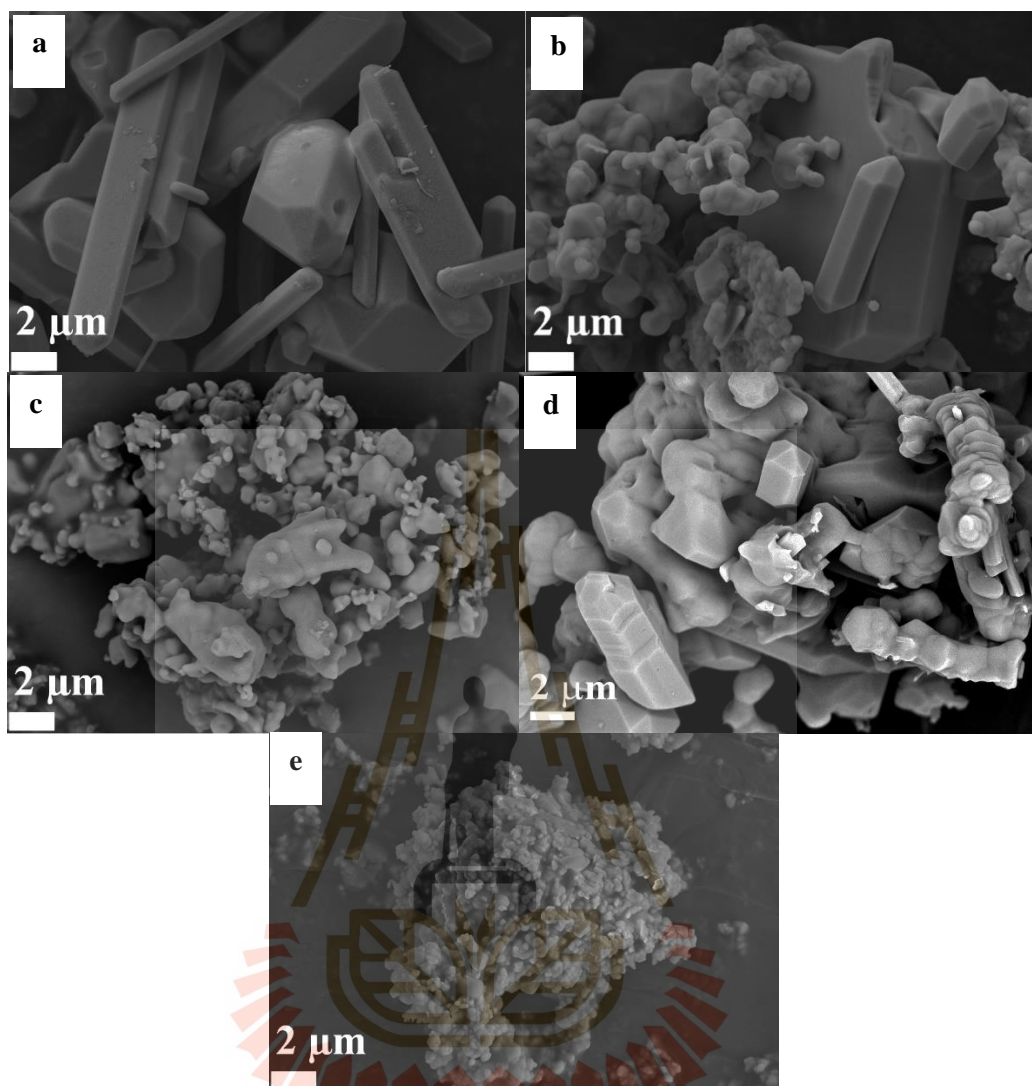
**Figure 4.32** SEM image of  $\text{NH}_4\text{MnPO}_4 \cdot \text{H}_2\text{O}$  powders prepared by chemical precipitation method with (a) water (b) PVP (c) PVA (d) Sucrose and (e) CTAB.



**Figure 4.33** SEM image of  $\text{NH}_4\text{FePO}_4 \cdot \text{H}_2\text{O}$  powders prepared by chemical precipitation method with (a) water (b) PVP (c) PVA (d) Sucrose and (e) CTAB.



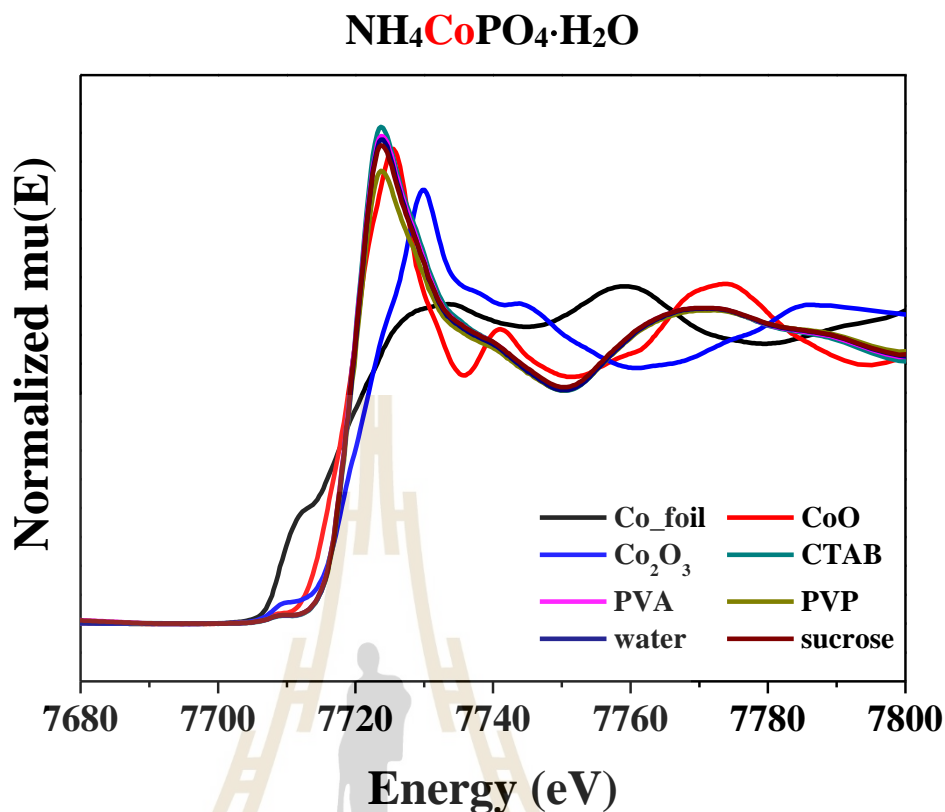
**Figure 4.34** SEM image of  $\text{NH}_4\text{NiPO}_4 \cdot \text{H}_2\text{O}$  powders prepared by chemical precipitation method with (a) water (b) PVP (c) PVA and (d) CTAB.



**Figure 4.35** SEM image of  $\text{NH}_4\text{ZnPO}_4$  powders prepared by chemical precipitation method with (a) water (b) PVP (c) PVA (d) Sucrose and (e) CTAB.

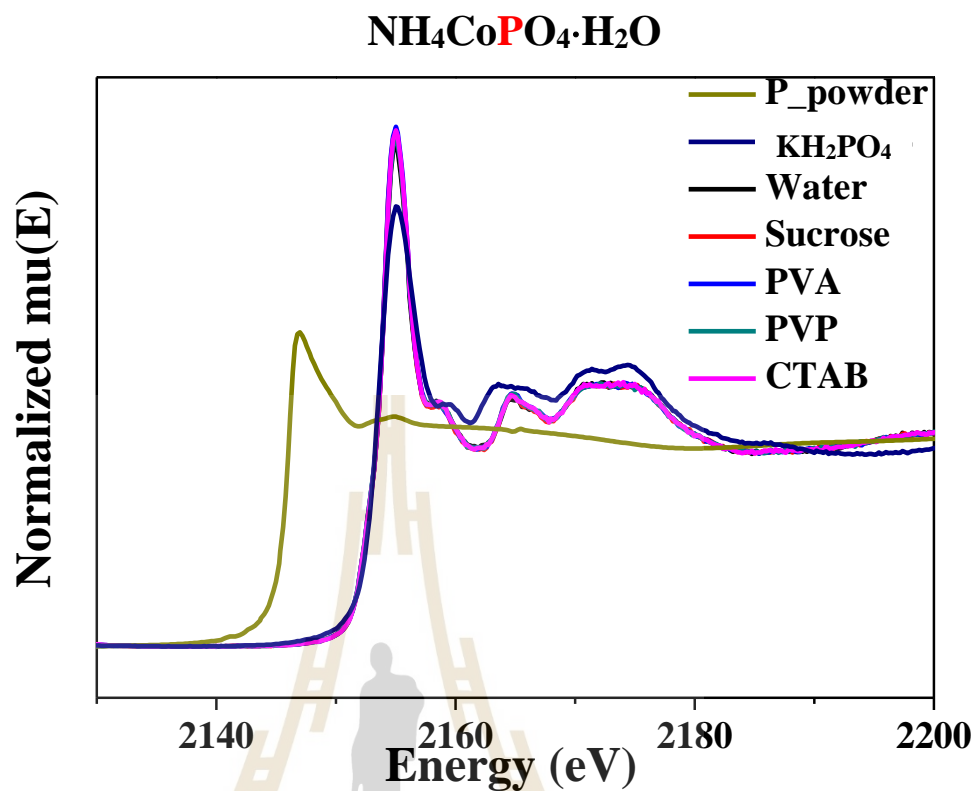
### 4.2.3 X-ray absorption spectroscopy study of the $\text{NH}_4\text{MPO}_4\cdot\text{H}_2\text{O}$ powders (M = Mg, Co, Fe, Mn, Ni, Zn, Cu) with water, PVP, PVA, Sucrose and CTAB

The X-ray absorption near-edge structure (XANES) spectrum of the  $\text{NH}_4\text{CoPO}_4\cdot\text{H}_2\text{O}$  was measured at Co K-edge at energy range of 7650-7800 eV to examine the chemical states of cobalt element in the samples. The XANES technique is used to distinguish the chemical species and oxidation states of Co in the samples. The energy edges were evaluated using Athena software, Figure 4.36 shows the normalized Co K-edge XANES spectra of the  $\text{NH}_4\text{CoPO}_4\cdot\text{H}_2\text{O}$  particles, which were compared with the standard compounds CoO ( $\text{Co}^{2+}$ ) and  $\text{Co}_2\text{O}_3$  ( $\text{Co}^{3+}$ ). The results indicated that the spectra feature of all samples show quite similar feature. In general, the edge and pre-edge energy positions of XANES spectra related to the valence state of the absorbing atom in the sample and shifted to higher energy when oxidation state of the absorbing atom increase. The edge energy positions of  $\text{NH}_4\text{CoPO}_4\cdot\text{H}_2\text{O}$  (water, PVP, PVA, Sucrose and CTAB) were 7720.04, 7719.51, 7719.43, 7719.97. and 7719.96 eV. The edge energy positions of all samples match with the edge energy positions of  $\text{Co}_2\text{O}_3$  ( $E_0 = 7722.33$  eV) and CoO ( $E_0 = 7719.86$  eV) standard samples. These results can be implied that Co ions in all samples have a  $\text{Co}^{2+}$  and  $\text{Co}^{3+}$  in the structure.



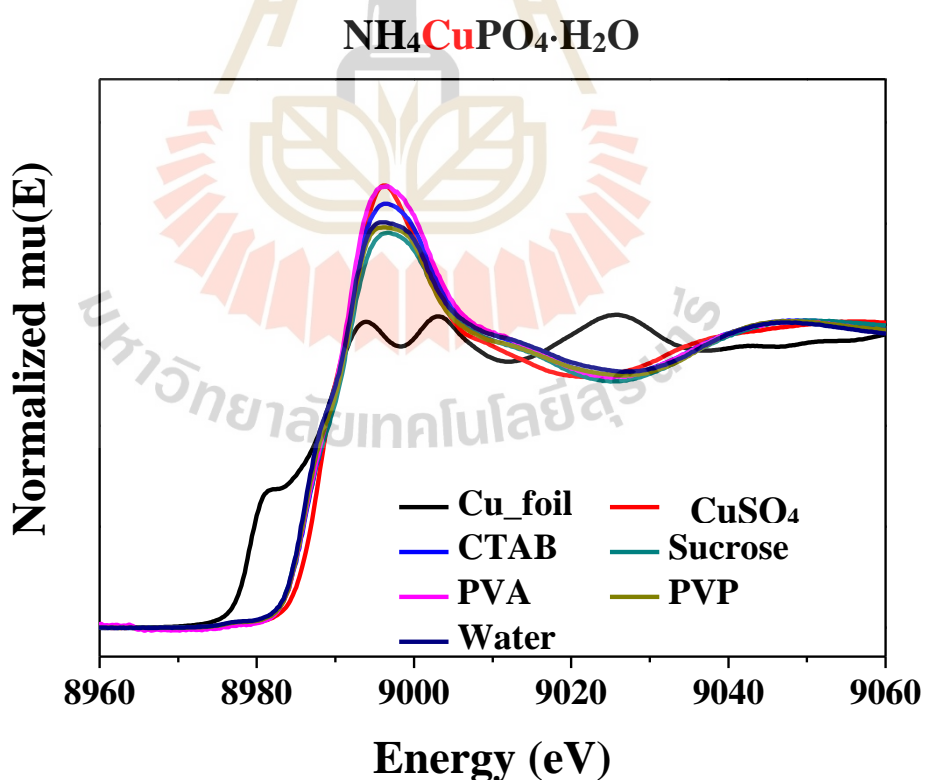
**Figure 4.36** Co K-edge XANES spectra of NH<sub>4</sub>CoPO<sub>4</sub>·H<sub>2</sub>O powder prepared by chemical precipitation method.

Figure 4.37 shows the normalized P K-edge XANES spectra of the NH<sub>4</sub>CoPO<sub>4</sub>·H<sub>2</sub>O with water, PVP, PVA, Sucrose and CTAB condition, which were compared with the standard compounds of P<sup>0+</sup> and P<sup>5+</sup>. The results indicated that the spectra feature of all samples show quite similar feature. The edge energy positions of samples match with edge energy positions of KH<sub>2</sub>PO<sub>4</sub> standard samples. These results can be concluded that P ions in all samples have a P<sup>5+</sup> in the structure.



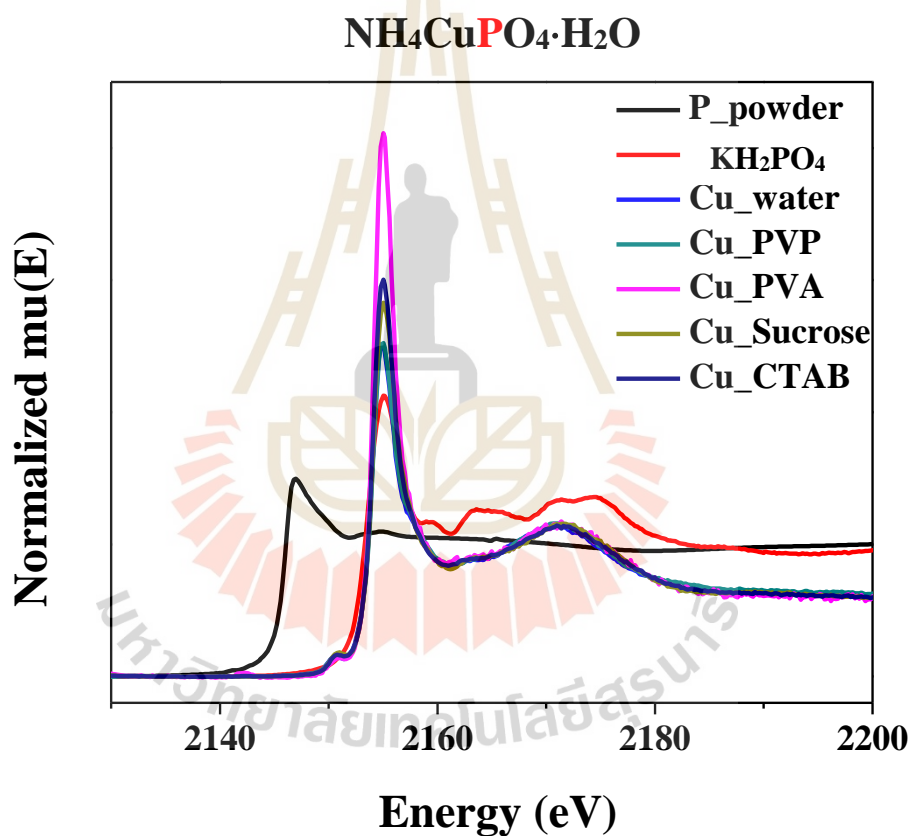
**Figure 4.37** P K-edge XANES spectra of  $\text{NH}_4\text{CoPO}_4 \cdot \text{H}_2\text{O}$  powders prepared by chemical precipitation method.

The XANES spectrum of  $\text{NH}_4\text{CuPO}_4\cdot\text{H}_2\text{O}$  at Cu K-edge was measured at energy range of 8950-9080 eV to examine the oxidation states of copper element in the samples. Figure 4.38 shows the normalized Cu K-edge XANES spectra of the  $\text{NH}_4\text{CuPO}_4\cdot\text{H}_2\text{O}$  with water, PVP, PVA, Sucrose and CTAB solution, which were compared with the standard compounds of Cu and  $\text{Cu}^{2+}$ . The edge energy positions of  $\text{NH}_4\text{CuPO}_4\cdot\text{H}_2\text{O}$  (water, PVP, PVA, Sucrose and CTAB) samples were at 8986.11, 8985.94, 8985.93, 8985.93 and 8986.07 eV, which were between the edge energy positions of Cu foil ( $E_0 = 8979.18$  eV) and  $\text{CuSO}_4$  ( $E_0 = 8987.73$  eV) standard samples. These results can be implied that Cu ions in all samples have mixing of Cu and  $\text{Cu}^{2+}$  in the structure.



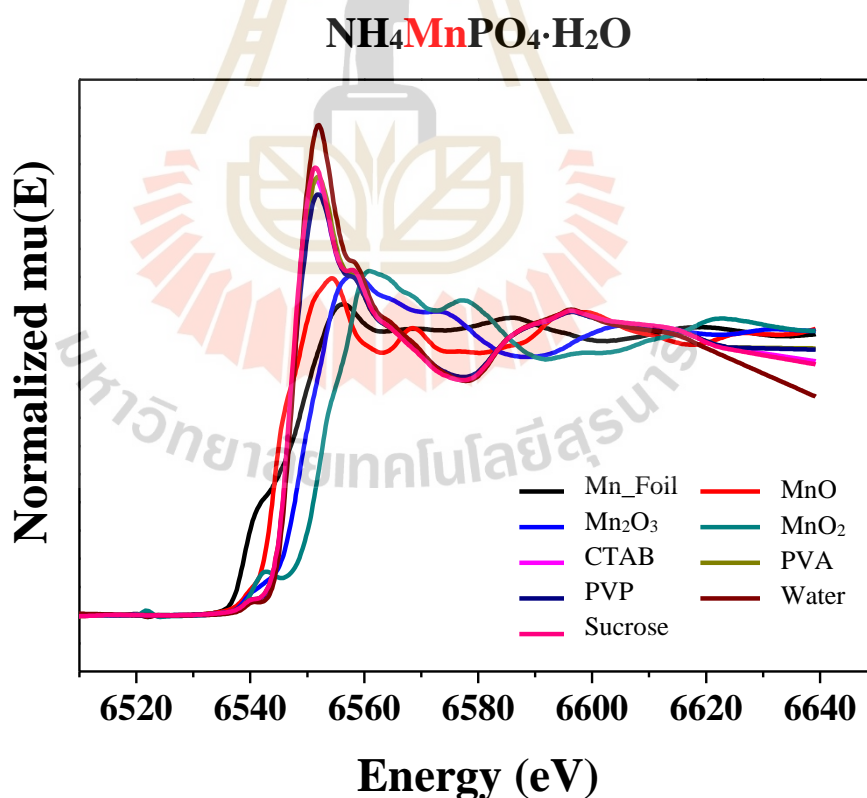
**Figure 4.38** Cu K-edge XANES spectra of  $\text{NH}_4\text{CuPO}_4\cdot\text{H}_2\text{O}$  powder prepared by chemical precipitation method.

Figure 4.39 shows the normalized P K-edge XANES spectra of the  $\text{NH}_4\text{CuPO}_4 \cdot \text{H}_2\text{O}$  with water, PVP, PVA, Sucrose and CTAB condition, which were compared with the standard compounds of  $\text{P}^{0+}$  and  $\text{P}^{5+}$ . The results indicated that the spectra feature of all samples show quite similar feature. The edge energy positions of samples match with edge energy positions of  $\text{KH}_2\text{PO}_4$  standard samples. These results can be concluded that P ions in all samples have a  $\text{P}^{5+}$  in the structure.



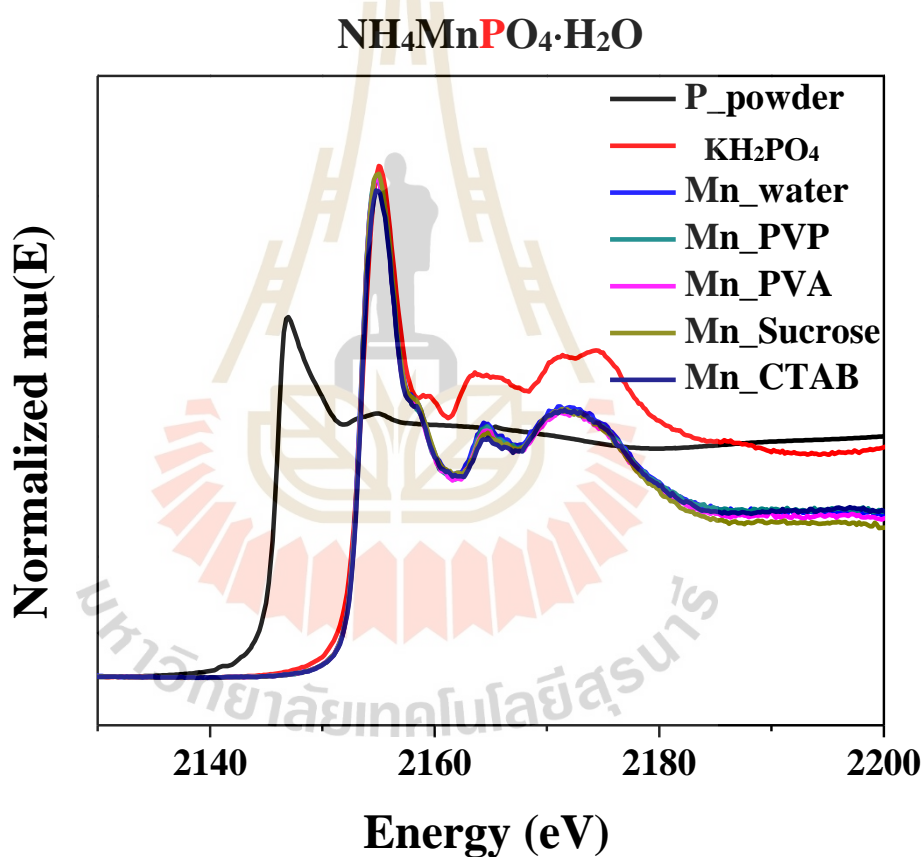
**Figure 4.39** P K-edge XANES spectra of  $\text{NH}_4\text{CuPO}_4 \cdot \text{H}_2\text{O}$  powder prepared by chemical precipitation method.

The XANES spectra of Mn K-edge XANES was measured at energy range 6500-6640 eV to examine the oxidation states of iron element in the samples. Figure 4.40 shows the normalized Mn K-edge XANES spectra of the  $\text{NH}_4\text{MnPO}_4\cdot\text{H}_2\text{O}$  with water, PVP, PVA, Sucrose and CTAB solution, which was compared with the standard compounds of  $\text{Mn}^{2+}$ ,  $\text{Mn}^{3+}$  and  $\text{Mn}^{4+}$ . The edge energy positions of the  $\text{NH}_4\text{MnPO}_4\cdot\text{H}_2\text{O}$  with water, PVP, PVA, Sucrose and CTAB solution were at 6547.45, 6547.46, 6547.46, 6547.46 and 6547.46 eV, which lied between the edge energy positions of MnO ( $E_0 = 6544.20$  eV,  $\text{Mn}_2\text{O}_3$   $E_0 = 6548.42$  eV) and  $\text{MnO}_2$  ( $E_0=76552.61$  eV) standard samples. These results can be implied that Mn ions in all samples have  $\text{Mn}^{+2}$  and  $\text{Mn}^{3+}$  in the structure.



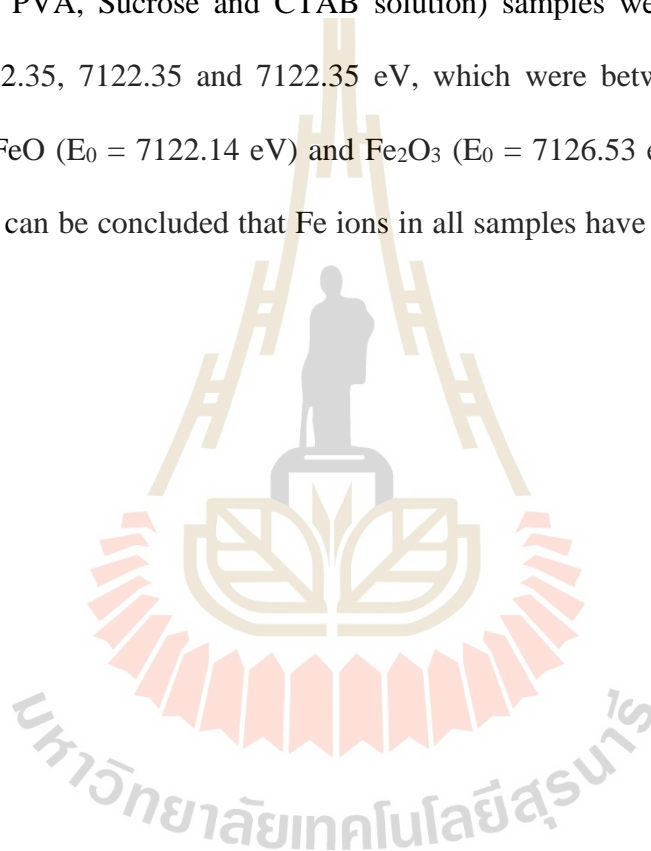
**Figure 4.40** Mn K-edge XANES spectra of  $\text{NH}_4\text{MnPO}_4\cdot\text{H}_2\text{O}$  powders prepared by chemical precipitation method.

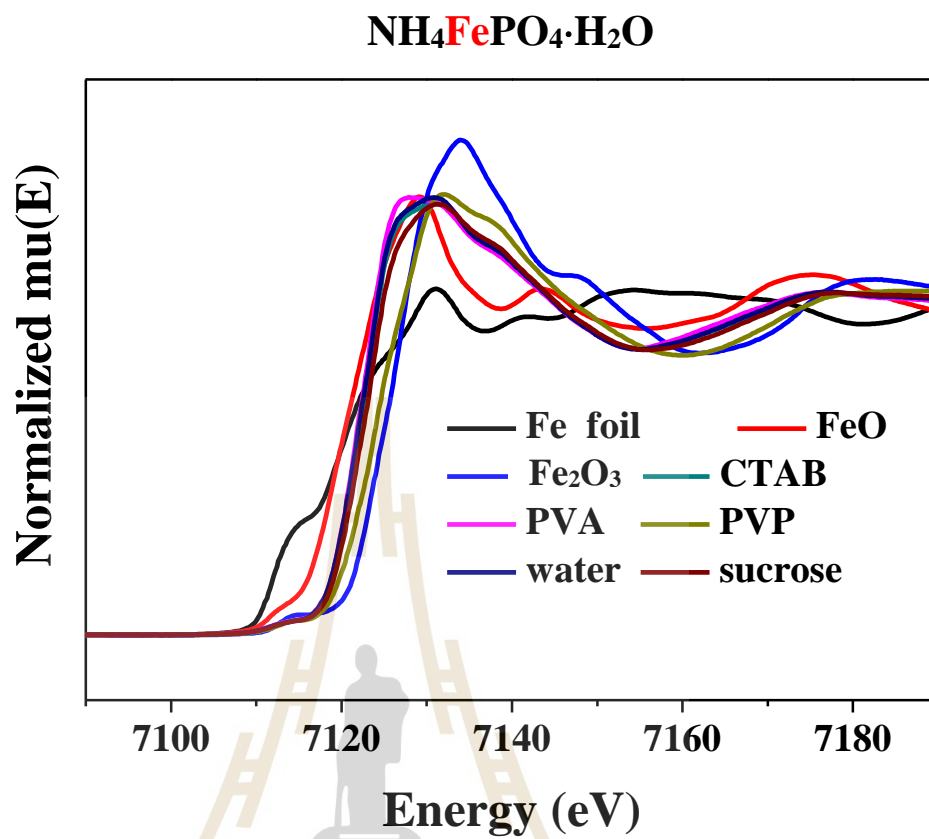
Figure 4.41 shows the normalized P K-edge XANES spectra of the  $\text{NH}_4\text{MnPO}_4\cdot\text{H}_2\text{O}$  with water, PVP, PVA, Sucrose and CTAB condition, which were compared with the standard compounds of  $\text{P}^{0+}$  and  $\text{P}^{5+}$ . The results indicated that the spectra feature of all samples show quite similar feature. The edge energy positions of samples match with edge energy positions of  $\text{KH}_2\text{PO}_4$  standard samples. These results can be concluded that P ions in all samples have a  $\text{P}^{5+}$  in the structure.



**Figure 4.41** P K-edge XANES spectra of  $\text{NH}_4\text{MnPO}_4\cdot\text{H}_2\text{O}$  powders prepared by chemical precipitation method.

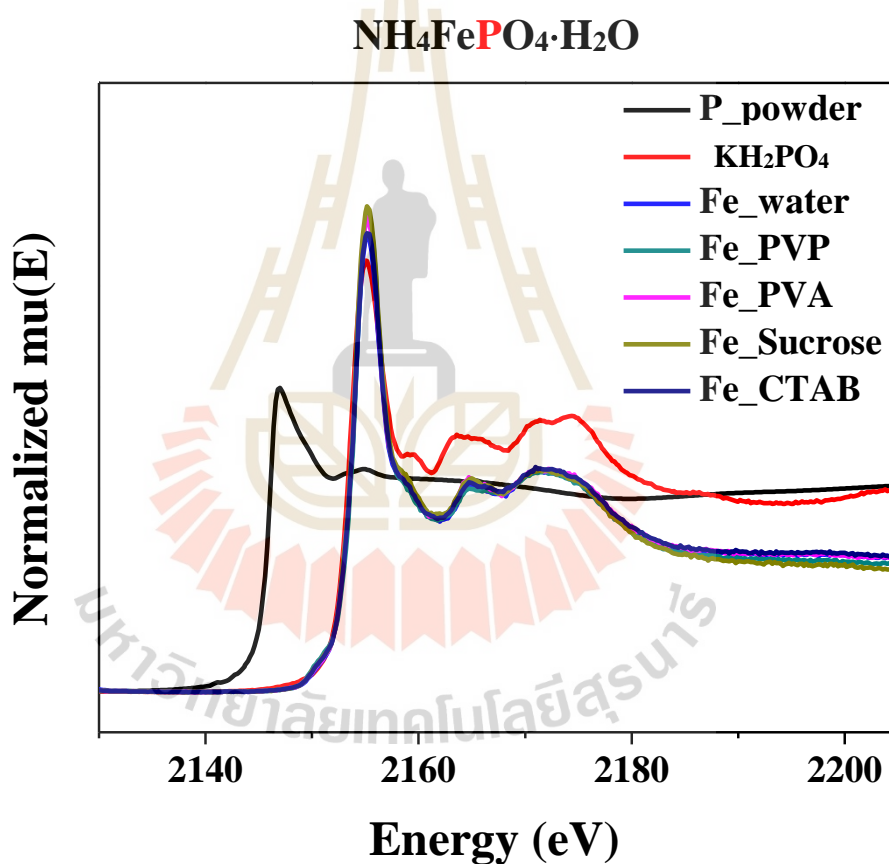
Figure 4.42 shows the normalized Fe K-edge XANES spectra of the  $\text{NH}_4\text{FePO}_4 \cdot \text{H}_2\text{O}$  with water, PVP, PVA, Sucrose and CTAB solution, which were compared with the standard compounds of Fe,  $\text{Fe}^{2+}$  and  $\text{Fe}^{3+}$ . The XANES spectra of  $\text{NH}_4\text{FePO}_4 \cdot \text{H}_2\text{O}$  at Fe K-edge was measured at energy range of 7080-7200 eV to examine the chemical states of iron element in the samples. The edge energy positions of  $\text{NH}_4\text{FePO}_4 \cdot \text{H}_2\text{O}$  (water, PVP, PVA, Sucrose and CTAB solution) samples were found at 7122.35, 7123.90, 7122.35, 7122.35 and 7122.35 eV, which were between the edge energy positions of FeO ( $E_0 = 7122.14$  eV) and  $\text{Fe}_2\text{O}_3$  ( $E_0 = 7126.53$  eV) standard samples. These results can be concluded that Fe ions in all samples have a  $\text{Fe}^{+2}$  and  $\text{Fe}^{3+}$  in the structure.





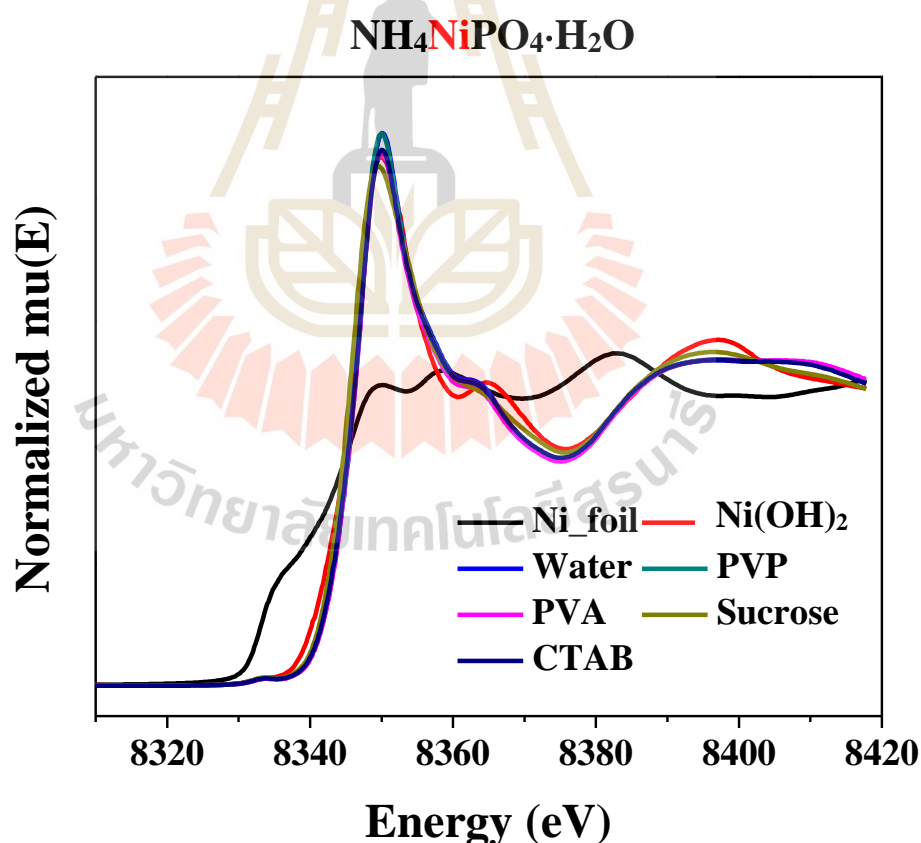
**Figure 4.42** Fe K-edge XANES spectra of NH<sub>4</sub>FePO<sub>4</sub>·H<sub>2</sub>O powders prepared by chemical precipitation method.

Figure 4.43 shows the normalized P K-edge XANES spectra of the  $\text{NH}_4\text{FePO}_4 \cdot \text{H}_2\text{O}$  with water, PVP, PVA, Sucrose and CTAB condition, which were compared with the standard compounds of  $\text{P}^{0+}$  and  $\text{P}^{5+}$ . The results indicated that the spectra feature of all samples show quite similar feature. The edge energy positions of samples match with edge energy positions of  $\text{KH}_2\text{PO}_4$  standard samples. These results can be concluded that P ions in all samples have a  $\text{P}^{5+}$  in the structure.



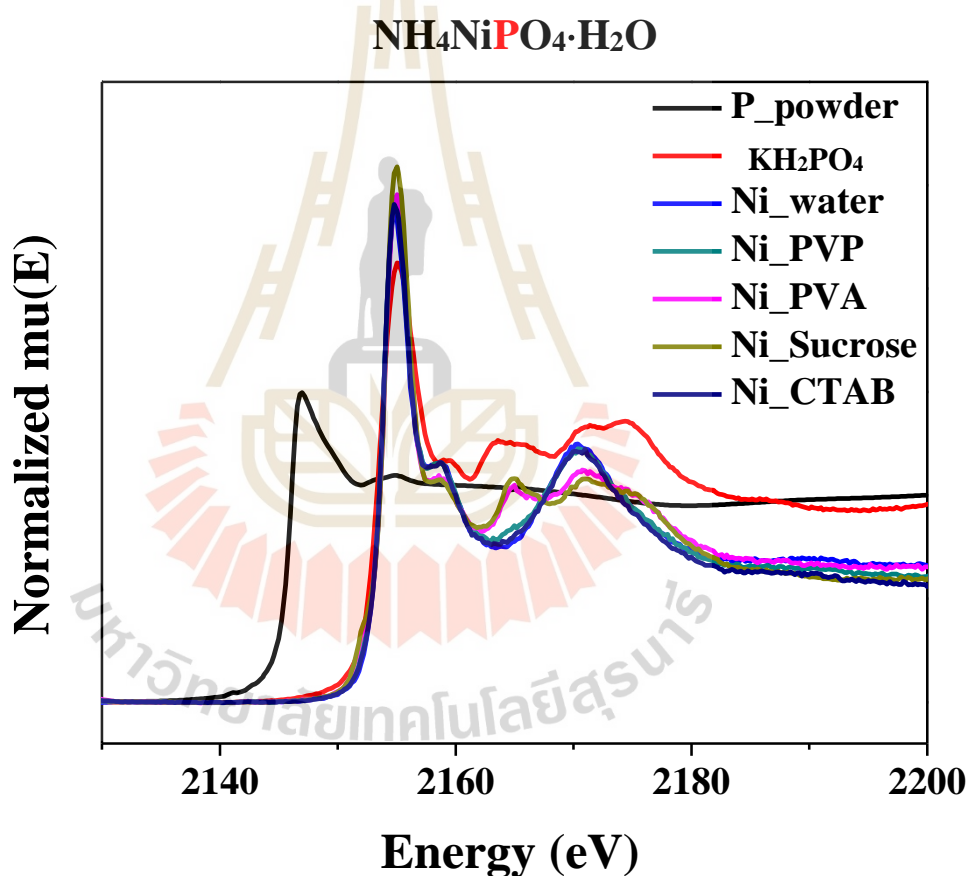
**Figure 4.43** P K-edge XANES spectra of  $\text{NH}_4\text{FePO}_4 \cdot \text{H}_2\text{O}$  powders prepared by chemical precipitation method.

Figure 4.44 shows the normalized Ni K-edge XANES spectra of the  $\text{NH}_4\text{NiPO}_4 \cdot \text{H}_2\text{O}$  with water, PVP, PVA, Sucrose and CTAB solution, which were compared with the standard compounds of Ni and  $\text{Ni}^{2+}$ . The XANES spectra of Ni K-edge XANES was measured at energy range 8300-8420 eV to examine the oxidation states of iron element in the samples. The edge energy positions of  $\text{NH}_4\text{NiPO}_4 \cdot \text{H}_2\text{O}$  (water, PVP, PVA, Sucrose and CTAB) samples were found at 8346.10, 8346.52, 8346.47, 8346.47 and 8346.43 eV, which lied on the edge energy positions of  $\text{Ni}(\text{OH})_2$  ( $E_0 = 8346.00\text{eV}$ ) standard samples. These results can be concluded that Ni ions in all samples are  $\text{Ni}^{+2}$  in the structure.



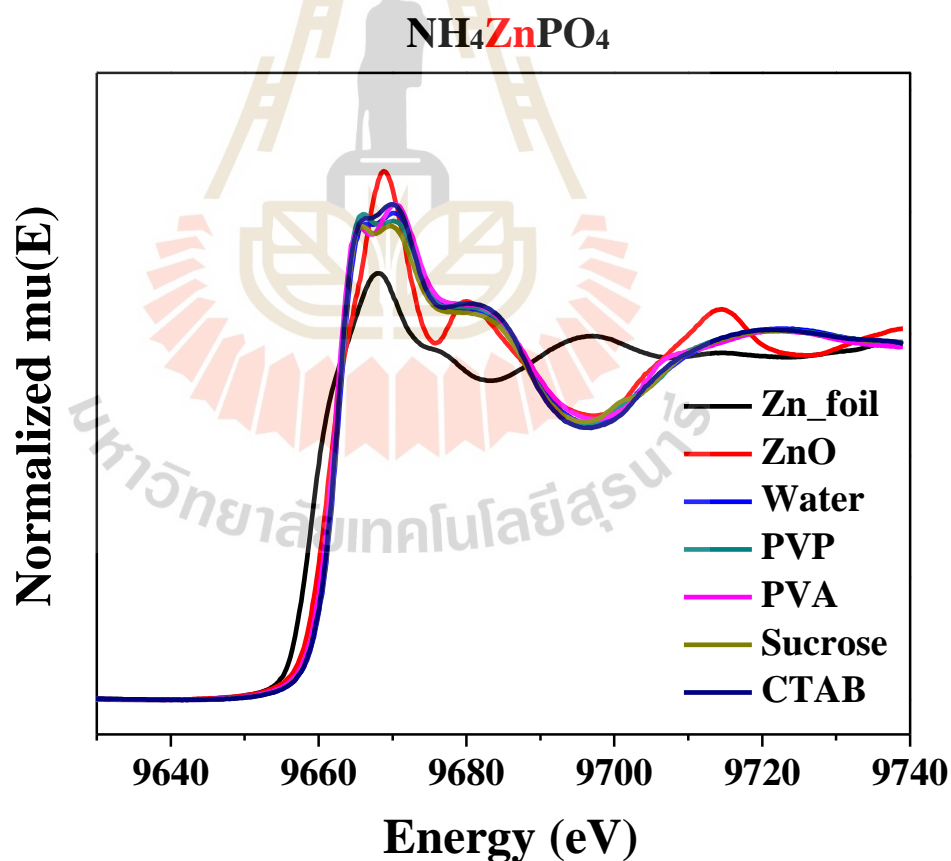
**Figure 4.44** Ni K-edge XANES spectra of  $\text{NH}_4\text{NiPO}_4 \cdot \text{H}_2\text{O}$  powders prepared by chemical precipitation method.

Figure 4.45 shows the normalized P K-edge XANES spectra of the  $\text{NH}_4\text{NiPO}_4\cdot\text{H}_2\text{O}$  with water, PVP, PVA, Sucrose and CTAB condition, which was compared with the standard compounds of  $\text{P}^{0+}$  and  $\text{P}^{5+}$ . The results indicated that the spectra feature of all samples show quite similar feature. The edge energy positions of samples match with edge energy positions of  $\text{KH}_2\text{PO}_4$  standard samples. These results can be concluded that P ions in all samples have a  $\text{P}^{5+}$  in the structure.



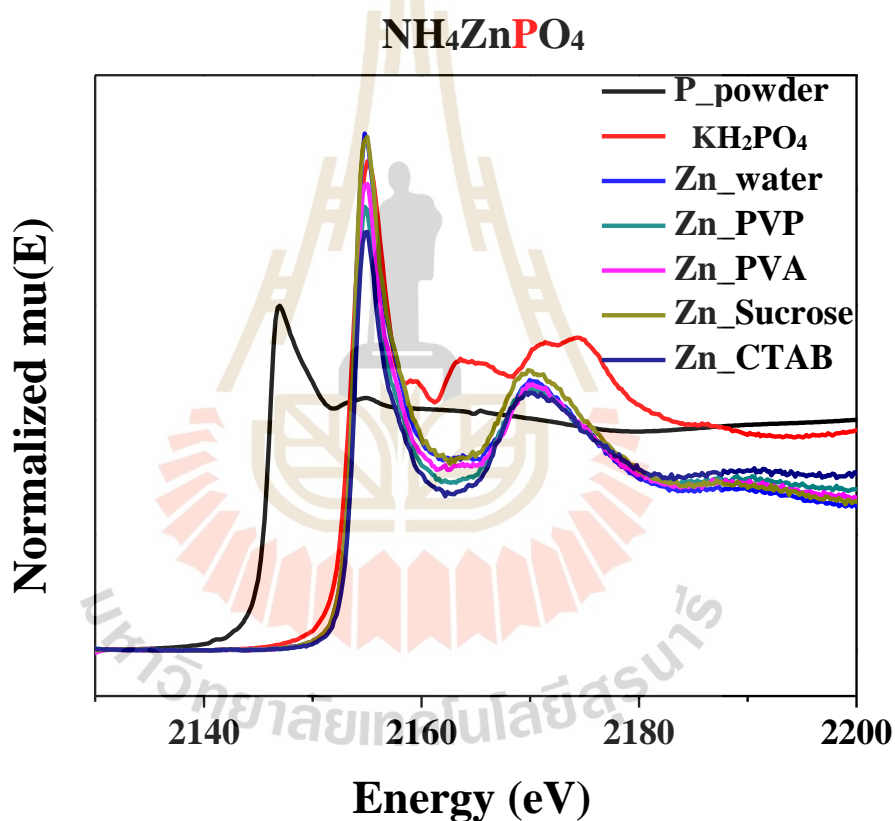
**Figure 4.45** P K-edge XANES spectra of  $\text{NH}_4\text{NiPO}_4\cdot\text{H}_2\text{O}$  powder prepared by chemical precipitation method.

The XANES spectra of  $\text{NH}_4\text{ZnPO}_4$  of Zn K-edge XANES were measured at energy range 9600-9760 eV to examine the oxidation states of iron element in the samples. Figure 4.46 shows the normalized Zn K-edge XANES spectra of the  $\text{NH}_4\text{ZnPO}_4$  with water, PVP, PVA, Sucrose and CTAB solution, which were compared with the standard compounds of Zn and  $\text{Zn}^{2+}$ . The edge energy positions of  $\text{NH}_4\text{ZnPO}_4$  (water, PVP, PVA, Sucrose and CTAB solution) samples were 9662.60, 9662.62, 9662.27, 9662.54 and 9662.50 eV, which lied on the edge energy positions of ZnO ( $E_0 = 9662.69$  eV) standard samples. These results can be implied that Zn ions in all samples have a  $\text{Zn}^{+2}$  in the structure.



**Figure 4.46** Zn K-edge XANES spectra of  $\text{NH}_4\text{ZnPO}_4$  powders prepared by chemical precipitation method.

Figure 4.47 shows the normalized P K-edge XANES spectra of the  $\text{NH}_4\text{ZnPO}_4$  with water, PVP, PVA, Sucrose and CTAB condition, which were compared with the standard compounds of  $\text{P}^{0+}$  and  $\text{P}^{5+}$ . The results indicated that the spectra feature of all samples show quite similar feature. The edge energy positions of samples match with edge energy positions of  $\text{KH}_2\text{PO}_4$  standard samples. These results can be concluded that P ions in all samples have a  $\text{P}^{5+}$  in the structure.



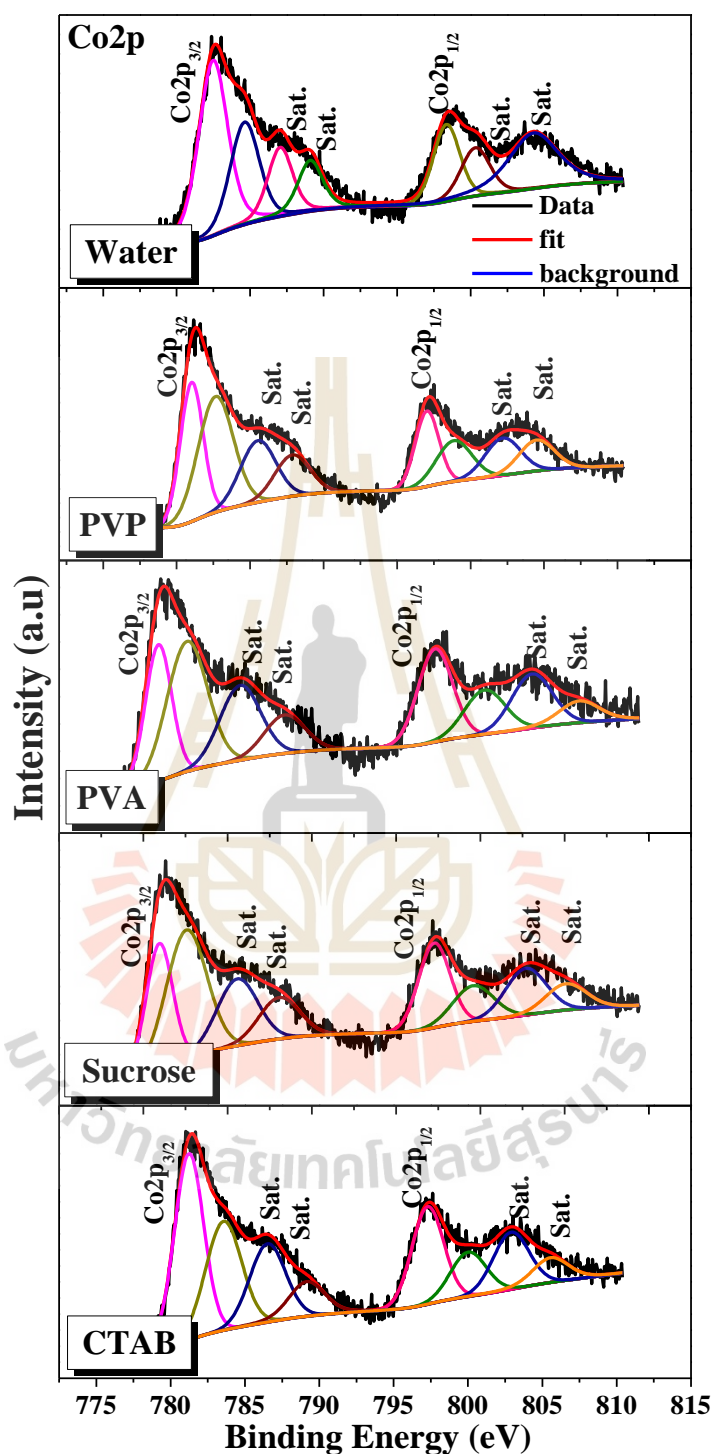
**Figure 4.47** P K-edge XANES spectra of  $\text{NH}_4\text{ZnPO}_4$  powders prepared by chemical precipitation method.

#### 4.2.4 X-ray photoelectron spectroscopy study of the $\text{NH}_4\text{MPO}_4\cdot\text{H}_2\text{O}$ powdes (M = Mg, Co, Fe, Mn, Ni, Zn, Cu)

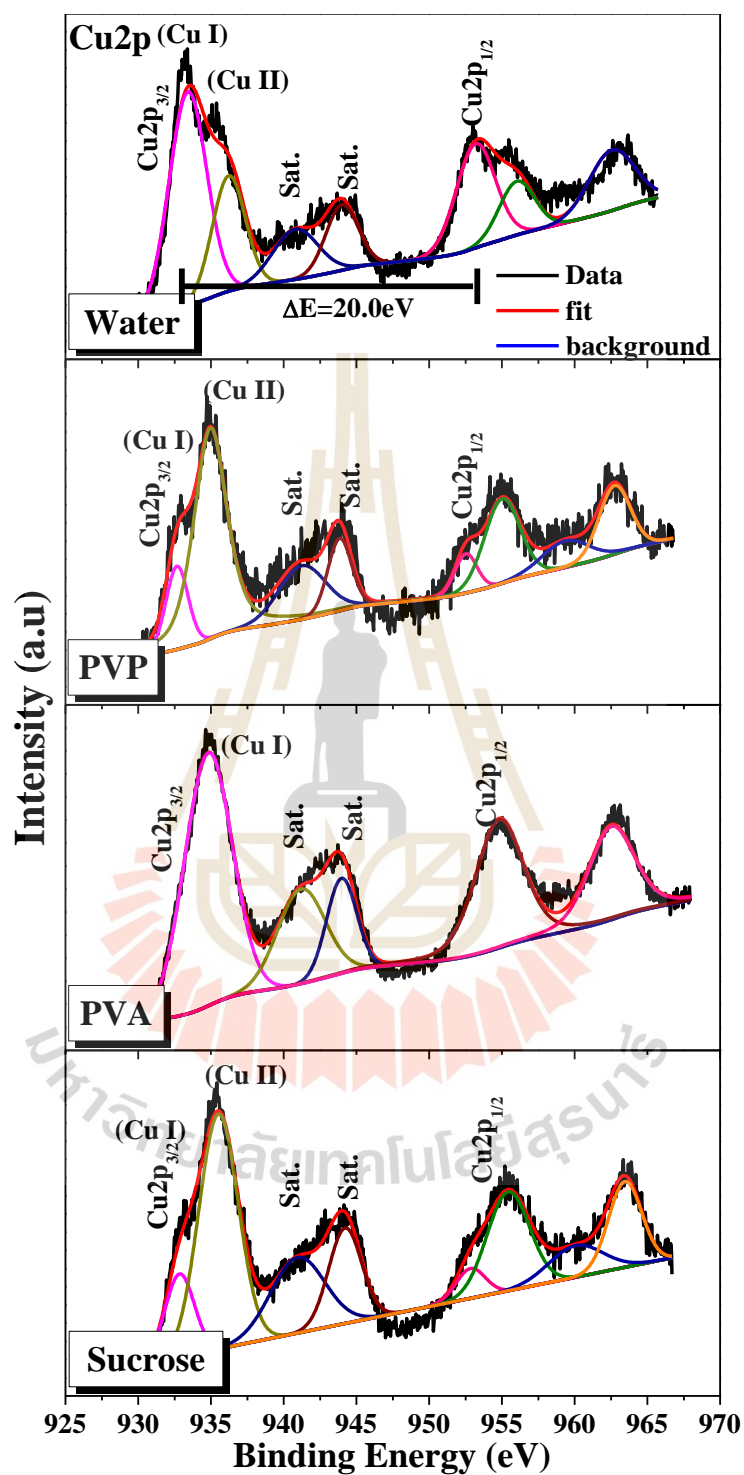
The XPS spectra in the Co 2p, Cu 2p, Fe 2p, Mg 2s, Mn 2p, Ni and Zn 2p regions of  $\text{NH}_4\text{MPO}_4\cdot\text{H}_2\text{O}$  powders (M = Co, Cu, Fe, Mg, Mn, Ni, Zn) with water, PVP, PVA, Sucrose and CTAB solution are shown in Figure 4.48 - 61. The XPS spectra of Co 2p of  $\text{NH}_4\text{CoPO}_4\cdot\text{H}_2\text{O}$  are shown in Figure 4.48. Peaks fit of both species of  $\text{Co}^{2+}$  ( $2p_{3/2}$  BE = ~781 eV) and  $\text{Co}^{3+}$  ( $2p_{3/2}$  BE = ~784 eV) are observed in all sample  $\text{NH}_4\text{CoPO}_4\cdot\text{H}_2\text{O}$  powder.

Figure 4.48 - 54 shows XPS spectra of Co 2p, Cu 2p, Fe 2p, Mg 2s, Mn 2p, Ni and Zn 2p of  $\text{NH}_4\text{MPO}_4\cdot\text{H}_2\text{O}$  indicating that  $\text{Co}^{2+}$  ( $2p_{3/2}$  BE = ~781 eV) and  $\text{Co}^{3+}$  ( $2p_{3/2}$  BE = ~784 eV),  $\text{Cu}^{1+}$  ( $2p_{3/2}$  BE = ~933 eV,  $2p_{1/2}$  BE = ~953 eV)  $\text{Cu}^{2+}$  ( $2p_{3/2}$  BE = ~936 eV,  $2p_{1/2}$  BE = ~956 eV). Except  $\text{NH}_4\text{CuPO}_4\cdot\text{H}_2\text{O}$  with PVA solution shows only  $\text{Cu}^{2+}$  in sample. Fe 2p of  $\text{NH}_4\text{FePO}_4\cdot\text{H}_2\text{O}$  confirm  $\text{Fe}^{2+}$  ( $2p_{3/2}$  BE = 710.09 eV,  $2p_{1/2}$  BE = 724.10 eV) and  $\text{Fe}^{3+}$  ( $2p_{3/2}$  BE = ~711 eV,  $2p_{1/2}$  BE = ~726 eV).  $\text{NH}_4\text{MgPO}_4\cdot\text{H}_2\text{O}$  shows  $\text{Mg}^{2+}$  (2s BE = 89.32 eV).  $\text{NH}_4\text{MnPO}_4\cdot\text{H}_2\text{O}$  shows  $\text{Mn}^{3+}$  ( $2p_{3/2}$  BE = ~641 eV,  $2p_{1/2}$  BE = ~653 eV)  $\text{Mn}^{4+}$  ( $2p_{3/2}$  BE = ~642 eV,  $2p_{1/2}$  BE = ~654.45 eV).  $\text{NH}_4\text{NiPO}_4\cdot\text{H}_2\text{O}$  shows  $\text{Ni}^{2+}$  ( $2p_{3/2}$  BE = ~856 eV,  $2p_{1/2}$  BE = ~874 eV) and  $\text{NH}_4\text{ZnPO}_4$  shows  $\text{Zn}^{2+}$  ( $2p_{3/2}$  BE = ~1022 eV)

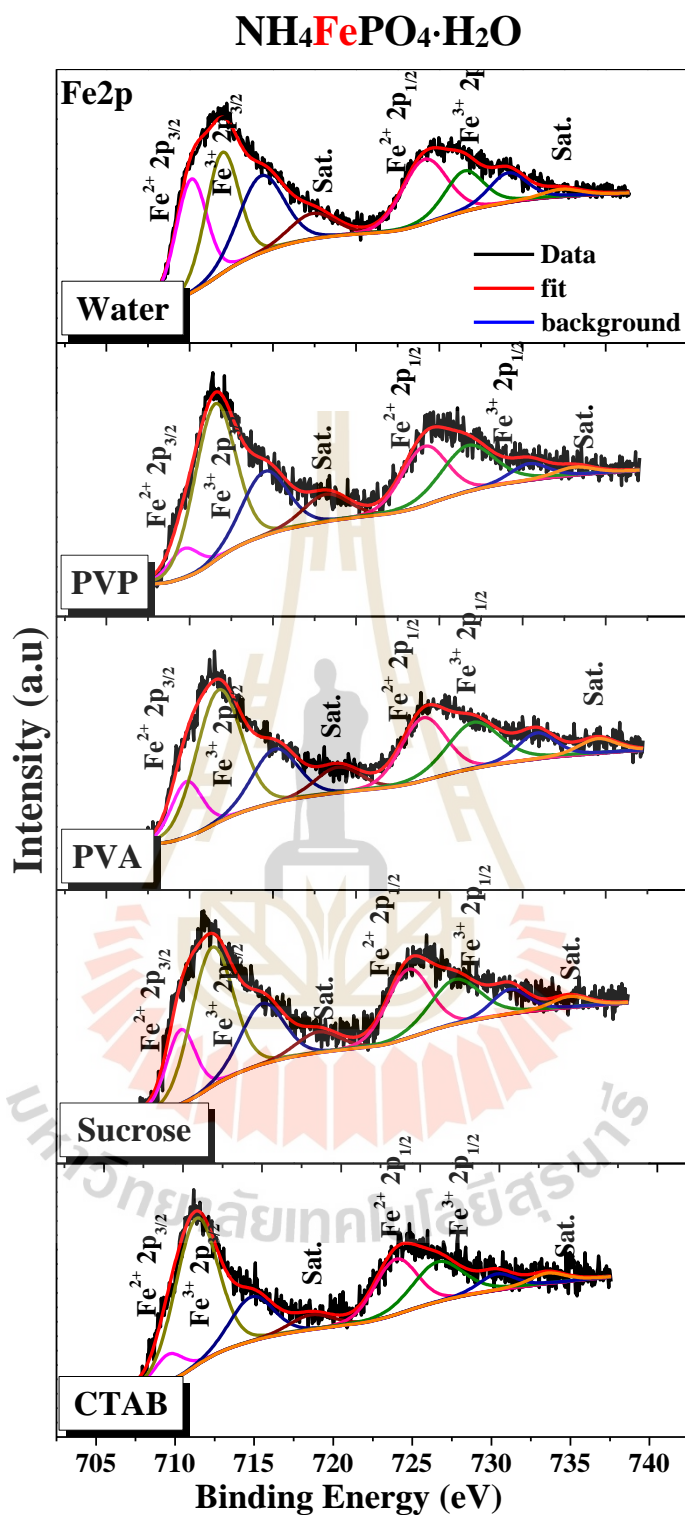
The XPS spectra of P 2p region of  $\text{NH}_4\text{MPO}_4\cdot\text{H}_2\text{O}$  sample (M = Co, Cu, Fe, Mg, Mn, Ni, Zn) with water, PVP, PVA, Sucrose and CTAB solution are shown in Figure 4.55 – 61. All of sample exhibit only peak of P 2p ( $2p_{3/2}$  BE = ~134 eV) are observed in  $\text{NH}_4\text{MPO}_4\cdot\text{H}_2\text{O}$ . These results indicated that  $\text{P}^{5+}$  ( $\text{NH}_4\text{MPO}_4\cdot\text{H}_2\text{O}$ ) in sample correspond XRD and XAS results.



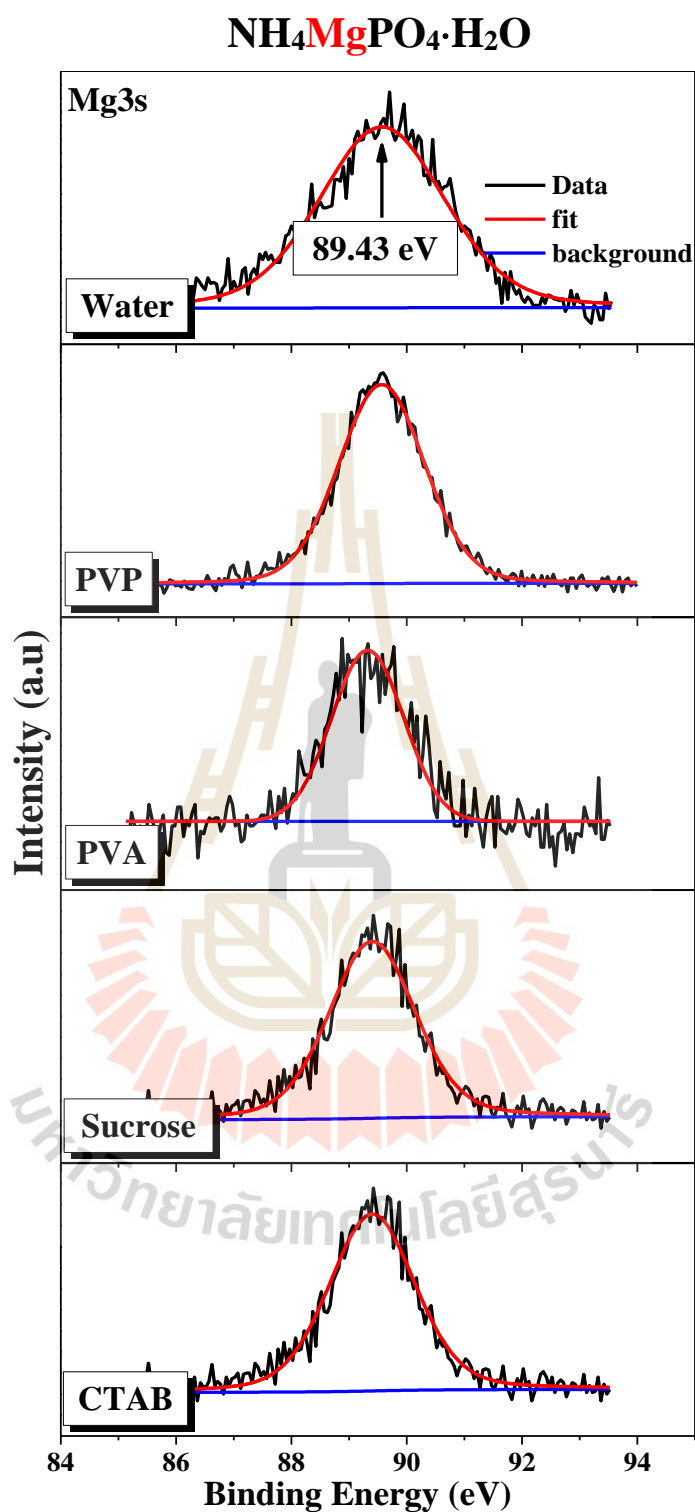
**Figure 4.48** Curve-fitting for Co<sub>2</sub>p and XPS spectra of  $\text{NH}_4\text{CoPO}_4\cdot\text{H}_2\text{O}$  samples with water, PVP, PVA, Sucrose and CTAB.

$$\text{NH}_4\text{CuPO}_4 \cdot \text{H}_2\text{O}$$


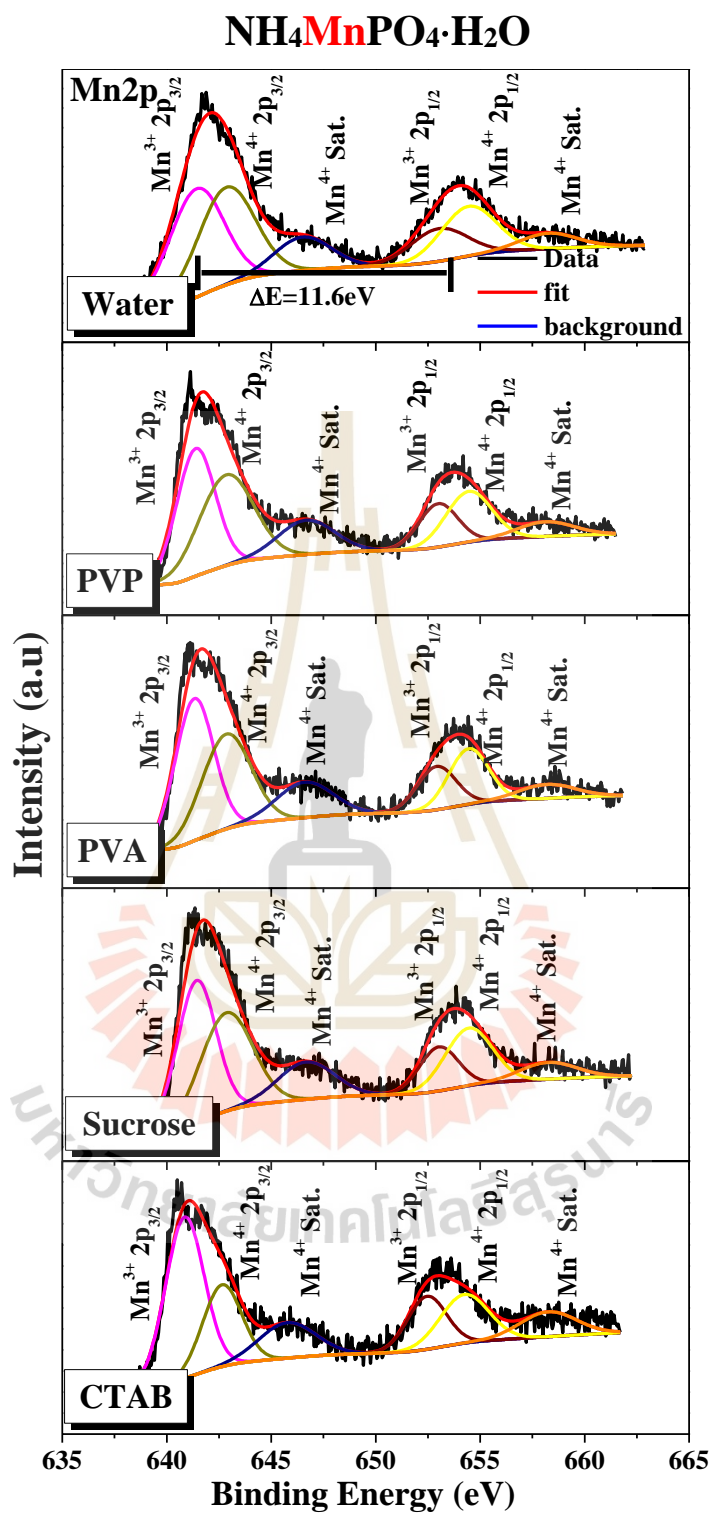
**Figure 4.49** Curve-fitting for Cu2p and XPS spectra of  $\text{NH}_4\text{CuPO}_4 \cdot \text{H}_2\text{O}$  samples with water, PVP, PVA and Sucrose.



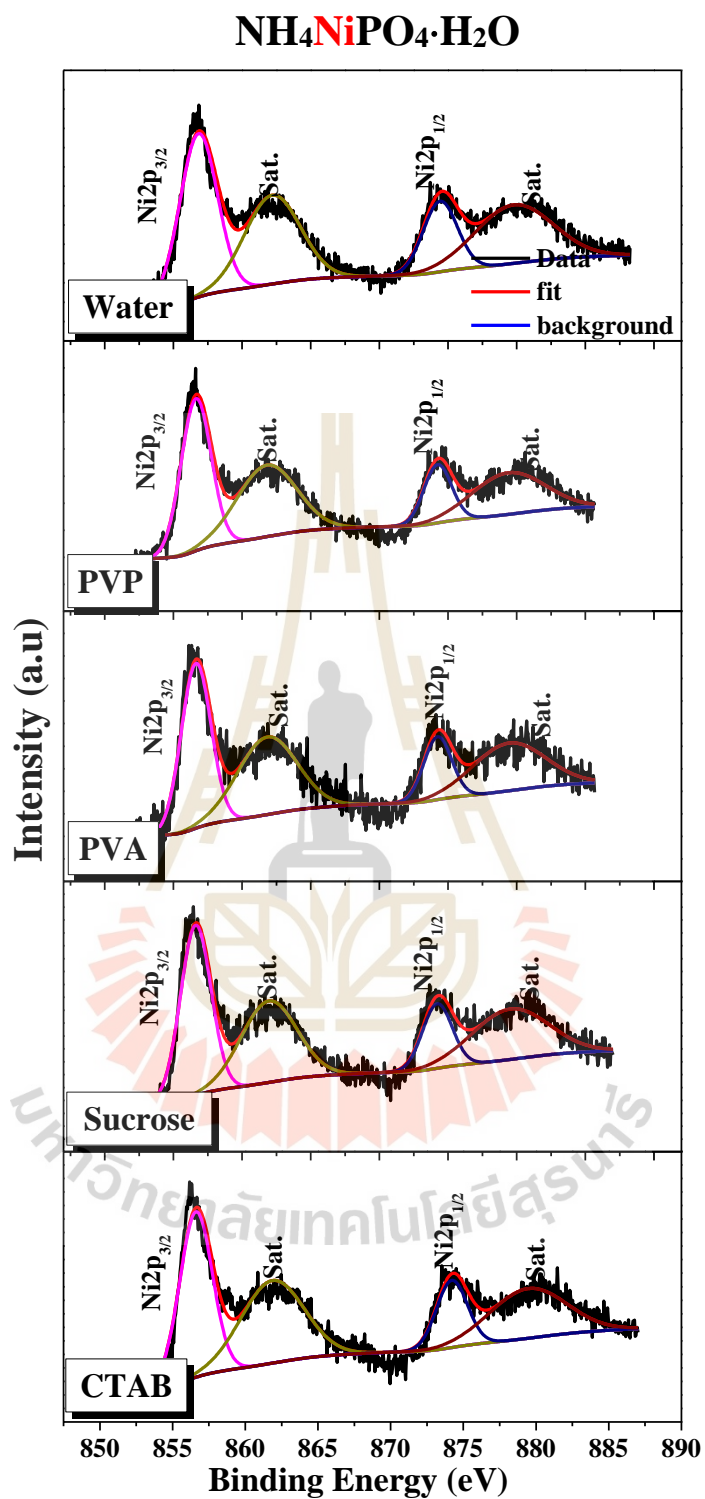
**Figure 4.50** Curve-fitting for Fe2p and XPS spectra of NH<sub>4</sub>FePO<sub>4</sub>·H<sub>2</sub>O samples with water, PVP, PVA Sucrose and CTAB.



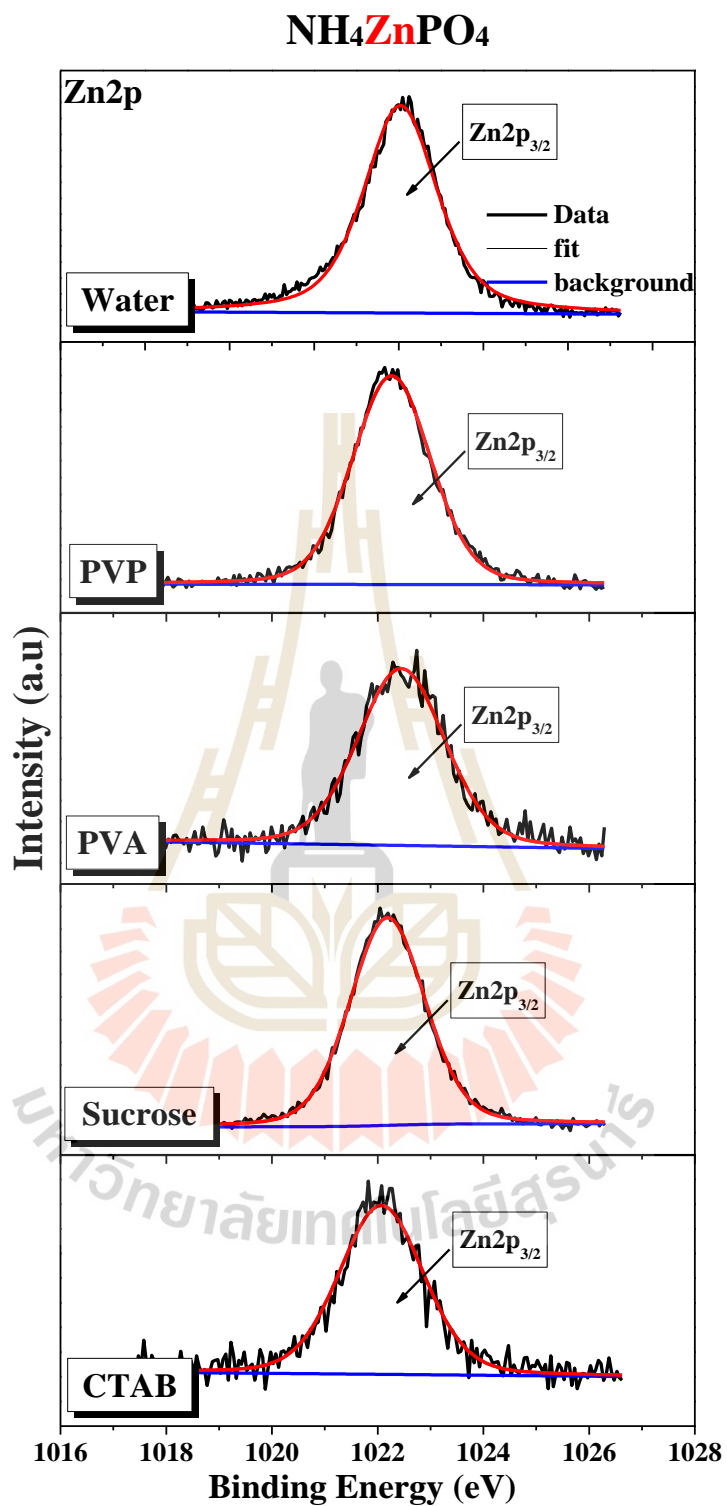
**Figure 4.51** Curve-fitting for Mg3s and XPS spectra of NH<sub>4</sub>MgPO<sub>4</sub>·H<sub>2</sub>O samples with water, PVP, PVA, Sucrose and CTAB.



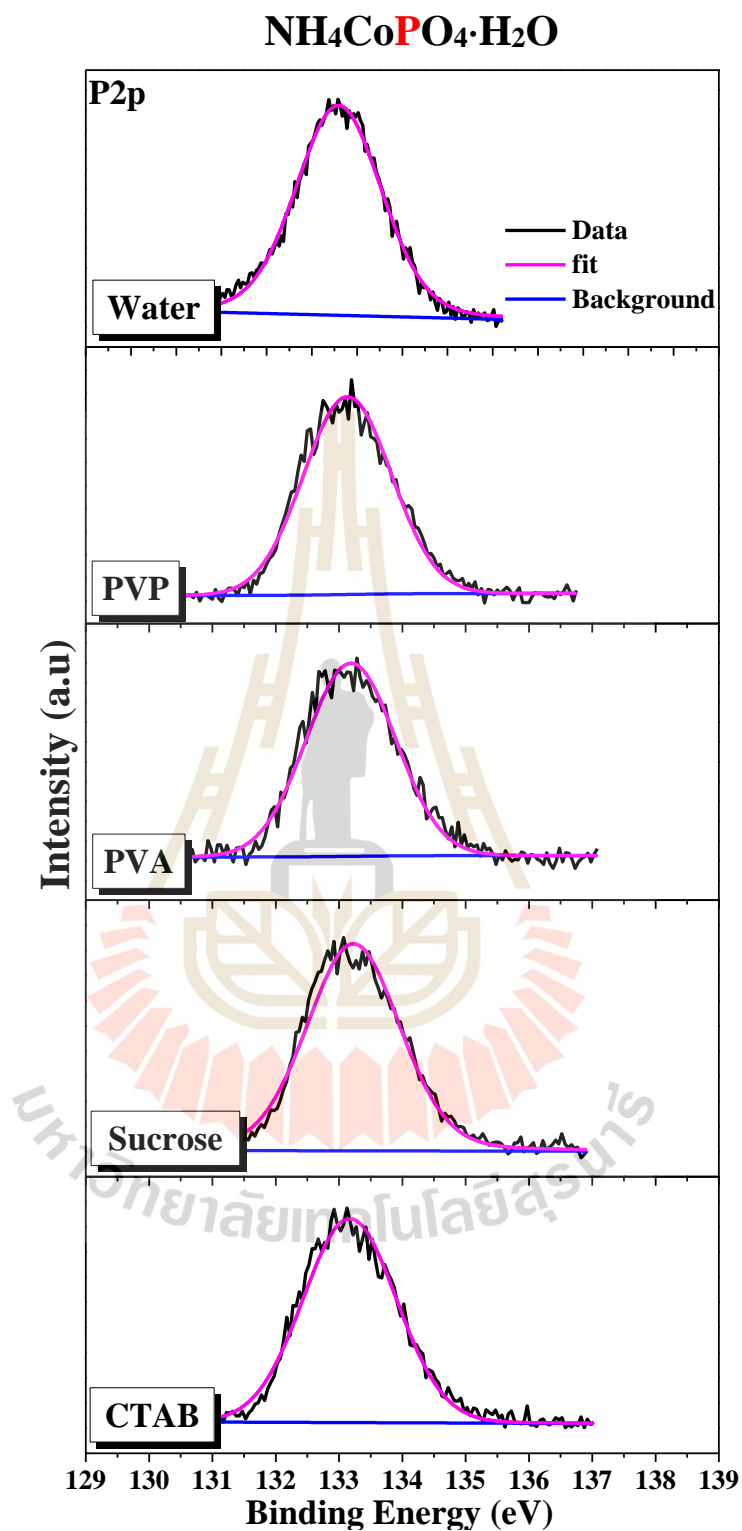
**Figure 4.52** Curve-fitting for Mn2p and XPS spectra of NH<sub>4</sub>MnPO<sub>4</sub>·H<sub>2</sub>O samples with water, PVP, PVA Sucrose and CTAB.



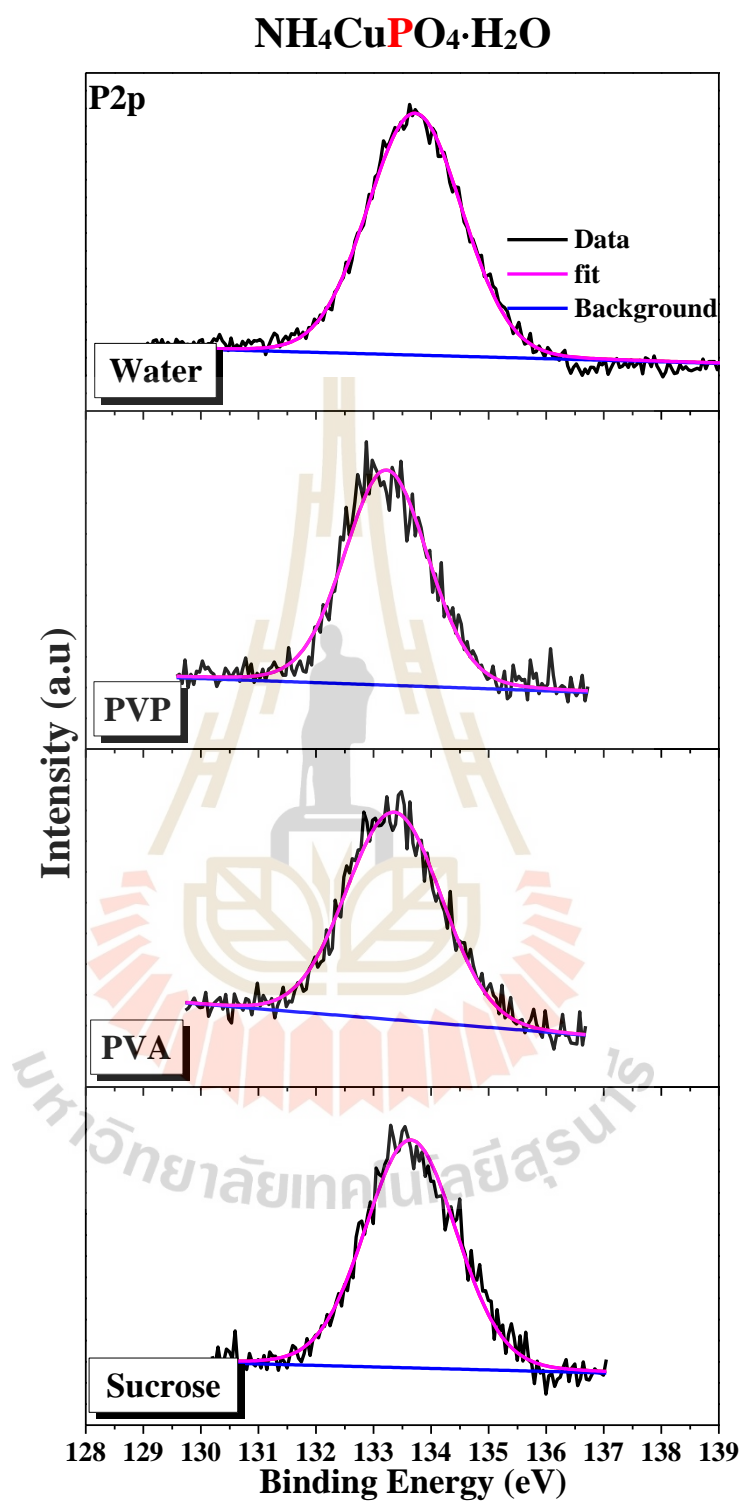
**Figure 4.53** Curve-fitting for Ni2p and XPS spectra of NH<sub>4</sub>NiPO<sub>4</sub>·H<sub>2</sub>O samples with water, PVP, PVA, Sucrose and CTAB.



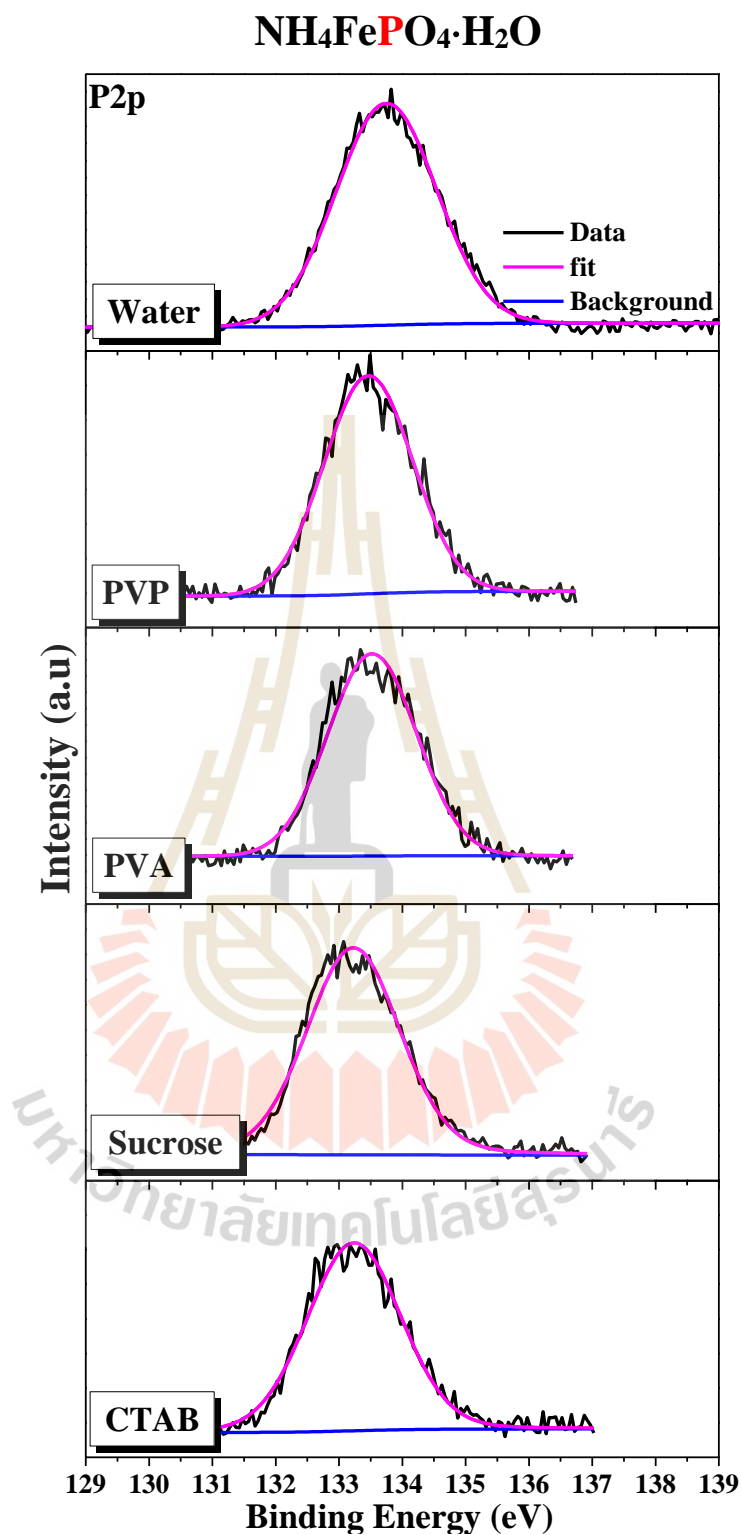
**Figure 4.54** Curve-fitting for Zn2p and XPS spectra of NH<sub>4</sub>ZnPO<sub>4</sub> samples with water, PVP, PVA Sucrose and CTAB.



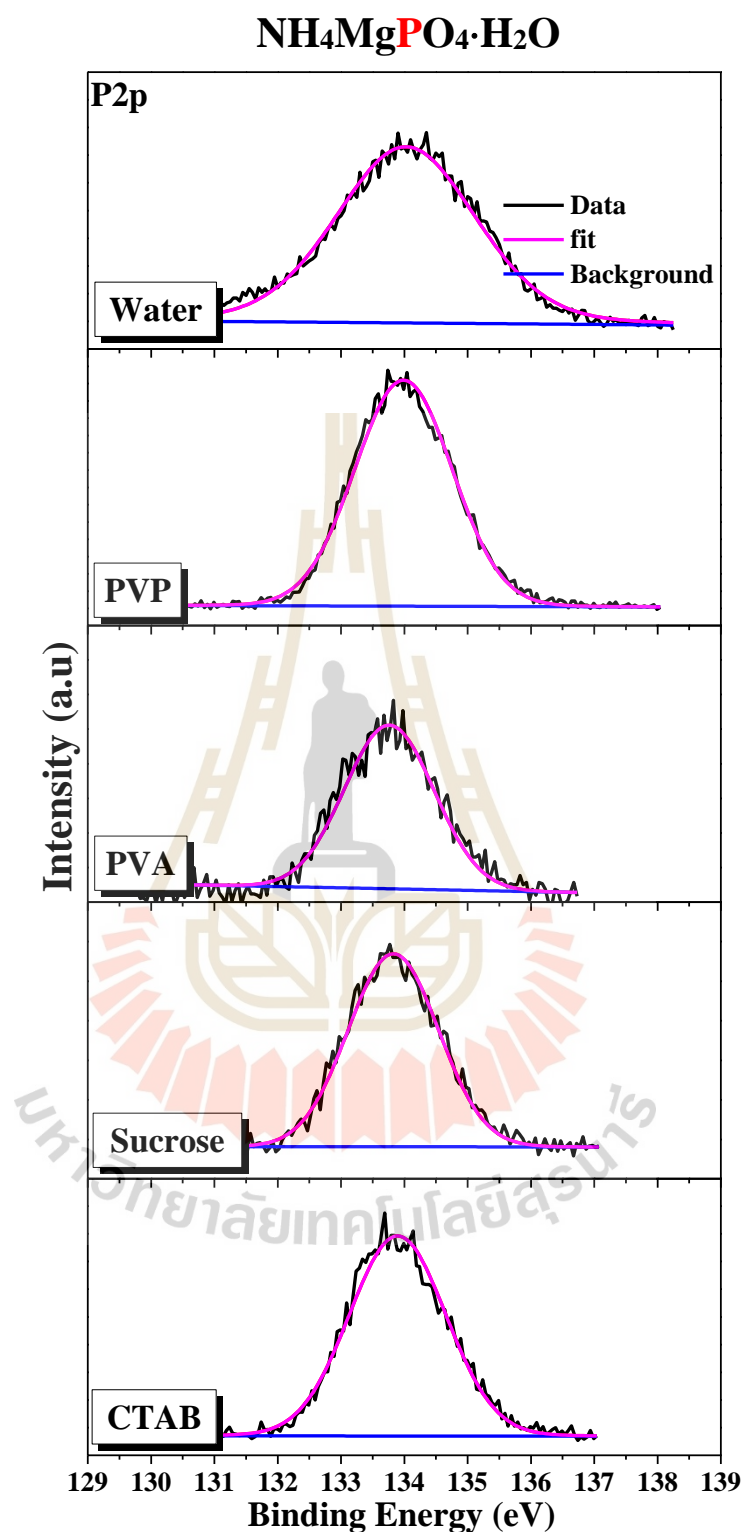
**Figure 4.55** Curve-fitting for P<sub>2</sub>p and XPS spectra of NH<sub>4</sub>CoPO<sub>4</sub>·H<sub>2</sub>O samples with water, PVP, PVA Sucrose and CTAB.



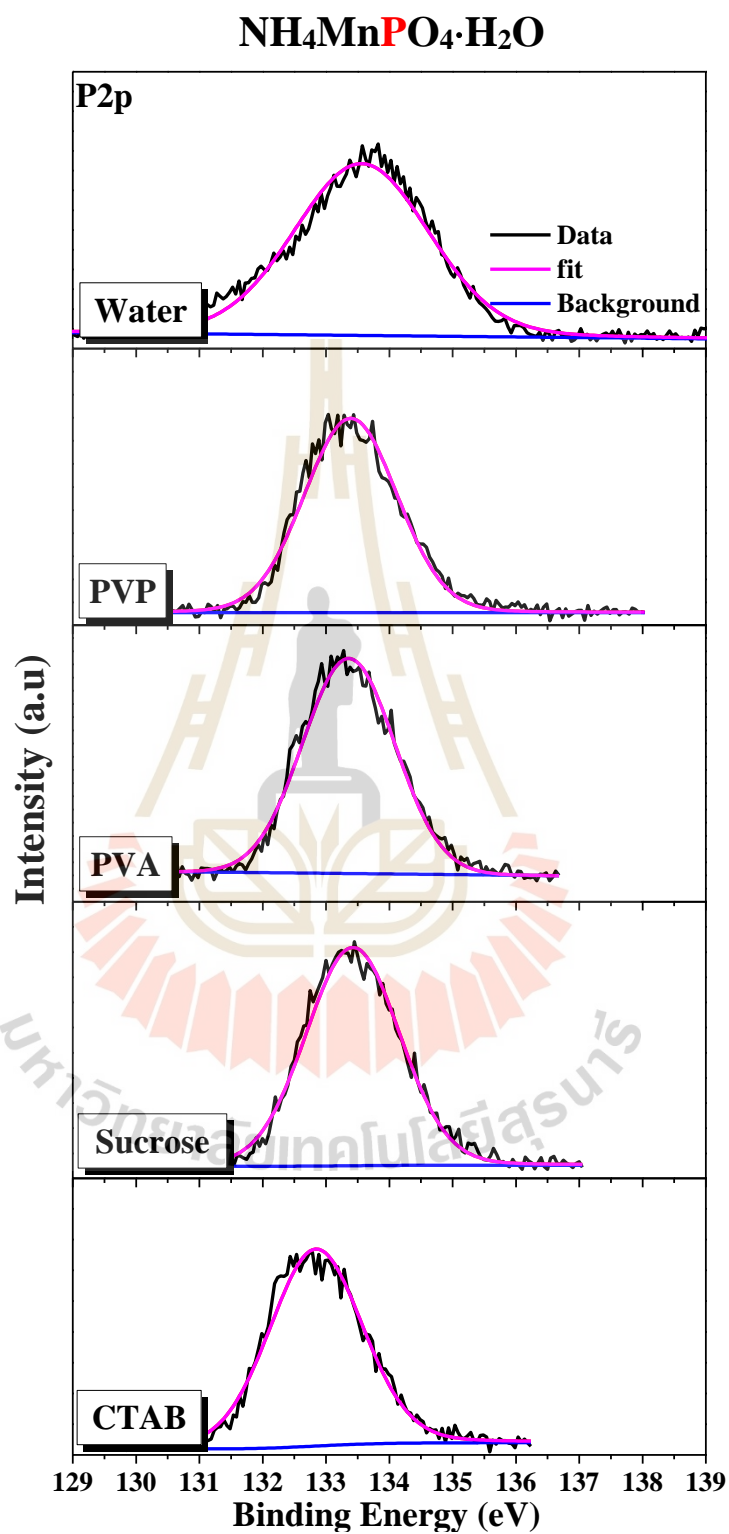
**Figure 4.56** Curve-fitting for P2p and XPS spectra of  $\text{NH}_4\text{CuPO}_4 \cdot \text{H}_2\text{O}$  samples with water, PVP, PVA and Sucrose



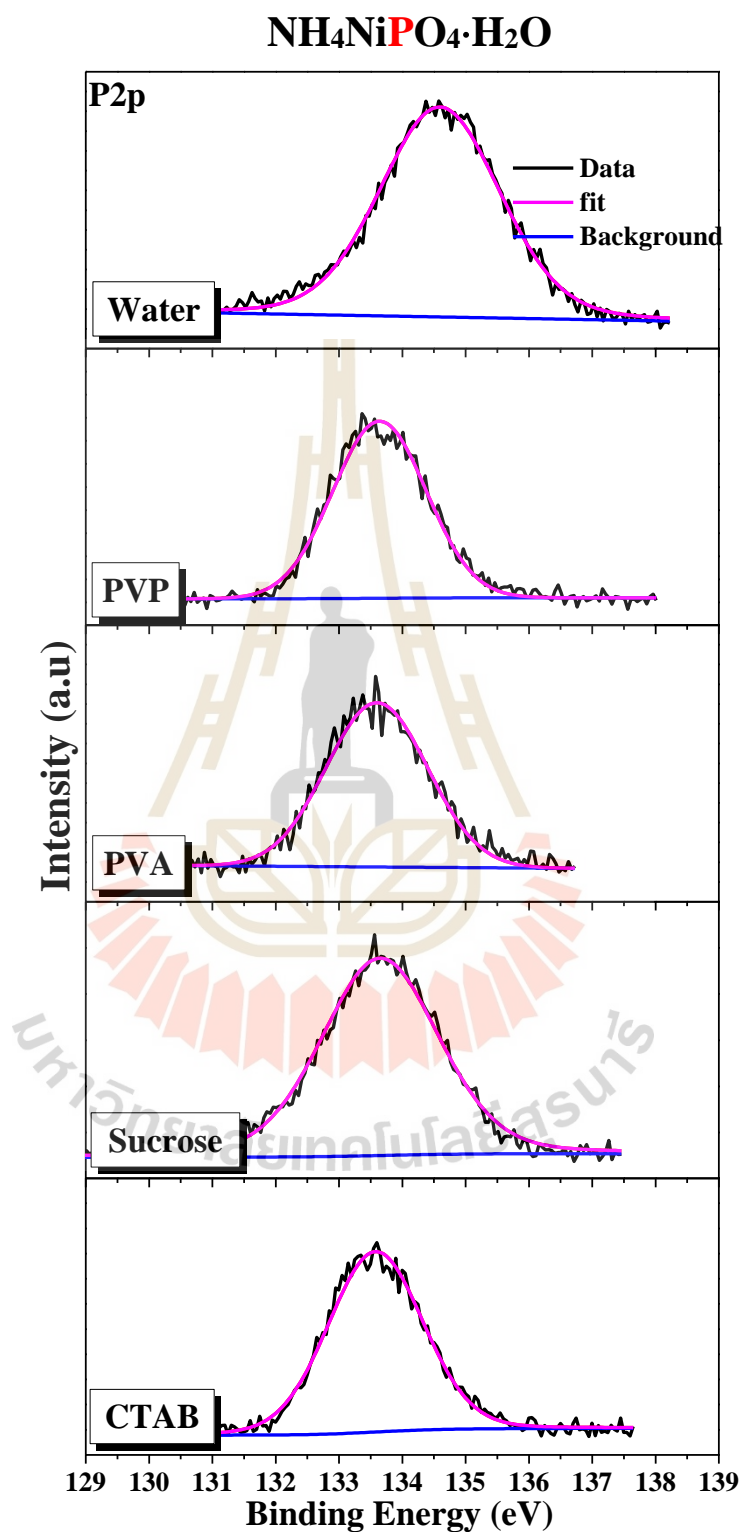
**Figure 4.57** Curve-fitting for P2p and XPS spectra of NH<sub>4</sub>FePO<sub>4</sub>·H<sub>2</sub>O samples with water, PVP, PVA Sucrose and CTAB.



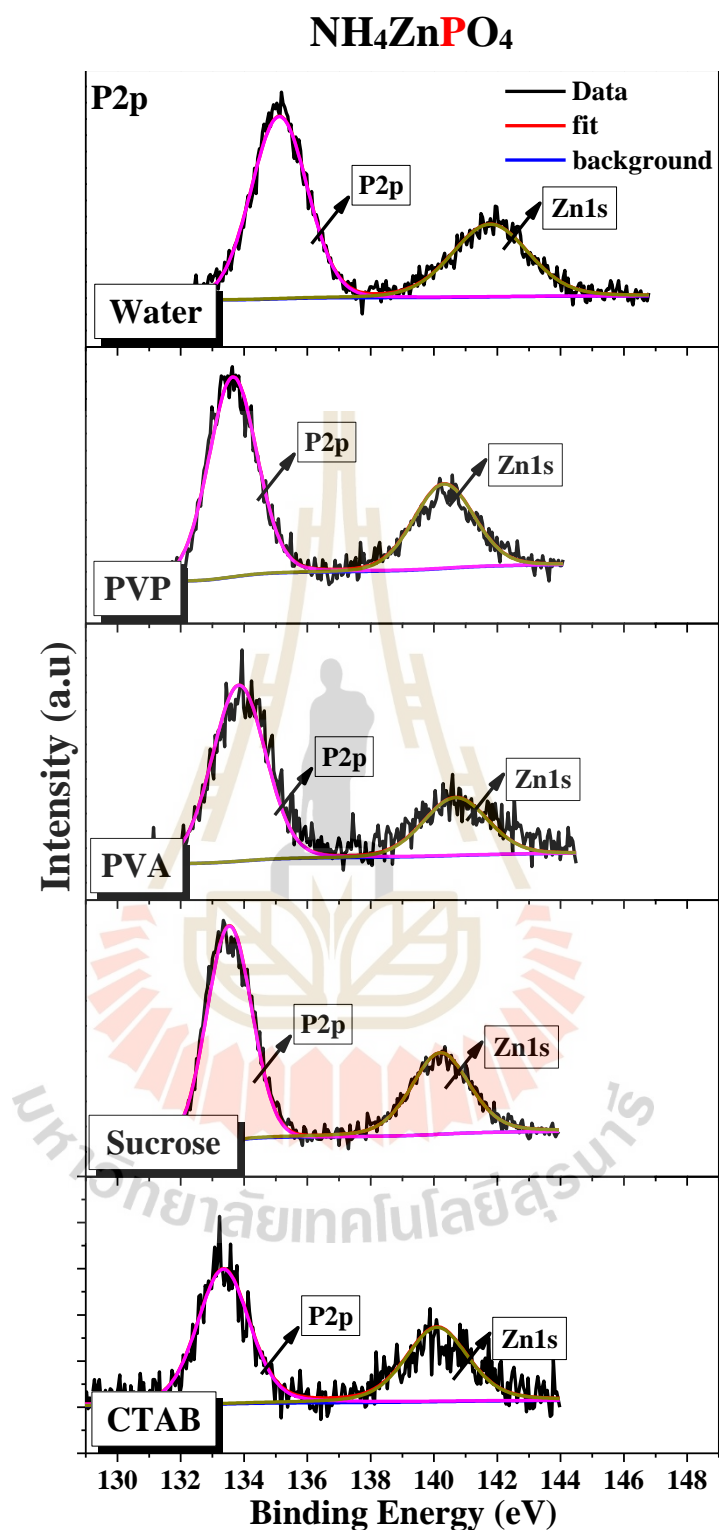
**Figure 4.58** Curve-fitting for P<sub>2</sub>p and XPS spectra of NH<sub>4</sub>MgPO<sub>4</sub>·H<sub>2</sub>O samples with water, PVP, PVA Sucrose and CTAB.



**Figure 4.59** Curve-fitting for P2p and XPS spectra of NH<sub>4</sub>MnPO<sub>4</sub>·H<sub>2</sub>O samples with water, PVP, PVA Sucrose and CTAB.



**Figure 4.60** Curve-fitting for P2p and XPS spectra of  $\text{NH}_4\text{NiPO}_4 \cdot \text{H}_2\text{O}$  samples with water, PVP, PVA Sucrose and CTAB.



**Figure 4.61** Curve-fitting for P2p and XPS spectra of NH<sub>4</sub>ZnPO<sub>4</sub> samples with water, PVP, PVA Sucrose and CTAB.

#### 4.2.5 Ion release properties

In addition to the crystal size and morphology, another important property is the ion release capacity of the potential slow-release fertilizer. The table 4.9 to 4.11 show the ion release from  $\text{NH}_4\text{MPO}_4\cdot\text{H}_2\text{O}$  (M= Mg, Co, Fe, Mn, Ni, Zn, Cu) water condition samples by inductively coupled plasma optical emission spectrometry (ICP-OES) method. In this study, the ion release measurement was used to clarify type of fertilizer in all  $\text{NH}_4\text{MPO}_4\cdot\text{H}_2\text{O}$  (M = Mg, Co, Fe, Mn, Ni, Zn, Cu) samples prepared by using water solution. From the table, it is found that all water condition samples emit phosphorus ions.  $\text{NH}_4\text{MPO}_4\cdot\text{H}_2\text{O}$  can be sorted from the release of phosphorus ion from high to low as follows  $\text{NH}_4\text{FePO}_4\cdot\text{H}_2\text{O}$  (105.0 mg/L),  $\text{NH}_4\text{MgPO}_4\cdot\text{H}_2\text{O}$  (91.0 mg/L),  $\text{NH}_4\text{NiPO}_4\cdot 6\text{H}_2\text{O}$  (88.1 mg/L),  $\text{NH}_4\text{MnPO}_4\cdot\text{H}_2\text{O}$  (57.9 mg/L),  $\text{NH}_4\text{CoPO}_4\cdot\text{H}_2\text{O}$  (34.7 mg/L),  $\text{NH}_4\text{ZnPO}_4$  (32.8 mg/L),  $\text{NH}_4\text{CuPO}_4\cdot\text{H}_2\text{O}$  (10.3 mg/L) and respectively.  $\text{NH}_4\text{MPO}_4\cdot\text{H}_2\text{O}$  (M= Mg, Co, Fe, Mn, Ni, Zn, Cu) can be sorted from the release of metal ion from high to low as follows  $\text{NH}_4\text{MgPO}_4\cdot\text{H}_2\text{O}$  (14.9 mg/L),  $\text{NH}_4\text{FePO}_4\cdot\text{H}_2\text{O}$  (7.4 mg/L),  $\text{NH}_4\text{ZnPO}_4$  (0.35 mg/L),  $\text{NH}_4\text{CuPO}_4\cdot\text{H}_2\text{O}$  (0.26 mg/L),  $\text{NH}_4\text{NiPO}_4\cdot\text{H}_2\text{O}$  (0.24 mg/L),  $\text{NH}_4\text{CoPO}_4\cdot\text{H}_2\text{O}$  (0 mg/L) and  $\text{NH}_4\text{MnPO}_4\cdot\text{H}_2\text{O}$  (0 mg/L), respectively.

In the case of all  $\text{NH}_4\text{MPO}_4\cdot\text{H}_2\text{O}$  (M = Mn, Fe, Co, Cu) samples prepared by using water solution. The results of ion release properties are summarized in Table 4.9 to 4.11. Based on the experimental results, the P ion releases of 57.90, 105.00, 34.7 and 10.30 mg/L were observed in the  $\text{NH}_4\text{MPO}_4\cdot\text{H}_2\text{O}$  samples where M = Mn, Fe, Co, and Cu, respectively. In case of the metal ion releases, the amounts of 0, 7.40, 0 and 0.26 mg/L were observed in the  $\text{NH}_4\text{MPO}_4\cdot\text{H}_2\text{O}$  samples where M = Mn, Fe, Co, and Cu,

respectively. According to the ion release result, mass of the highest amount of P and Fe ion releases in the sample of  $\text{NH}_4\text{FePO}_4\cdot\text{H}_2\text{O}$  was calculated to be 298 mg in 1g of this compound. By combining the value of P (105.00 mg/L) and Fe ion (7.40 mg/L) release, the value of approximately 11.24 mg out of 298 mg of P and Fe ions corresponding to around 3.8 % of the total mass was released in 24 h. Based on the obtained results, our  $\text{NH}_4\text{MPO}_4\cdot\text{H}_2\text{O}$  (M =Mn, Fe, Co, Cu) powders can be classified as a slow release fertilizer where less than 15% of the ions was released in 24 h (Trenkel, 2010). For comparison between Fe products and the commercial iron foliar fertilizer (Agrichem Co., Ltd.) could release Fe ions ~10 mg/L with the assistance of acidic additives. For  $\text{NH}_4\text{FePO}_4\cdot\text{H}_2\text{O}$ , the release of Fe ions was approximately 7.40 mg/L in the aqueous phase which is lower than that of commercial fertilizer. More importantly, the  $\text{NH}_4\text{FePO}_4\cdot\text{H}_2\text{O}$  products can be used without the assistance of acidic additives resulting in an easy to use and reducing costs. For  $\text{NH}_4\text{CuPO}_4\cdot\text{H}_2\text{O}$  sample, the releases of Cu and P ions were observed to be 0.26 and 10.30 mg/L, respectively. In photosynthesis process, the Cu concentration should be between 2.2 and 6.9 mg/kg (Römheld and Marschner, 1991). Therefore, our products can be used for practical purposes by increasing the concentration to support the nutritional needs of the plant. In the case of  $\text{NH}_4\text{MnPO}_4\cdot\text{H}_2\text{O}$  products, the critical deficiency concentration of manganese in leaf is 10-15 mg/kg dry weight (Römheld and Marschner, 1991) thus the Mn ion would be 4-6 mg/L if all Mn ions were in the aqueous solution (the average water content in leaf is ~70 wt. %) (Li et al., 2014). Then,  $\text{NH}_4\text{MnPO}_4\cdot\text{H}_2\text{O}$  could not release ions (0 mg/L) in the aqueous phase, which is lower than that of commercial fertilizer. Similarly, the obtained  $\text{NH}_4\text{CoPO}_4\cdot\text{H}_2\text{O}$  could not release the Co ions.

However, all samples have a high phosphorus ion release whereas the data of the commercial phosphorus ion fertilizer does not available. This suggests that our simple facile route can be used to synthesize a  $\text{NH}_4\text{MPO}_4\cdot\text{H}_2\text{O}$  (M =Mn, Fe, Co, Cu) based slow-release fertilizer

In the case of all  $\text{NH}_4\text{MgPO}_4\cdot\text{H}_2\text{O}$  samples prepared by using water, PVA, PVP, sucrose and CTAB solution. The results of ion release properties are summarized in Table 4.9. It was found that the P ion releases of 91.0, 75.7, 170.0, 104.0, and 102.0 mg/L were observed in the  $\text{NH}_4\text{MgPO}_4\cdot\text{H}_2\text{O}$  prepared in water, PVA, PVP, sucrose and CTAB solution, respectively. The Mg ion releases of 14.9, 11.1, 32.0, 63.8 and 66.0 mg/L were observed in the  $\text{NH}_4\text{MgPO}_4\cdot\text{H}_2\text{O}$  prepared in water, PVA, PVP, sucrose and CTAB solution, respectively.

In the case of all  $\text{NH}_4\text{CoPO}_4\cdot\text{H}_2\text{O}$  samples prepared by using water, PVP, PVA, sucrose and CTAB solution. The results of ion release properties are summarized in Table 4.9. It was found that the P ion releases of 34.7, 27.0, 58.8, 54.9, and 63.6 mg/L were observed in the  $\text{NH}_4\text{CoPO}_4\cdot\text{H}_2\text{O}$  prepared in water, PVA, PVP, sucrose and CTAB solution, respectively. The Co ion releases of 0 mg/L were observed in the all condition of  $\text{NH}_4\text{CoPO}_4\cdot\text{H}_2\text{O}$ .

In the case of all  $\text{NH}_4\text{FePO}_4\cdot\text{H}_2\text{O}$  samples prepared by using water, PVA, PVP, sucrose and CTAB solution. The results of ion release properties are summarized in Table 4.10. It was found that the P ion releases of 105.0, 81.2, 83.3, 88.1, and 50.6 mg/L were observed in the  $\text{NH}_4\text{FePO}_4\cdot\text{H}_2\text{O}$  prepared in water, PVA, PVP, sucrose and CTAB solution, respectively. The Fe ion releases of 7.4, 45.8, 19.9, 54.2 and 0.41 mg/L were

observed in the  $\text{NH}_4\text{FePO}_4\cdot\text{H}_2\text{O}$  prepared in water, PVA, PVP, sucrose and CTAB solution, respectively.

In the case of all  $\text{NH}_4\text{MnPO}_4\cdot\text{H}_2\text{O}$  samples prepared by using water, PVA, PVP, sucrose and CTAB solution. The results of ion release properties are summarized in Table 4.10. It was found that the P ion releases of 57.9, 52.8, 58.8, 54.9, and 63.6 mg/L were observed in the  $\text{NH}_4\text{MnPO}_4\cdot\text{H}_2\text{O}$  prepared in water, PVA, PVP, sucrose and CTAB solution, respectively. The Mn ion releases of 0 mg/L were observed in the all condition of  $\text{NH}_4\text{MnPO}_4\cdot\text{H}_2\text{O}$ .

In the case of all  $\text{NH}_4\text{NiPO}_4\cdot\text{H}_2\text{O}$  samples prepared by using water, PVA, PVP, sucrose and CTAB solution. The results of ion release properties are summarized in Table 4.9 to 4.11. It was found that the P ion releases of 88.1, 67.7, 33.6, 28.1, and 46.4 mg/L were observed in the  $\text{NH}_4\text{NiPO}_4\cdot\text{H}_2\text{O}$  prepared in water, PVA, PVP, sucrose and CTAB solution, respectively. The Ni ion releases of 0.24, 3.88, 5.10, 5.54 and 5.05 mg/L were observed in the  $\text{NH}_4\text{NiPO}_4\cdot\text{H}_2\text{O}$  prepared in water, PVA, PVP, sucrose and CTAB solution, respectively.

In the case of all  $\text{NH}_4\text{CuPO}_4\cdot\text{H}_2\text{O}$  samples prepared by using water, PVA, PVP, sucrose and CTAB solution. The results of ion release properties are summarized in Table 4.9. It was found that the P ion releases of 10.3, 4.78, 15.6, 76.7, and 23.8 mg/L were observed in the  $\text{NH}_4\text{CuPO}_4\cdot\text{H}_2\text{O}$  prepared in water, PVA, PVP, sucrose and CTAB solution, respectively. The Cu ion releases of 0.26, 6.36, 7.51, 38.6 and 0.16 mg/L were observed in the  $\text{NH}_4\text{CuPO}_4\cdot\text{H}_2\text{O}$  prepared in water, PVA, PVP, sucrose and CTAB solution, respectively.

In the case of all  $\text{NH}_4\text{ZnPO}_4$  samples prepared by using water, PVP, PVA, sucrose and CTAB solution. The results of ion release properties are summarized in Table 4.11. It was found that the P ion releases of 32.8, 41.4, 33.6, 46.0, and 26.5 mg/L were observed in the  $\text{NH}_4\text{ZnPO}_4$  prepared in water, PVP, PVA, sucrose and CTAB solution, respectively. The Zn ion releases of 0.35, 1.63, 0.66, 4.22 and 0 mg/L were observed in the  $\text{NH}_4\text{ZnPO}_4$  prepared in water, PVP, PVA, sucrose and CTAB solution, respectively. From these results, it can be seen that Zn and P ions with hexagonal structure are released more than those having monoclinic structure. Also, the Zn and P ions are released with a higher proportion of Hopeite. Considering the molar mass ratio of  $\text{NH}_4\text{ZnPO}_4$  prepared in sucrose solution, the mass of P and Zn ions can be calculated to be around 540 mg in 1 g of this compound. By combining the value of P and Zn ion release (52.5 mg/L), approximately 5 mg out of 540 mg of P and Zn ions corresponding to around 1% of the total mass was released in 24 h. Based on the obtained results, our  $\text{NH}_4\text{ZnPO}_4$  powders can be classified as a slow-release fertilizer where less than 15% of the ions was released in 24 h (Trenkel, 2010). Specifically, the Zn ion release of 4.17 mg/L is comparable with previous reports of the  $\text{Zn}(\text{OH})_2$  (9.62 mg/L) (Li et al., 2012), the core-shell  $\text{ZnSO}_4$  (3.8 mg/L) (Yuvaraj and Subramanian, 2015), the zeolite-based  $\text{ZnSO}_4$  (4.5 mg/L) (Yuvaraj and Subramanian, 2018) as well as the commercial ZnO-based fertilizer (1-2 mg/L) (Li et al., 2012). This suggests that our simple facile route can be used to synthesize a  $\text{NH}_4\text{ZnPO}_4$ -based slow-release fertilizer.

**Table 4.9** Ion release from  $\text{NH}_4\text{MPO}_4\cdot\text{H}_2\text{O}$  (M= Mg, Co, Cu) samples by Inductively Coupled Plasma Optical Emission Spectrometry (ICP-OES) method.

Samples	Ion release from samples		
		M(mg/L)	P (mg/L)
$\text{NH}_4\text{CoPO}_4\cdot\text{H}_2\text{O}$	Water	0	34.7
	PVA	0.05	27.0
	PVP	0.05	24.3
	Sucrose	0.08	55.2
	CTAB	0	58.8
$\text{NH}_4\text{CuPO}_4\cdot\text{H}_2\text{O}$	Water	0.26	10.3
	PVA	6.36	4.78
	PVP	7.51	15.6
	Sucrose	38.6	76.7
	CTAB	0.16	23.8
$\text{NH}_4\text{MgPO}_4\cdot\text{H}_2\text{O}$	Water	14.9	91.0
	PVA	11.1	75.7
	PVP	32.0	170.0
	Sucrose	63.8	104
	CTAB	66.0	102

**Table 4. 10** Ion release from  $\text{NH}_4\text{MPO}_4\cdot\text{H}_2\text{O}$  (M= Fe, Mn) samples by Inductively Coupled Plasma Optical Emission Spectrometry (ICP-OES) method.

Samples	Ion release from samples		
		M(mg/L)	P (mg/L)
$\text{NH}_4\text{MnPO}_4\cdot\text{H}_2\text{O}$	Water	0	57.9
	PVA	0	52.8
	PVP	0	58.8
	Sucrose	0	54.9
	CTAB	0	63.6
$\text{NH}_4\text{FePO}_4\cdot\text{H}_2\text{O}$	Water	7.4	105.0
	PVA	45.8	81.2
	PVP	19.9	83.3
	Sucrose	54.2	88.1
	CTAB	0.41	50.6

**Table 4. 11** Ion release from  $\text{NH}_4\text{MPO}_4\cdot\text{H}_2\text{O}$  (M= Ni, Zn) samples by Inductively Coupled Plasma Optical Emission Spectrometry (ICP-OES) method.

Samples	Ion release from samples		
		M(mg/L)	P (mg/L)
$\text{NH}_4\text{NiPO}_4\cdot\text{H}_2\text{O}$	Water	0.24	88.1
	PVA	3.88	67.7
	PVP	5.10	33.6
	Sucrose	5.54	28.1
	CTAB	5.05	46.4
$\text{NH}_4\text{ZnPO}_4$	Water	0.35	32.8
	PVA	0.66	33.6
	PVP	1.63	41.4
	Sucrose	4.22	46.0
	CTAB	0	26.5

## CHAPTER V

### CONCLUSION AND SUGGESTION

In this work,  $\text{NH}_4\text{MPO}_4\cdot\text{H}_2\text{O}$  ( $\text{M} = \text{Mg}, \text{Co}, \text{Fe}, \text{Mn}, \text{Ni}, \text{Zn}, \text{Cu}$ ) particles have been successfully synthesized by a simple coprecipitation method in water solution. The effects of solvents on  $\text{NH}_4\text{MPO}_4\cdot\text{H}_2\text{O}$  ( $\text{M} = \text{Mg}, \text{Co}, \text{Fe}, \text{Mn}, \text{Ni}, \text{Zn}, \text{Cu}$ ) structure were studied by dissolving PVP, PVA, sucrose and CTAB in DI water. The surface morphology, structure formation and local structure of the prepared powder were characterized by XRD, TEM, SEM, XAS and XPS techniques. The magnetic and ion release properties were determined by VSM and ICP-OES techniques, respectively. From the results and discussion, the conclusions of the whole thesis can be summarized as follows:

#### 5.1 The structure and morphology characterization

The XRD results of the prepared  $\text{NH}_4\text{MPO}_4\cdot\text{H}_2\text{O}$  ( $\text{M} = \text{Co}, \text{Fe}, \text{Mn}, \text{Ni}$ ) samples by a simple coprecipitation method exhibit the formation of the orthorhombic structure with the Pmn21 space group without detected other phases impurities. On the other hand, the formation of hexagonal and monoclinic structures was revealed in  $\text{NH}_4\text{ZnPO}_4$  and  $\text{NH}_4\text{CuPO}_4\cdot\text{H}_2\text{O}$  samples, respectively. However, the phase impurity of  $\text{NH}_4\text{MgPO}_4\cdot 6\text{H}_2\text{O}$  could be detected in the replacement of  $\text{M} = \text{Mg}$  sample. Therefore, the replacement of  $\text{M}$  with different Mg, Co, Fe, Mn, Ni, Zn, and Cu in the  $\text{NH}_4\text{MPO}_4\cdot\text{H}_2\text{O}$  structure provides the different crystal structures.

For thermal decomposition studies, TG/DSC curves of the  $\text{NH}_4\text{MPO}_4\cdot\text{H}_2\text{O}$  ( $\text{M} = \text{Mg, Co, Fe, Mn, Ni, Zn, Cu}$ ) samples were stable under  $100^\circ\text{C}$ . For the studies of microstructure, the SEM images of the samples revealed that the obtained all of particles were microparticle and the morphology is plate-like shape with the size about  $10\ \mu\text{m}$ . In contrast, microflower with nearly spherical shape was observed in  $\text{NH}_4\text{MnPO}_4\cdot\text{H}_2\text{O}$  sample. Additionally, TEM bright field images confirmed that the obtained particles were micro size and the SAED patterns show lattice fringes and spot patterns of orthorhombic structure  $\text{NH}_4\text{MPO}_4\cdot\text{H}_2\text{O}$  ( $\text{M} = \text{Co, Fe, Mn, Ni, Cu}$ ) without detected any secondary phases. These results are in good agreement with XRD results.

For the local structure, the X-ray absorption near-edge structure (XANES) spectra of the  $\text{NH}_4\text{MPO}_4\cdot\text{H}_2\text{O}$  ( $\text{M} = \text{Mg, Co, Fe, Mn, Ni, Zn, Cu}$ ) were evaluated at the M K-edge energy. XANES results imply that Co, Cu, Fe, and Mn ions in  $\text{NH}_4\text{CoPO}_4\cdot\text{H}_2\text{O}$ ,  $\text{NH}_4\text{CuPO}_4\cdot\text{H}_2\text{O}$ ,  $\text{NH}_4\text{FePO}_4\cdot\text{H}_2\text{O}$ , and  $\text{NH}_4\text{MnPO}_4\cdot\text{H}_2\text{O}$  samples have the mixing oxidation state of  $\text{Co}^{2+}$  and  $\text{Co}^{3+}$ , Cu and  $\text{Cu}^{2+}$ ,  $\text{Fe}^{+2}$  and  $\text{Fe}^{3+}$ , and  $\text{Mn}^{+2}$  and  $\text{Mn}^{3+}$  in the structures. On the contrary, XANES spectra revealed that the oxidation states of Ni and Zn ions in the samples are  $2+$  and the oxidation state of P in all samples is  $5+$ .

For the studies of chemical compositions, XPS survey spectra confirmed the presence of C, N, O, P, Mg, Co, Fe, Mn, Ni, Zn, and Cu elements on the samples surface. Peak fitting of N 1s region in high resolution XPS spectra of  $\text{NH}_4\text{MPO}_4\cdot\text{H}_2\text{O}$  ( $\text{M} = \text{Co, Fe, Mn, Ni, Cu}$ ) sample show two main regions of N and NH indicating that the materials are suitable for fertilizer application. In the metal region, the high resolution XPS spectra show the transition metal of  $\text{Co}^{2+}$ ,  $\text{Co}^{3+}$ ,  $\text{Cu}^{1+}$ ,  $\text{Cu}^{2+}$ ,  $\text{Fe}^{2+}$ ,  $\text{Fe}^{3+}$ ,  $\text{Mn}^{3+}$ ,  $\text{Mn}^{4+}$ , and  $\text{Ni}^{2+}$ . Interesting result is that the high resolution XPS spectra in P 2p

region show the strong peak, implying rich P in all samples. As mention before, phosphorus (P) is one of the primary nutrients which is required by plants in relatively large quantities. Therefore, this result clearly confirms the suitable applications of these materials in plants.

## 5.2 The magnetic properties

For magnetic properties, the VSM measurements were taken at room temperature. In case of  $\text{NH}_4\text{MgPO}_4\cdot\text{H}_2\text{O}$  and  $\text{NH}_4\text{ZnPO}_4$  samples, the magnetization values decrease with increasing external magnetic field indicating diamagnetic behavior. The magnetization of the prepared  $\text{NH}_4\text{MPO}_4\cdot\text{H}_2\text{O}$  with  $M = \text{Co, Cu, Fe, Mn,}$  and  $\text{Ni}$  samples was obtained to be 14.98, 2.14, 17.52, 26.17 and 4.83 emu/g, respectively. Clearly, the results indicate that the magnetization value depends on the oxidation state in the structure of the materials which was investigated by XPS and XAS techniques. For the prepared  $\text{NH}_4\text{MPO}_4\cdot\text{H}_2\text{O}$  ( $M = \text{Co, Cu, Fe, Mn, Ni}$ ) samples, VSM results show the antiferromagnetism behavior which can be described via superexchange mechanism.

## 5.3 The ion release properties

To clarify type of fertilizer, the ion release properties of the materials were studied by ICP-OES. The results indicated that all water condition samples emitted phosphorus (P) ions in which the  $\text{NH}_4\text{FePO}_4\cdot\text{H}_2\text{O}$  sample released the highest amount of P ions (105 mg/L). In contrast, the release rates of metal ions from high to low are 14.9, 7.4, 0.35, 0.26, 0.24, 0, and 0 mg/L for  $\text{NH}_4\text{MgPO}_4\cdot\text{H}_2\text{O}$ ,  $\text{NH}_4\text{FePO}_4\cdot\text{H}_2\text{O}$ ,  $\text{NH}_4\text{ZnPO}_4$ ,  $\text{NH}_4\text{CuPO}_4\cdot\text{H}_2\text{O}$ ,  $\text{NH}_4\text{NiPO}_4\cdot\text{H}_2\text{O}$ ,  $\text{NH}_4\text{CoPO}_4\cdot\text{H}_2\text{O}$  and  $\text{NH}_4\text{MnPO}_4\cdot\text{H}_2\text{O}$

samples, respectively. In comparison with the commercial ion foliar fertilizer, the prepared  $\text{NH}_4\text{FePO}_4\cdot\text{H}_2\text{O}$  sample released ions higher than that of the commercial product ( $\sim 10$  mg/L). Among all the polymer sources, the Mg ion released the highest amount of 14.9 mg/L in the  $\text{NH}_4\text{MgPO}_4\cdot\text{H}_2\text{O}$  sample prepared by using sucrose. On the other hand, the highest amount of P ions (170.0 mg/L) was observed in the  $\text{NH}_4\text{MgPO}_4\cdot\text{H}_2\text{O}$  sample prepared by using PVP as a polymer source. Therefore, the use of polymer sources of PVP and sucrose seems to enhance the metal ions release properties, especially in the prepared samples of  $\text{NH}_4\text{MgPO}_4\cdot\text{H}_2\text{O}$ ,  $\text{NH}_4\text{CuPO}_4\cdot\text{H}_2\text{O}$  and  $\text{NH}_4\text{FePO}_4\cdot\text{H}_2\text{O}$ .

#### **5.4 Effect of solvent on $\text{NH}_4\text{MPO}_4\cdot\text{H}_2\text{O}$ (M= Mg, Co, Fe, Mn, Ni, Zn, Cu) structures**

The effect of solvent on  $\text{NH}_4\text{MPO}_4\cdot\text{H}_2\text{O}$  (M = Mg, Co, Fe, Mn, Ni, Zn, Cu) structure was studied by dissolving polymer sources of PVP, PVA, sucrose and CTAB in DI water. The obtained samples were characterized by XRD, SEM, XAS and XPS techniques. The XRD patterns of the  $\text{NH}_4\text{MPO}_4\cdot\text{H}_2\text{O}$  (M = Co, Mn, Fe) sample with different polymer sources of water, PVP, PVA, sucrose and CTAB can be indexed as orthorhombic structure with Pmn21 space group. No structural change of  $\text{NH}_4\text{MPO}_4\cdot\text{H}_2\text{O}$  (M = Co, Mn, Fe) was observed by using medium solutions of water, PVP, PVA, sucrose and CTAB. In case of the prepared  $\text{NH}_4\text{CuPO}_4\cdot\text{H}_2\text{O}$  by using polymer sources of PVA and sucrose, diffraction peaks are broad implying amorphous structure in these materials. By using water, PVP, PVA, sucrose and CTAB, phase structure of  $\text{NH}_4\text{MgPO}_4\cdot\text{H}_2\text{O}$  changes to  $\text{NH}_4\text{MgPO}_4\cdot 6\text{H}_2\text{O}$ . The phase structure of  $\text{NH}_4\text{NiPO}_4\cdot 6\text{H}_2\text{O}$  presented after PVP, PVA, Sucrose and CTAB were used in the

preparation of  $\text{NH}_4\text{NiPO}_4\cdot\text{H}_2\text{O}$  and the presence of monoclinic structure of  $\text{NH}_4\text{ZnPO}_4$  shown after PVP and CTAB were used.

For the studies of microstructure, SEM image of the prepared  $\text{NH}_4\text{CuPO}_4\cdot\text{H}_2\text{O}$  and  $\text{NH}_4\text{MgPO}_4\cdot\text{H}_2\text{O}$  powder using PVA, sucrose, and CTAB solution revealed the reduction of particle size into nanometer range. On the other hand, the reduction of particle in the prepared  $\text{NH}_4\text{CoPO}_4\cdot\text{H}_2\text{O}$  sample by using PVA and sucrose was also observed but the particle could not reach in nanometer size. Additionally, the reduction of particle size was also presented in the prepared  $\text{NH}_4\text{MnPO}_4\cdot\text{H}_2\text{O}$  sample by using PVP, PVA, Sucrose and CTAB. The water, PVP, PVA, Sucrose and CTAB solution cannot reduce size of the  $\text{NH}_4\text{FePO}_4\cdot\text{H}_2\text{O}$ . By using PVP, PVA and CTAB solution, the change of morphology was observed in  $\text{NH}_4\text{NiPO}_4\cdot\text{H}_2\text{O}$  sample and the change of particle size to nanoparticle in  $\text{NH}_4\text{ZnPO}_4$  was also observed by using these solutions.

For the local structure, X-ray absorption near-edge structure (XANES) spectra of the prepared  $\text{NH}_4\text{MPO}_4\cdot\text{H}_2\text{O}$  (M = Mg, Co, Fe, Mn, Ni, Zn, Cu) samples by using water, PVP, PVA, sucrose and CTAB were evaluated at M K-edge. The XANES results imply that Co, Cu, Mn, and Fe ions in the samples have the mixing oxidation states of  $\text{Co}^{2+}$  and  $\text{Co}^{3+}$ , Cu and  $\text{Cu}^{2+}$ ,  $\text{Mn}^{2+}$  and  $\text{Mn}^{3+}$ , and  $\text{Fe}^{+2}$  and  $\text{Fe}^{3+}$  in the structures, respectively. In case of  $\text{NH}_4\text{NiPO}_4\cdot 6\text{H}_2\text{O}$  and  $\text{NH}_4\text{ZnPO}_4$  samples, the XANES spectra are well matched with  $\text{Ni}^{2+}$  and  $\text{Zn}^{2+}$  standard data. Moreover, the oxidation state of P ions in the  $\text{NH}_4\text{MPO}_4\cdot\text{H}_2\text{O}$  sample is 5+ due to the matching edge energy between the prepared and standard samples.

For the studies of chemical compositions, the XPS spectra in the Co 2p, Cu 2p, Fe 2p, Mg 2s, Mn 2p, Ni and Zn 2p regions of  $\text{NH}_4\text{MPO}_4\cdot\text{H}_2\text{O}$  (M = Co, Cu, Fe, Mg,

Mn, Ni, Zn) powder with water, PVP, PVA, sucrose and CTAB solution are shown in the samples indicating  $\text{Co}^{2+}$  and  $\text{Co}^{3+}$ ,  $\text{Cu}^{1+}$  and  $\text{Cu}^{2+}$ . Except for  $\text{NH}_4\text{CuPO}_4\cdot\text{H}_2\text{O}$  with PVA solution, XPS spectra show only  $\text{Cu}^{2+}$  in the sample. For  $\text{NH}_4\text{FePO}_4\cdot\text{H}_2\text{O}$ ,  $\text{NH}_4\text{MgPO}_4\cdot\text{H}_2\text{O}$ ,  $\text{NH}_4\text{MnPO}_4\cdot\text{H}_2\text{O}$ ,  $\text{NH}_4\text{NiPO}_4\cdot\text{H}_2\text{O}$ , and  $\text{NH}_4\text{ZnPO}_4$  samples, the oxidation states are confirmed to be  $\text{Fe}^{2+}$  and  $\text{Fe}^{3+}$ ,  $\text{Mg}^{2+}$ ,  $\text{Mn}^{3+}$  and  $\text{Mn}^{4+}$ ,  $\text{Ni}^{2+}$  and  $\text{Zn}^{2+}$ , respectively. In addition, the XAS spectra in P 2p region of  $\text{NH}_4\text{MPO}_4\cdot\text{H}_2\text{O}$  sample ( $\text{M} = \text{Co}, \text{Cu}, \text{Fe}, \text{Mg}, \text{Mn}, \text{Ni}, \text{Zn}$ ) with water, PVP, PVA, sucrose and CTAB solution exhibit only peak of P 2p indicating that the oxidation state of P in the samples is 5+ and these results are in good agreement with XRD and XAS results.

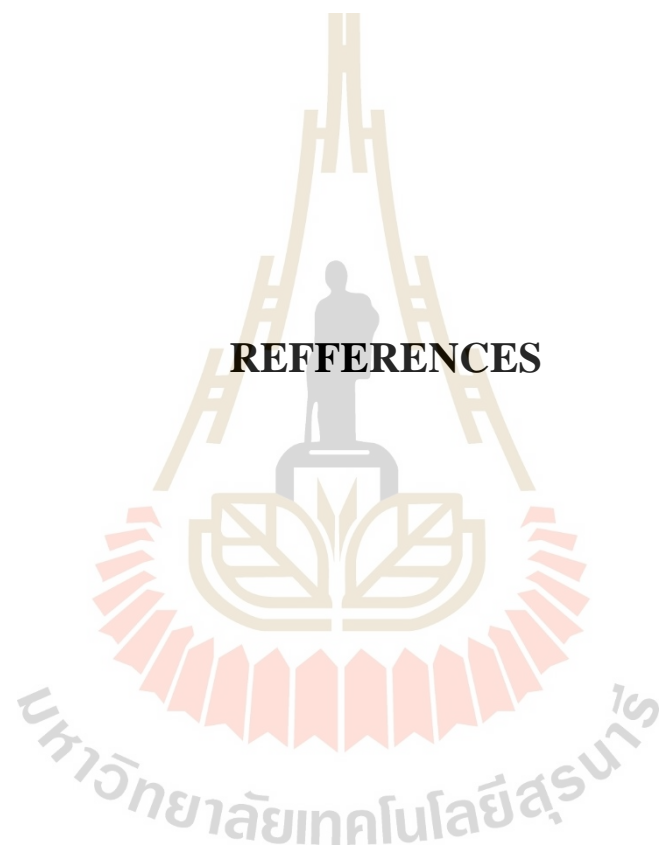
## 5.5 Suggestion for future work

This work showed successful preparation of the  $\text{NH}_4\text{MPO}_4\cdot\text{H}_2\text{O}$  ( $\text{M} = \text{Mg}, \text{Co}, \text{Fe}, \text{Mn}, \text{Ni}, \text{Zn}, \text{Cu}$ ) powders by a simple coprecipitation method in water and other template solution. This method can be extended for the preparation of other metal-oxide or complex-oxide micro-nanoparticles. The findings in this research suggest the future works as follows:

5.4.1 Investigation of the specific surface area and pore size distribution analysis of  $\text{NH}_4\text{MPO}_4\cdot\text{H}_2\text{O}$  ( $\text{M} = \text{Mg}, \text{Co}, \text{Fe}, \text{Mn}, \text{Ni}, \text{Zn}, \text{Cu}$ ) by using Brunauer-Emmett-Teller (BET) and Barrett-Joyner-Halenda (BJH) methods, along with the studying of the ion release on the prepared materials.

5.4.2 Updating application of  $\text{NH}_4\text{MPO}_4\cdot\text{H}_2\text{O}$  ( $\text{M} = \text{Mg}, \text{Co}, \text{Fe}, \text{Mn}, \text{Ni}, \text{Zn}, \text{Cu}$ ) within water, PVP, PVA, Sucrose and CTAB for uptake in plants by using fertilizer release process.

## REFERENCES



## REFERENCES

- Amghouz, Z., Ramajo, B., Khainakov, S. A., Da Silva, I., Castro, G. R., García, J. R. and García-Granda, S. (2014). Dimensionality changes in the solid phase at room temperature: 2D  $\rightarrow$  1D  $\rightarrow$  3D evolution induced by ammonia sorption-desorption on zinc phosphates. **Chemical Communications** 50(51): 6729-6732.
- Asgari-Vadeghani, T., Ghanbari, D., Mozdianfar, M. R., Salavati-Niasari, M., Bagheri, S. and Saberyan, K. (2016). Sugar and Surfactant-Assisted Synthesis of Mg(OH)<sub>2</sub> Nano-flower and PVA Nanocomposites. **Journal of Cluster Science** 27(1): 299-314.
- Attfield, J. P. (2001). **Phosphates: Encyclopedia of Materials: Science and Technology**. P. Veysière et al. Oxford, Elsevier: 6896-6901.
- Azeem, B., KuShaari, K., Man, Z. B., Basit, A. and Thanh, T. H. (2014). Review on materials & methods to produce controlled release coated urea fertilizer. **Journal of Controlled Release** 181: 11-21.
- Barros, N., Airoidi, C., Simoni, J. A., Ramajo, B., Espina, A. and Garcia, J. R. (2006). Calorimetric determination of the effect of ammonium-iron(II) phosphate monohydrate on Rhodic Eutrudox Brazilian soil. **Thermochimica Acta** 441(1): 89-95.
- Bica, I. (1999). Nanoparticle production by plasma. **Materials Science and Engineering B-Advanced Functional Solid-State Materials** 68(1): 5-9.

- Bridger, G. L., Salutsky, M. L. and Starostka, R. W. (1962). Micronutrient Sources, Metal Ammonium Phosphates as Fertilizers. **Journal of Agricultural and Food Chemistry** 10(3): 181-188.
- Byrappa, K., Chandrashekar, C. K., Basavalingu, B., LokanathaRai, K. M., Ananda, S. and Yoshimura, M. (2007). Growth, morphology and mechanism of rare earth vanadate crystals under mild hydrothermal conditions. **Journal of Crystal Growth** 306(1): 94-101.
- Caglar, M. and Yakuphanoglu, F. (2012). Structural and optical properties of copper doped ZnO films derived by sol-gel. **Applied Surface Science** 258(7): 3039-3044.
- Chen, C., Zhang, N., Liu, X., He, Y., Wan, H., Liang, B., Ma, R., Pan, A. and Roy, V. A. (2016). Polypyrrole-modified  $\text{NH}_4\text{NiPO}_4 \cdot \text{H}_2\text{O}$  nanoplate arrays on Ni foam for efficient electrode in electrochemical capacitors. **ACS Sustainable Chemistry & Engineering** 4(10): 5578-5584.
- Chen, Q., Wang, Y., Zheng, M., Fang, H. and Meng, X. (2018). Nanostructures confined self-assembled in biomimetic nanochannels for enhancing the sensitivity of biological molecules response. **Journal of Materials Science: Materials in Electronics** 29(23): 19757-19767.
- Debray, M. (1864). **Comptes Rendus Hebdomadaires des Seances de l'Aeademie des Sciences** 59(4): 40.
- FAO. (2012). "State of food insecurity in the world: economic growth is necessary but not sufficient to accelerate reduction of hunger and malnutrition. ." from <http://www.fao.org/docrep/016/i3027e/i3027e.pdf>.

- Hänsch, R. and Mendel, R. R. (2009). Physiological functions of mineral micronutrients (Cu, Zn, Mn, Fe, Ni, Mo, B, Cl). **Current Opinion in Plant Biology** 12(3): 259-266.
- Harrison, W. T. A., Sobolev, A. N. and Phillips, M. L. F. (2001). Hexagonal ammonium zinc phosphate,  $(\text{NH}_4)\text{ZnPO}_4$ , at 10 K. **Acta Crystallographica Section C-Crystal Structure Communications** 57(5): 508-509.
- Jiang, T., Wang, Y., Meng, D., Wu, X., Wang, J. and Chen, J. (2014). Controllable fabrication of CuO nanostructure by hydrothermal method and its properties. **Applied Surface Science** 311: 602-608.
- Jiang, Z., Xie, J., Jiang, D., Wei, X. and Chen, M. (2013). Modifiers-assisted formation of nickel nanoparticles and their catalytic application to p-nitrophenol reduction. **Crystengcomm** 15(3): 560-569.
- Jie, C., Jing-zhang, C., Man-zhi, T. and Zi-tong, G. (2002). Soil degradation: a global problem endangering sustainable development. **Journal of Geographical Sciences** 12(2): 243-252.
- Karaphun, A., Chirawatkul, P., Maensiri, S. and Swatsitang, E. (2018). Influence of calcination temperature on the structural, morphological, optical, magnetic and electrochemical properties of  $\text{Cu}_2\text{P}_2\text{O}_7$  nanocrystals. **Journal of Sol-Gel Science and Technology** 88(2): 407-421.
- Koo, H.-J. and Whangbo, M.-H. (2008). On the correct spin lattice for the spin-gapped magnetic solid  $\text{NH}_4\text{CuPO}_4 \cdot \text{H}_2\text{O}$ . **Journal of Solid State Chemistry** 181(2): 276-281.

- Kyrychenko, A., Pasko, D. A. and Kalugin, O. N. (2017). Poly(vinyl alcohol) as a water protecting agent for silver nanoparticles: the role of polymer size and structure. **Physical Chemistry Chemical Physics** 19(13): 8742-8756.
- Lapina, L. M. (1968). Metal Ammonium Phosphates and Their New Applications. **Russian Chemical Reviews** 37(9): 693.
- Li, P., Du, Y., Li, L., Huang, L., Rudolph, V., Nguyen, A. V. and Xu, Z. P. (2014). Preparation and characterisation of manganese and iron compounds as potential control-release foliar fertilisers. **Biointerface Research in Applied Chemistry** 4(3): 746-753.
- Li, P., Xu, Z. P., Hampton, M. A., Vu, D. T., Huang, L., Rudolph, V. and Nguyen, A. V. (2012). Control Preparation of Zinc Hydroxide Nitrate Nanocrystals and Examination of the Chemical and Structural Stability. **The Journal of Physical Chemistry C** 116(18): 10325-10332.
- Li, Y., Liu, Q. and Shen, W. (2011). Morphology-dependent nanocatalysis: metal particles. **Dalton Transactions** 40(22): 5811-5826.
- López-Quintela, M. A. and Rivas, J. (1993). Chemical Reactions in Microemulsions: A Powerful Method to Obtain Ultrafine Particles. **Journal of Colloid and Interface Science** 158(2): 446-451.
- Maensiri, S., Masingboon, C., Boonchom, B. and Seraphin, S. (2007). A simple route to synthesize nickel ferrite (NiFe<sub>2</sub>O<sub>4</sub>) nanoparticles using egg white. **Scripta Materialia** 56(9): 797-800.
- Mishra, V., Mishra, R. K., Dikshit, A. and Pandey, A. C. (2014). **Chapter 8 - Interactions of Nanoparticles with Plants: An Emerging Prospective in the Agriculture Industry: Emerging Technologies and Management of Crop**

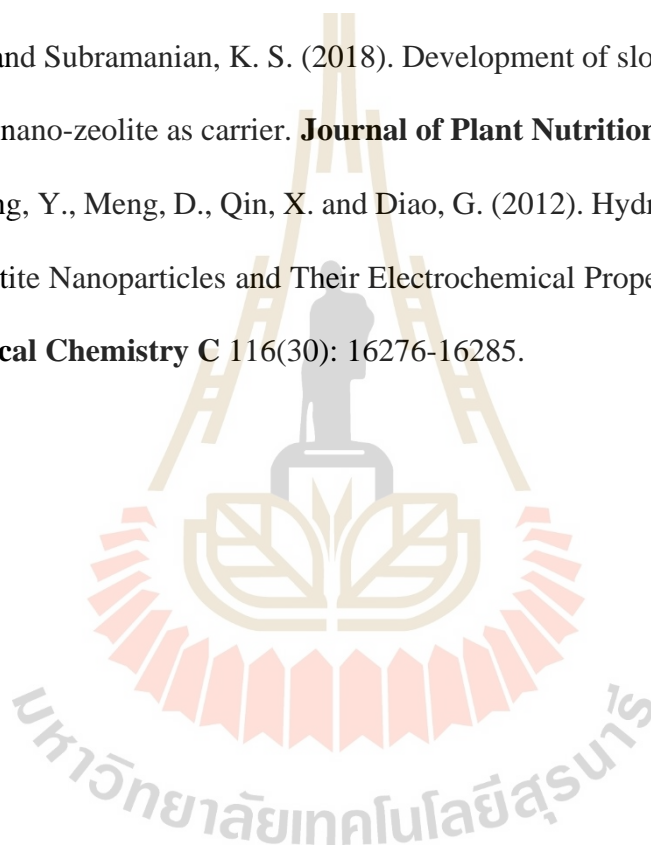
- Stress Tolerance.** P. Ahmad and S. Rasool. San Diego, Academic Press: 159-180.
- Olesik, J. W. (1991). Elemental analysis using ICP-OES and ICP/MS. **Analytical Chemistry** 63(1): 12A-21A.
- Pan, Y., Heryadi, D., Zhou, F., Zhao, L., Lestari, G., Su, H. and Lai, Z. (2011). Tuning the crystal morphology and size of zeolitic imidazolate framework-8 in aqueous solution by surfactants. **Crystengcomm** 13(23): 6937-6940.
- Pang, H., Yan, Z., Ma, Y., Li, G., Chen, J., Zhang, J., Du, W. and Li, S. (2013). Cobalt pyrophosphate nano/microstructures as promising electrode materials of supercapacitor. **Journal of Solid State Electrochemistry** 17(5): 1383-1391.
- Pang, H., Yan, Z., Wang, W., Chen, J., Zhang, J. and Zheng, H. (2012). Facile fabrication of  $\text{NH}_4\text{CoPO}_4 \cdot \text{H}_2\text{O}$  nano/microstructures and their primarily application as electrochemical supercapacitor. **Nanoscale** 4(19): 5946-5953.
- Pang, H., Yan, Z., Wang, W., Wei, Y., Li, X., Li, J., Chen, J., Zhang, J. and Zheng, H. (2012). Template-free Controlled Fabrication of  $\text{NH}_4\text{MnPO}_4 \cdot \text{H}_2\text{O}$  and  $\text{Mn}_2\text{P}_2\text{O}_7$  Micro-Nanostructures and Study of Their Electrochemical Properties. **International Journal of Electrochemical Science** 7(12): 12340-12353.
- Park, M. (2001). **2 - A brief history: The Fertilizer Industry.** M. Park, Woodhead Publishing: 2-page 19.
- Patel, D. D. and Anderson, B. D. (2013). Maintenance of supersaturation II: Indomethacin crystal growth kinetics versus degree of supersaturation. **Journal of Pharmaceutical Sciences** 102(5): 1544-1553.

- Pysiak, J., Prodan, E. A., Samuskevich, V. V., Pacewska, B. and Shkorik, N. A. (1993). Thermal transformations of  $\text{NH}_4\text{M}^{\text{II}}\text{PO}_4 \cdot \text{H}_2\text{O}$  (where  $\text{M}^{\text{II}}$  is Mg, Mn, Co, Cu). **Thermochimica Acta** 222(1): 91-103.
- Rezlescu, L., Rezlescu, E., Popa, P. D. and Rezlescu, N. (1999). Fine barium hexaferrite powder prepared by the crystallisation of glass. **Journal of Magnetism and Magnetic Materials** 193(1–3): 288-290.
- Römheld, V. and Marschner, H. (1991). **Function of Micronutrients in Plants: Micronutrients in agriculture.** J. J. Mortvedt: 297-328.
- Sronsri, C., Noisong, P. and Danvirutai, C. (2014). Synthesis, non-isothermal kinetic and thermodynamic studies of the formation of  $\text{LiMnPO}_4$  from  $\text{NH}_4\text{MnPO}_4 \cdot \text{H}_2\text{O}$  precursor. **Solid State Sciences** 32: 67-75.
- Sun, X., Zheng, C., Zhang, F., Yang, Y., Wu, G., Yu, A. and Guan, N. (2009). Size-Controlled Synthesis of Magnetite ( $\text{Fe}_3\text{O}_4$ ) Nanoparticles Coated with Glucose and Gluconic Acid from a Single Fe(III) Precursor by a Sucrose Bifunctional Hydrothermal Method. **The Journal of Physical Chemistry C** 113(36): 16002-16008.
- Thanh, N. T. K., Maclean, N. and Mahiddine, S. (2014). Mechanisms of Nucleation and Growth of Nanoparticles in Solution. **Chemical Reviews** 114(15): 7610-7630.
- Torre-Fernández, L., Trobajo, C., de Pedro, I., Alfonso, B. F., Fabelo, O., Blanco, J. A., García, J. R. and García-Granda, S. (2013). Ammonium–cobalt–nickel phosphates,  $\text{NH}_4[\text{Co}_{1-x}\text{Ni}_x\text{PO}_4] \cdot \text{H}_2\text{O}$ . **Journal of Solid State Chemistry** 206: 75-84.

- Touaiher, M., Bettach, M., Benkhrouja, K., Zahir, M., Aranda, M. A. G. and Bruque, S. (2001). Synthesis and structure of  $\text{NH}_4\text{CoPO}_4 \cdot 6\text{H}_2\text{O}$ . **Annales de Chimie Science des Matériaux** 26(3): 49-54.
- Treesukkasem, N., Chokradjaroen, C., Theeramunkong, S., Saito, N. and Watthanaphanit, A. (2019). Synthesis of Au Nanoparticles in Natural Matrices by Liquid-Phase Plasma: Effects on Cytotoxic Activity against Normal and Cancer Cell Lines. **ACS Applied Nano Materials** 2(12): 8051-8062.
- Trenkel, M. E. (2010). **Slow- and Controlled-release and Stabilized Fertilizers: An Option for Enhancing Nutrient Use Efficiency in Agriculture**, International fertilizer industry Association.
- Wang, S., Pang, H., Zhao, S., Shao, W., Zhang, N., Zhang, J., Chen, J. and Li, S. (2014).  $\text{NH}_4\text{CoPO}_4 \cdot \text{H}_2\text{O}$  microbundles consisting of one-dimensional layered microrods for high performance supercapacitors. **RSC Advances** 4(1): 340-347.
- Wang, X., Jian, H., Xiao, Q. and Huang, S. (2018). In-situ fabrication of 3D flower-like  $\text{NH}_4\text{NiPO}_4$  on Ni foam without nickel salts added for high sensitive nonenzymatic glucose detection. **Materials Research Bulletin** 100: 407-412.
- Wang, Y., Jiang, T., Meng, D., Yang, J., Li, Y., Ma, Q. and Han, J. (2014). Fabrication of nanostructured CuO films by electrodeposition and their photocatalytic properties. **Applied Surface Science** 317: 414-421.
- Wannasen, L., Chanlek, N., Maensiri, S. and Swatsitang, E. (2019). Composition effect of Co/Ni on the morphology and electrochemical properties of  $\text{NH}_4\text{Co}_{1-x}\text{Ni}_x\text{PO}_4 \cdot \text{H}_2\text{O}$  nanocrystallites prepared by a facile hydrothermal method. **Journal of Materials Science: Materials in Electronics** 30(8): 7794-7807.

- Wenwei, W., Yanjin, F., Xuehang, W., Sen, L. and Shushu, L. (2009). Preparation via solid-state reaction at room temperature and characterization of layered nanocrystalline  $\text{NH}_4\text{MnPO}_4 \cdot \text{H}_2\text{O}$ . **Journal of Physics and Chemistry of Solids** 70(3-4): 584-587.
- Wenwei, W., Yanjin, F., Xuehang, W., Sen, L. and Shushu, L. (2009). Preparation via solid-state reaction at room temperature and characterization of layered nanocrystalline  $\text{NH}_4\text{MnPO}_4 \cdot \text{H}_2\text{O}$ . **Journal of Physics and Chemistry of Solids** 70(3-4): 584-587.
- Wu, W., Li, S., Wu, X., Liao, S. and Cao, J. (2010). Novel Method for Preparing  $\text{NH}_4\text{NiPO}_4 \cdot 6\text{H}_2\text{O}$ : Hydrogen Bonding Coacervate Selective Self-assembly. **Chinese Journal of Chemistry** 28(12): 2389-2393.
- Yan, B. and Gu, J. (2009). Morphology controlled solvo-thermal synthesis and luminescence of  $\text{NH}_4\text{ZnPO}_4: \text{Eu}^{3+}$  submicrometer phosphor. **Journal of Alloys and Compounds** 479(1-2): 536-540.
- Yuan, A., Wu, J., Bai, L., Ma, S., Huang, Z. and Tong, Z. (2008). Standard molar enthalpies of formation for ammonium/3d-Transition metal phosphates  $\text{NH}_4\text{MPO}_4 \cdot \text{H}_2\text{O}$  (M=  $\text{Mn}^{2+}$ ,  $\text{Co}^{2+}$ ,  $\text{Ni}^{2+}$ ,  $\text{Cu}^{2+}$ ). **Journal of Chemical & Engineering Data** 53(5): 1066-1070.
- Yuan, A., Wu, J., Bai, L., Ma, S., Huang, Z. and Tong, Z. (2008). Standard Molar Enthalpies of Formation for Ammonium/3d-Transition Metal Phosphates  $\text{NH}_4\text{MPO}_4 \cdot \text{H}_2\text{O}$  (M =  $\text{Mn}^{2+}$ ,  $\text{Co}^{2+}$ ,  $\text{Ni}^{2+}$ ,  $\text{Cu}^{2+}$ ). **Journal of Chemical & Engineering Data** 53(5): 1066-1070.

- Yuan, A., Wu, J., Huang, Z., Wu, K., Liao, S. and Tong, Z. F. (2008). Synthesis of  $\text{NH}_4\text{FePO}_4 \cdot \text{H}_2\text{O}$  nano-plates via solid-state reaction at low temperature and its thermochemistry properties. **Materials Research Bulletin** 43(6): 1339-1345.
- Yuvaraj, M. and Subramanian, K. S. (2015). Controlled-release fertilizer of zinc encapsulated by a manganese hollow core shell. **Soil Science and Plant Nutrition** 61(2): 319-326.
- Yuvaraj, M. and Subramanian, K. S. (2018). Development of slow release Zn fertilizer using nano-zeolite as carrier. **Journal of Plant Nutrition** 41(3): 311-320.
- Zhu, M., Wang, Y., Meng, D., Qin, X. and Diao, G. (2012). Hydrothermal Synthesis of Hematite Nanoparticles and Their Electrochemical Properties. **The Journal of Physical Chemistry C** 116(30): 16276-16285.



## CURRICULUM VITAE

**Name** Mr. Santi Phumying  
**Date of Birth** Mach 29, 1983  
**Place of Birth** 68 Nonsang Tambol Nonsang, Nonsang District,  
Nongbualamphu Province, 39140, Thailand.

### Education

1999 – 2002 High school  
Nonsang Wittayakarn School, Nongbualamphu Province, Thailand.

2002 – 2007 B.Sc. (Physics)  
Department of Physics, Faculty of Science, Khon Kaen University,  
Thailand

2009 – 2012 M.Sc. (Material Science and Nanotechnology)  
Department of Physics, Faculty of Science, Khon Kaen University,  
Thailand

